

Direct Laser Cooling of Polyatomic Molecules

Benjamin L. Augenbraun, Loïc Anderegg, Christian Hallas, Zack D. Lasner, Nathaniel B. Vilas, John M. Doyle

Department of Physics, Harvard University, Cambridge, MA 02138, USA

Harvard-MIT Center for Ultracold Atoms, Cambridge, MA 02138, USA

Abstract

Over the past decade, tremendous progress has been made to extend the tools of laser cooling and trapping to molecules. Those same tools have recently been applied to polyatomic molecules (molecules containing three or more atoms). In this review, we discuss the scientific drive to bring larger molecules to ultralow temperatures, the features of molecular structure that provide the most promising molecules for this pursuit, and some technical aspects of how lasers can be used to control the motion and quantum states of polyatomic molecules. We also present opportunities for and challenges to the use of polyatomic molecules for science and technology.

Keywords: ultracold molecules, laser cooling, polyatomic molecules

DRAFT: February 18, 2023

Email addresses: augenbraun@g.harvard.edu (Benjamin L. Augenbraun),
jdoyle@g.harvard.edu (John M. Doyle)

Preprint submitted to Advances in Atomic, Molecular and Optical Physics February 21, 2023

Direct Laser Cooling of Polyatomic Molecules

Benjamin L. Augenbraun, Loïc Anderegg, Christian Hallas, Zack D. Lasner, Nathaniel B. Vilas, John M. Doyle

Department of Physics, Harvard University, Cambridge, MA 02138, USA

Harvard-MIT Center for Ultracold Atoms, Cambridge, MA 02138, USA

Contents

1	Introduction	4
1.1	Polyatomic molecules for quantum science	5
1.1.1	Quantum information processing	7
1.1.2	Quantum simulation	8
1.2	Precision measurements	9
1.3	Collisions and chemistry	13
1.4	Experimental approaches besides direct laser cooling	16
1.5	Direct laser cooling	17
1.5.1	Forming closed cycling transitions	17
1.5.2	Effects of multilevel systems on laser cooling	19
2	Molecular structure for laser cooling experiments	20
2.1	Electronic structure	20
2.2	Vibrational structure	24
2.2.1	Vibrational state notation	27
2.2.2	Anharmonic coupling	28
2.3	Rotational structure	28
2.3.1	Linear molecules	29
2.3.2	Spherical top molecules	29
2.3.3	Symmetric top molecules	29
2.3.4	Asymmetric top molecules	30

Email addresses: augenbraun@g.harvard.edu (Benjamin L. Augenbraun),
jdoyle@g.harvard.edu (John M. Doyle)

Preprint submitted to Advances in Atomic, Molecular and Optical Physics February 21, 2023

2.3.5	Dependence on spin and electronic angular momenta	30
2.3.6	Hyperfine effects and nuclear spin statistics	32
2.4	Transitions	33
2.4.1	Electronic transitions	33
2.4.2	Vibrational transitions	34
2.4.3	Measuring vibrational branching ratios	35
2.4.4	Repumping transition spectroscopy	39
2.4.5	Designing an optical cycle	42
2.4.6	Rotational transitions	43
2.5	Perturbations	51
3	Experimental techniques	53
3.1	Cryogenic buffer-gas beams	53
3.2	Optical cycling	57
3.3	Optical forces	59
3.4	Transverse cooling	60
3.5	Molecular deceleration	61
3.5.1	Radiative slowing	63
3.5.2	Zeeman-Sisyphus deceleration	64
3.6	Magneto-optical trapping	69
3.7	Sub-Doppler cooling	72
3.7.1	Grey molasses	72
3.7.2	Λ -enhanced grey molasses	73
3.7.3	Single-frequency cooling	75
3.8	Optical trapping	76
3.9	Preparation and coherent control of single quantum states	78
4	Outlook and challenges	80
4.1	Toward larger molecules	80
4.2	Other molecular motifs	81
4.3	Challenges and possibilities for other polyatomic molecules	82
5	Conclusion	85
6	Acknowledgments	86

1. Introduction

Detailed understanding of polyatomic molecules (those containing three or more atoms) is central to such diverse fields as chemistry, biology, and interstellar science. Beyond the inherent interest in their structures and interactions, physicists also hope to fully control polyatomic molecules at the single quantum state level for next-generation explorations. The diversity of electronic structures, geometries, and atomic constituents present in polyatomic molecules may provide powerful building blocks for quantum information processing and precision tests of fundamental physics, e.g. searching for dark matter or for new particles that help explain the matter-antimatter asymmetry of the universe. However, using complex molecules for these applications requires us to confront one of their most defining—and daunting—characteristics: their immensely rich and varied internal structures. Attempts to tame polyatomic molecules, for example by controlling their internal (e.g. vibrational/rotational) and external (motional) states have a long history both in atomic, molecular, and optical (AMO) physics and in physical chemistry. It is the purpose of this review to describe recent advances that have introduced direct laser cooling as a new element in the toolkit of polyatomic molecular control.

The already achieved exquisite control over certain quantum systems has been realized in no small part by using optical photons—this is a hallmark of modern quantum science and physical chemistry. The most recent wave of advances with atoms and molecules relies on the ability to cool, control, and detect molecules efficiently (and, ideally, nondestructively). Optical cycling, a process in which molecules are made to rapidly and repeatedly scatter many hundreds or thousands of photons, can be an effective way to carry out these tasks. Using photon cycling, scientists have exploited the mechanical effects of light to prepare and interrogate individual atoms and diatomic molecules in pristine and dynamically controllable traps (Barredo et al. (2016); Endres et al. (2016)). Optical photons also allow scientists to probe the fragile quantum effects that form the heart of modern quantum technologies (Haroche (2013); Wineland (2013)). The creation of quantum gases of atoms and the production of useful architectures for quantum computing also rely on these experimental feats. These wide ranging impacts span many frontiers of quantum science, as well as cold chemistry, and precision searches for new fundamental (particle) physics.

1.1. Polyatomic molecules for quantum science

Ultracold molecules are a promising platform for quantum simulation and quantum information processing due to their large electric dipole moments and the intrinsically long coherence times achievable in low-lying rotational states. Heteronuclear molecules have molecule-frame electric dipole moments, typically on the order of several debye (D), that can be accessed in the electronic ground state, eliminating the need for the short-lived excited electronic levels often employed in atomic systems. The molecules may interact via the electric dipole-dipole interaction, whose long-range and anisotropic behavior enables access to a diverse variety of Hamiltonians for quantum simulation, as well as enabling entangling gates for quantum information applications. While not always required to achieve interactions, it can be advantageous to realize a molecular dipole moment in the laboratory frame by aligning the atoms or molecules with an external electric field (either DC or microwave).

While polyatomic molecules, compared to diatomic molecules, possess greater complexity and additional degrees of freedom that need to be controlled, many of the structures present in polyatomic molecules have no analogue in atoms or diatomic molecules. One especially appealing feature of polyatomic molecules is the existence of parity-doubled states in the ground electronic manifold. These “parity doublets” comprise nearly-degenerate pairs of quantum states with opposite parity that can be mixed by a small DC electric field (often $\lesssim 100$ V/cm depending on the molecule), enabling the molecule to be easily polarized in the laboratory frame. Moreover, because this method of polarizing the molecule does not mix end-over-end rotational levels (which requires much larger electric fields, typically >1 kV/cm), the polarized molecules contain states with positive, negative, and near-zero lab-frame dipole moment (see Fig. 1).

The existence of parity-doubled states is a general feature of molecules that have a nonzero projection of the total angular momentum along the molecule-frame dipole moment. In particular, for a molecule with total angular momentum J , whose projection onto the laboratory Z axis is M and whose projection onto the molecular symmetry axis is K , the states $2^{1/2}|\pm\rangle = |J, K, M\rangle \pm (-1)^{J-K}|J, -K, M\rangle$ have opposite parity. States with $K \neq 0$ are universally present in polyatomic molecules: linear polyatomic molecules have angular momentum about the internuclear axis in vibrational bending modes, while nonlinear polyatomic molecules have nonzero moments of inertia about the symmetry axis even in the electronic and vibrational

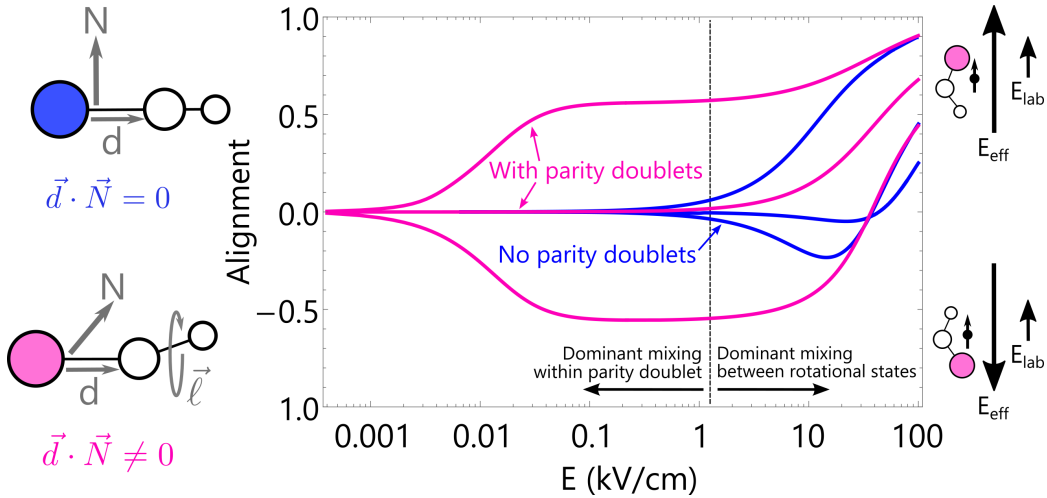


Figure 1: Molecular polarization as a function of applied laboratory electric field. Parameters are typical of YbOH molecules. Blue lines show alignment in a state without parity doubling ($N \leq 2$, $|M_N| \leq 1$ plotted). Pink lines show alignment of $N = 1$ sublevels in a vibrational level that has parity doubling, e.g. the fundamental bending vibrational state. We indicate two electric-field regimes: one where mixing occurs within a single rotational state and another where mixing occurs among many rotational states.

ground state. The degeneracy of these parity doublets is lifted by a range of mechanisms, including Coriolis interactions, nuclear spin-rotation interactions, hyperfine interactions, or molecular asymmetry (Klemperer et al. (1993)). The resulting energy splitting can be as large as tens of MHz (notably in linear polyatomic molecules) or as small as tens of Hz or kHz (e.g., in singlet symmetric top molecules).

For the parity doublet states $|\pm\rangle$ described above, the Hamiltonian under the influence of an external DC electric field \mathcal{E} is

$$H = \begin{pmatrix} -\hbar\Delta/2 & -d\mathcal{E} \\ -d\mathcal{E} & \hbar\Delta/2 \end{pmatrix} \quad (1)$$

where Δ is the parity doublet splitting and

$$d\mathcal{E} \equiv \langle +|\vec{d} \cdot \vec{\mathcal{E}}|-\rangle = d_0\mathcal{E} \frac{KM}{J(J+1)} \quad (2)$$

where d_0 is the permanent dipole moment of the molecule. The energy eigen-

values are therefore

$$E_{\pm} = \pm \frac{1}{2} \hbar \Delta \left[1 + 4 \left(\frac{d\mathcal{E}}{\hbar \Delta} \right)^2 \right]^{1/2} \quad (3)$$

At low electric fields $d\mathcal{E}/\hbar\Delta \ll 1$ the states split apart quadratically, while at high electric fields $d\mathcal{E}/\hbar\Delta \gg 1$ the molecule becomes aligned in the laboratory frame and follows linear Stark shifts:

$$E \approx -d_0 \mathcal{E} \frac{KM}{J(J+1)}, \quad (4)$$

where K and M are signed quantities. The structure of the molecule in this “polarized” regime is amenable to a number of interesting quantum simulation and quantum information applications.

1.1.1. Quantum information processing

Since the seminal proposal by DeMille (2002), ultracold polar molecules have generated significant interest as a platform for quantum information applications, see e.g., Yelin et al. (2006); Ni et al. (2018); Sawant et al. (2019). The key element of these proposals is the fact that polar molecules have many long-lived rotational and vibrational degrees of freedom which enable storage of quantum information, while dipole-dipole interactions enable transfer of information and entanglement between individual molecules. Recent progress toward this goal has been realized with diatomic molecules by Holland et al. (2022) and Bao et al. (2022), who demonstrated dipolar coupling and entanglement between CaF molecules trapped in a tweezer array.

The linear Stark shifts discussed above for polyatomic molecules make them especially appealing for certain quantum computing and entanglement schemes, including those proposed by André et al. (2006); Wei et al. (2011); Yu et al. (2019); Zhang and Liu (2017). For example, Wei et al. (2011) studied theoretically entanglement generation in polar symmetric top molecules and identified two sets of polarized states that could be used as qubits in a quantum computer. They additionally proposed a method for realizing a CNOT entangling gate between two such molecules. Interestingly, it was also pointed out that polarized symmetric top molecules share certain similarities with the NMR quantum computing platform (see, e.g., Cory et al. (2000)). However, molecules in optical tweezer arrays offer the possibility of isolating

individual qubits and controlling entanglement on demand more cleanly than has been done with liquid-phase NMR and with intrinsic scalability.

Yu et al. (2019) proposed a quantum computing scheme harnessing the parity-doublet structure of symmetric top molecules, wherein the qubit states are contained within the $M = 0$ manifold, which eliminates first-order electric field sensitivity, thereby improving robustness to external perturbations. Interactions are switched on using a third state in either the $M = +1$ or $M = -1$ manifold, and entanglement is generated using an interaction blockade mechanism. Using the linear Stark shift structure to switch dipole-dipole interactions on and off in this manner is a key advantage of polyatomic molecules.

The large number of rotational and vibrational degrees of freedom in polyatomic molecules also has potential advantages for quantum information applications. For instance, error-correcting logical qubits could be constructed from coherent superpositions of rotational states, as proposed by Albert et al. (2020). The large number of internal states in polyatomic molecules could also make them uniquely amenable to “qudit” schemes where multiple bits of information are stored in the same molecule, as described by Tesch and de Vivie-Riedle (2002); Sawant et al. (2019). Such schemes could significantly increase the speed and fidelity of molecular quantum computers by performing the majority of gates using single-molecule operations, and only coupling molecules via dipole-dipole interactions when necessary. Full cooling and control of larger polyatomic molecules with many nuclear spins could also enable platforms where NMR-based quantum computing is performed within a single molecule, while scalability is achieved by coupling individual molecules with dipole-dipole interactions. More theoretical work is required to explore the feasibility of such schemes.

1.1.2. Quantum simulation

The long range and anisotropic dipolar interactions between polar molecules lend themselves to quantum simulation applications, in particular to simulation of quantum magnetism models where molecules pinned in a lattice act as effective spins (Carr et al. (2009); Bohn et al. (2017)). Wall et al. (2015a) provide a review of this topic. To date, much of this work has been focused on diatomic molecules, which are naturally suited to simulation of Heisenberg XY models, as first demonstrated experimentally by Yan et al. (2013) using KRb molecules. In theoretical work by Micheli et al. (2006), it was shown that microwave-dressed diatomic molecules with unpaired elec-

tron spins can be used to simulate even more general spin models, though the technical requirements of this proposal have not yet been realized in present day experiments.

Compared to diatomic molecules, polyatomic molecules are naturally suited to simulation of a greater diversity of quantum magnetism models, such as those described by Wall et al. (2013, 2015b,a). For instance, the unique rotational structure of molecules with parity doublet structure enables simulation of XYZ spin models via microwave dressing, as proposed by Wall et al. (2015b). Critically, the technical requirements of this proposal are significantly reduced compared to the method of Micheli et al. (2006) for simulating an XYZ Hamiltonian with diatomic molecules, which requires more microwave frequencies and significantly smaller lattice spacings to compensate for the molecules' sparser internal structure. Another benefit of large polyatomic molecules may be their small fine and hyperfine splittings, which can be made comparable to the dipole-dipole interaction energy at larger molecular spacings. For instance, operating in the regime where the dipolar interaction energy is comparable to the spin-rotation interaction energy in molecules with an unpaired spin would enable simulation of a diverse array of lattice spin models, as described in Micheli et al. (2006). These small energy-level splittings could, however, present a challenge for achieving full control of individual quantum states in the molecule, e.g., due to off-resonant excitations during control pulses.

Wall et al. (2013) have also proposed to use the (nearly) linear Stark shifts present in many polyatomic molecules as a way to simulate lattice spin models involving polarized dipoles. Because this proposal involves using electric dipole moments to simulate magnetic dipoles, the experimental interaction strengths can be several orders of magnitude larger. Importantly, this analogy can be extended to molecular states with arbitrarily large J , enabling quantum simulation of magnetic dipoles with integer spin $S = J$. These features could have interesting applications in simulation of lattice spin models as well as in the study of bulk dipolar gases (see Lahaye et al. (2009) for a review on the subject), which have previously been studied using magnetic atoms with much smaller interaction energies.

1.2. Precision measurements

Polyatomic molecules hold further promise for a variety of precision measurements probing the Standard Model (SM) and beyond-Standard-Model (BSM) physics (see Hutzler (2020) for a focused review). At least three

distinctive features of polyatomic molecules can be leveraged for improved precision measurements. The first such feature is the closely-spaced pairs of opposite-parity states described above, which can be directly mixed by electric fields to orient molecules in the lab frame, or brought to degeneracy via magnetic fields.

Mixing opposite-parity states to orient a molecule in the lab frame is useful for electron electric dipole moment (eEDM) searches, as well as Schiff moment and magnetic quadrupole moment searches operating in a similar manner. The proposals by Kozyryev and Hutzler (2017); Maison et al. (2019); Oleynichenko et al. (2022); Yu and Hutzler (2021); Zakharova and Petrov (2021) describe experiments using polyatomic molecules in which this capability is useful. The basic principle of an eEDM measurement using oriented molecules is as follows. If the electron possesses an electric dipole moment, \vec{d}_e , then it must be oriented along or against the electron spin, so that $|\vec{d}_e \cdot \vec{S}| \neq 0$. In a given molecular state, the energy shift associated with the eEDM is $\langle H_{de} \rangle = d_e \langle \vec{S} \cdot \vec{\mathcal{E}}_{\text{eff}} \rangle$, where the “effective electric field” vector $\vec{\mathcal{E}}_{\text{eff}}$ is a state-dependent constant oriented in the molecular frame, for example along an internuclear axis. In a parity eigenstate, the electron spin has no average orientation in the molecular frame, and $\langle \vec{S} \cdot \vec{\mathcal{E}}_{\text{eff}} \rangle$ vanishes. The simplest way to obtain a non-vanishing eEDM interaction is to orient the molecule in the lab frame so that $\vec{\mathcal{E}}_{\text{eff}} \parallel \hat{Z}$, where \hat{Z} is the lab z -axis, and to simultaneously orient the electron spin along or against the same axis (e.g., via angular momentum selection rules on electronic transitions) so that $M_S \neq 0$. In this ideal case, $\langle \vec{S} \cdot \vec{\mathcal{E}}_{\text{eff}} \rangle$ will have maximal magnitude and $\langle H_{de} \rangle$ can be probed. More generally, as long as the parity of a molecular state is at least partially mixed, then $\langle \vec{S} \cdot \vec{\mathcal{E}}_{\text{eff}} \rangle \neq 0$ and the eEDM can be measured via $\langle H_{de} \rangle$. Heteronuclear diatomic molecules in ${}^2\Sigma$ electronic states have rotational states of both positive and negative parity, but they are generally spaced by tens of GHz and require electric fields on the order of tens of kV/cm to saturate the energy shifts associated with the eEDM. By contrast, the parity doublets generically found in polyatomic molecules can be fully mixed at fields at or below 1 kV/cm. Furthermore, in contrast to rotational states, the structure of parity doublets found in polyatomic molecules, for example K -doublets in symmetric top molecules or ℓ -doublets in vibrational bending modes of polyatomic molecules, enables the orientation of molecules to be spectroscopically reversed in a fixed external electric field. This feature can also be found in Λ - or Ω -doublets of diatomic molecules, and it has already been a valuable tool

for systematic error rejection in ThO and HfF⁺, such as the experiments described in ACME Collaboration (2018); Cairncross et al. (2017). The special feature of polyatomic molecules is that such parity doublets can be obtained irrespective of the electronic structure of the selected polyatomic species.

Another case where near-degenerate opposite-parity states are useful is in probing intrinsic parity-violating Standard Model (SM) effects such as the vector electron-axial nucleon electroweak current coupling and the nuclear anapole moment. The total parity-violating interaction in a given electronic state is characterized by the constant W_p . By determining the value of W_p in multiple nuclei of the same molecular species, the contribution of each SM effect could be independently determined. A sensitive method to probe W_p is Stark interference (see DeMille et al. (2008)), where an electric dipole transition drives a molecule between opposite-parity states separated by energy Δ . The population transfer contains an interference term between the driving electric field E_0 and the parity-violating interaction W (which is proportional to W_p but contains additional factors from the molecular state). By comparing measurements with opposite phases of the driving electric field, a measured quantity proportional to W/Δ can be obtained. Thus the experimental signal is enhanced when the states under consideration are brought to near-degeneracy. Whereas rotational states of diatomic molecules can be brought to near-degeneracy with Tesla-scale magnetic fields, Norrgard et al. (2019b) showed that in a large class of linear polyatomic molecules, degeneracy can be achieved with fields of 10 mT or less, dramatically reducing the experimental complexity of operating an experiment within the bore of a superconducting magnet. By measuring nuclear-spin-independent parity-violating effects in light molecules, where calculations of Standard Model effects are not prohibitively challenging, parity-violating interactions in the SM may be probed and, perhaps, distinguished from BSM effects.

A second feature of polyatomic molecules that can be exploited in precision measurements of BSM physics is the multiplicity of rotational and vibrational modes. Whereas diatomic molecules have one rotational mode and one vibrational mode, every polyatomic molecule contains at least three vibrational modes and up to three rotational modes. Thus accidental near-degeneracies between rovibronic states can be commonly found at low energies (e.g., below 1000 cm⁻¹), and are nearly guaranteed at higher rovibronic energies where the density of states increases. As described by Jansen et al. (2014), these near-degeneracies are useful for probing potential variation of the proton-to-electron mass ratio, $\mu \equiv m_p/m_e$, over time: as μ changes, each

rovibrational level shifts since rotational and vibrational energies depend directly on the masses of atomic nuclei according to $\delta E = \partial E / \partial \mu \times \delta \mu$. (Here, changes in physical quantities associated with changes in μ are indicated by the prepended symbol δ .) Pure rotational energies and anharmonic vibrational energies obey $\delta E = -E \times \delta \mu / \mu$, while pure harmonic vibrational energies obey $\delta E = -\frac{1}{2} E \times \delta \mu / \mu$. In each case, the *absolute* energy sensitivity δE to μ variation scales with the overall energy E . In cases of accidental near-degeneracies, it is possible to obtain $\omega \approx 0$ even when the absolute frequency sensitivity of a transition $\delta \omega \equiv \delta E_2 - \delta E_1$ does not vanish because E_1 and E_2 depend differently on μ . For example, rovibronic transitions between near-degenerate states can exploit the relatively large absolute frequency shifts of vibrational energy levels ($E \sim 10$ THz) while being amenable to the technical convenience of lower-frequency microwave sources ($\omega \sim 10$ GHz) where stable frequency references are readily available and certain systematic errors like Doppler shifts are suppressed. Transitions where $\delta \omega / \omega \gg 1$ have been used to set limits on μ variation in molecules including methanol, ammonia, and KRb (where a degeneracy between an excited vibrational state and a metastable electronic state was used by Kobayashi et al. (2019)). Laser-cooled polyatomic molecules possess convenient rovibronic near-degeneracies to sensitively probe μ variation in a platform offering ultracold temperatures, long trap lifetimes, and full quantum control. Kozyryev et al. (2021) identified a promising near-degeneracy in the energy levels of SrOH that could be used for such an experiment.

The third, and final, feature of polyatomic molecules that we note for precision measurements is chirality. Because chirality requires three distinct molecular axes, it can only be found in molecules with at least four atoms. Parity-violating effects in the Standard Model are predicted to result in energy splittings between chiral molecules at the level of \sim mHz to Hz in various species of experimental interest (Cournol et al. (2019)). In principle, even in the absence of parity violation, any chiral molecule could convert to its enantiomer via the tunneling of some set of nuclei through a vibrational energy barrier, resulting in a double-well-type energy structure and associated splitting ΔE_{\pm} between molecular eigenstates. In many molecules such as hydrogen peroxide (HOOH) or the chiral isotopologue of ammonia (NHDT), the tunneling splitting dominates parity-violating effects, $\Delta E_{\pm} \gg \Delta E_{\text{pv}}$, and the symmetry breaking between left- and right-handed molecules occurs only “*de facto*,” i.e. due to initial conditions described by Quack et al. (2022). Nevertheless, in this case it is possible to measure the

effect of parity-violating interactions, for example by observing an initial parity eigenstate acquire a non-zero amplitude of an opposite-parity eigenstate upon free evolution (Quack (1986)). The other limiting case is where the parity-violating energy shifts are large compared to the tunneling splitting, $\Delta E_{\text{pv}} \gg \Delta E_{\pm}$, so that the symmetry breaking between enantiomers is “*de lege*,” i.e. due to intrinsic dynamics of the molecular energies. In this case, the energies of two enantiomers can be directly spectroscopically measured (e.g., via high-sensitivity infrared absorption experiments) and compared. Most molecules with heavier constituents, including species of interest such as CHFClBr and S₂Cl₂, are expected to exhibit “*de lege*” parity violation due to the large reduced tunneling mass (Quack et al. (2008)). Chiral molecules are also sensitive to parity-violating cosmic fields associated with certain dark matter candidates, as pointed out by Gaul et al. (2020). Thus precise measurements of enantiomeric energy splittings can be a definitive probe of parity-violating weak interactions and beyond-Standard Model interactions in suitably chosen molecules. Laser-cooled polyatomic chiral molecules (for example CaOCHDT, a chiral analogue of CaOCH₃) could potentially enable measurements of these parity-violating effects for the first time due to the possibility of longer interaction times and full quantum control (Augenbraun et al. (2020a)).

1.3. Collisions and chemistry

Collisions of polyatomic molecules—both with atoms and other molecules—are of great scientific interest to a number of disciplines across physics and chemistry. A distinction is typically made between two different temperature regimes, namely “cold” collisions at temperatures of $\lesssim 1$ K, and the “ultra-cold” collision regime, defined by temperatures sufficiently low that only a single partial wave participates in the collision. The ultracold collision regime is sometimes defined informally as $\lesssim 1$ mK, though the actual temperature for collisions to only include a single partial wave can be much lower for heavier molecules. In addition, there are subtleties involved in defining the single-partial-wave regime for dipolar collisions where all partial waves may contribute even at low collisional energies, see Chomaz et al. (2023). Numerous techniques have been developed for studying collisions at cold temperatures, and cold collision dynamics for a number of molecules, including polyatomic species, have already been investigated. These experiments have typically relied on beam-based approaches, though a variety of different experimental techniques have been employed, including slowing techniques to

reduce collisional temperatures, e.g., Stark (van de Meerakker and Meijer (2009)), Zeeman (Plomp et al. (2020)), and “cryofuge” (Wu et al. (2017)) deceleration. Trapping of the molecular species—from slowed or buffer-gas-cooled (Hummon et al. (2011)) molecular beams—has allowed for increased molecular interaction times, and has led to novel studies of cold dipolar collisions. Stark deceleration followed by magnetic trapping has, for example, been used to study dipolar collisions between OH and ND₃ molecules in a magnetic trap (Sawyer et al. (2011)), and cryofuge deceleration has recently been combined with electric trapping to study dipolar collisions between CH₃F molecules (Koller et al. (2022)). Collision studies at cold temperatures play a particularly important role in astrophysics, specifically for studying the astrochemical reactions that result in the molecular compositions observed in interstellar environments, see Herbst and van Dishoeck (2009). For more extensive reviews of cold collision studies, we refer interested readers to the articles by Toscano et al. (2020); Heazlewood and Softley (2021). The ultracold regime remains largely unexplored due to the difficulty in producing ultracold molecules, especially for polyatomic molecules. The extension of direct laser cooling techniques to polyatomic molecules could potentially provide a path towards realizing collision studies at ultracold temperatures. Below we provide a few key highlights of some of the novel collision dynamics and chemistry that are expected to arise at ultracold temperatures and which could potentially be explored with ultracold polyatomic molecules.

In the ultracold regime, the de Broglie wavelength of the colliding molecules exceeds their classical size, requiring a quantum-mechanical description of the collision process. Molecular interactions in this regime are therefore characterized by quantum statistics and quantum threshold behavior, and a host of different quantum collision and chemistry phenomena are expected to arise as a result (Carr et al. (2009)). For example, due to the delocalized wavelike nature of molecules in this regime, long-range dipolar interactions are expected to be essential for determining collision rates between polar molecules at ultracold temperatures. This bears important implications for chemical reaction rates. While reaction rates are “classically” expected to increase with temperature, many chemical reactions instead proceed at much accelerated rates in the limit of absolute zero (Richter et al. (2015)). Some of these quantum effects are already starting to be explored with ultracold diatomic molecules. Seminal experiments with ultracold KRb molecules created by photoassociation of laser-cooled atoms have, for example, probed long-range interactions in ultracold KRb–KRb (Ospelkaus et al. (2010); Ni

et al. (2010); Hu et al. (2021)) and KRb–Rb (Nichols et al. (2022)) collisions. Ultracold collision experiments have since also been performed with a range of other alkali species (Ye et al. (2018); Gregory et al. (2021); Bause et al. (2021)). Similar experiments could be imagined with polyatomic molecules, which would grant still broader access to new quantum collision and chemistry phenomena. As an example, it has been proposed that collective many-body effects in a Bose degenerate gas of triatomic molecules may lead to a “Bose-stimulated” photodissociative process in which branching to either of two decay channels, $ABC \rightarrow AB + C$ or $ABC \rightarrow A + BC$, can be significantly amplified (Moore and Vardi (2002)). Ultracold collision experiments with polyatomic molecules would also, along with experiments with diatomic molecules, provide important experimental benchmarks for new scattering theories and quantum chemistry at ultracold temperatures.

An essential implication of the quantum nature of the ultracold regime is that both elastic and inelastic collision rates are expected to have a strong dependence on the exact molecular quantum states (Carr et al. (2009)). External fields, too, can have strong and potentially very different effects on elastic and inelastic rates, for example by changing the relative orientation of two colliding molecules (Tscherbul and Krems (2006); Tscherbul et al. (2009); Brouard et al. (2014); Tscherbul and Krems (2015)). This provides the capability for separately “tuning” elastic as well as inelastic collision rates, which, as we discuss below, may be important for the realization of degenerate gases of polyatomic molecules. In the context of chemical reactions, this provides a path to controlled chemistry at ultracold temperatures in which chemical reactions can be very precisely studied and, possibly, engineered (Krems (2008); Balakrishnan (2016); Bohn et al. (2017)). These points are especially pertinent to polyatomic molecules, whose many internal degrees of freedom may provide additional tools for external field control, and, in particular, allow for easy orientation of the molecules. Recent experiments with CaF molecules have demonstrated that direct laser cooling in combination with optical trapping is a feasible approach for realizing the level of control required to characterize the quantum state and field dependencies of collision rates (Cheuk et al. (2020); Anderegg et al. (2021)). Optical trapping of ultracold polyatomic molecules additionally opens the door to probing collisional dynamics in confined geometries in which collision dynamics take on qualitatively distinct behavior compared to that of an unconfined gas (Carr et al. (2009)).

Finally, understanding the collisional processes of polyatomic molecules at

ultracold temperatures is likely to have a fundamental impact on the potential realization of Bose or Fermi degenerate polyatomic gases. In particular, the experiments with alkali molecules mentioned earlier have demonstrated that, in the ultracold regime, even molecules that are not chemically reactive can exhibit large inelastic collision losses due to forming long-lived complexes in so-called “sticky collisions” (Bause et al. (2022)). This prevents efficient evaporative cooling, which is the typical approach used for creating degenerate atomic gases (Pethick and Smith (2002)). The tunability of the reaction rates mentioned above is in this regard important and can enhance the elastic-to-inelastic collision ratio by several orders of magnitude using external fields. Several “shielding” techniques have already been demonstrated for diatomic molecules (Matsuda et al. (2020); Valtolina et al. (2020); Anderegg et al. (2021); Li et al. (2021)). Recently, Schindewolf et al. (2022) showed that quantum degeneracy could be reached for diatomic species using this shielding technique. Similar methods are likely required for the realization of degenerate gases of polyatomic molecules. A scheme for field-induced shielding in collisions between CaOH molecules has been proposed by Augustovičová and Bohn (2019). Alternative prospects for collisional cooling using sympathetic molecule-atom collisions have also recently been explored by Wójcik et al. (2019) for complex polyatomic molecules such as benzene and azulene.

1.4. Experimental approaches besides direct laser cooling

Achieving any of the diverse goals summarized above requires exquisite control over the molecules to be probed. In order to reap the benefits of polyatomic molecules, we must cool them to cold ($\lesssim 4$ K) or ultracold ($\lesssim 1$ mK) temperatures. This cooling is required to “compress” the molecular population into a small number of quantum states and to slow their thermal velocities to tens of meters per second; the former increases an experiment’s signal-to-noise ratio and the latter enables long interrogation times to improve achievable precision and control. Because polyatomic molecules contain many internal degrees of freedom, cooling them can be a very difficult task. Many research groups have tackled this problem, and we review some relevant methods here. A variety of approaches have been explored to realize this control.

A very successful method of producing ultracold diatomic molecules involves laser cooling atoms and then binding these pre-cooled atoms together (using photoassociation, magnetoassociation, etc.); see Ni et al. (2008); Molony

et al. (2014); Park et al. (2015); Guo et al. (2016); Rvachov et al. (2017); Cairncross et al. (2021). While this has produced a number of ultracold diatomic molecules in single quantum states, including degenerate gases, it is not clear it can be generalized to produce *polyatomic* molecules. However, very recent work by Yang et al. (2022) has shown some evidence for production of triatomic molecules in a mixture of $^{23}\text{Na}^{40}\text{K}$ and ^{40}K . It is also unclear whether this exciting result can be extended to other species (or larger ones), especially those containing difficult-to-cool atomic species such as O, C, and/or H.

Optoelectrical Sisyphus cooling, described by Zeppenfeld et al. (2012); Prehn et al. (2016), uses state-dependent energy shifts and repeated microwave transitions/optical pumping steps to cool molecules as they move through an electric trap. Energy is removed by ensuring molecules move away from the trap’s center along a “steep” potential and return to the center along a “shallow” potential. This technique relies on the linear Stark shifts that can be achieved in symmetric or asymmetric top molecules. It has been used to produce trapped samples of CH_3F and H_2CO at $\sim\text{mK}$ temperatures and could potentially be used to observe molecule-molecule collisions in the trap. To date, the molecules that have been cooled using this method do not offer convenient optical transitions, so vibrational transitions with relatively long lifetimes have been used instead. The method could likely be adapted to make use of the optical transitions offered by some of the molecules discussed in this review, speeding up the cooling rates considerably.

1.5. Direct laser cooling

Direct laser cooling is a promising approach because it may be widely applicable to diverse structures of molecules and brings with it the possibility of high-efficiency quantum state preparation and readout using optical photons. The direct laser cooling approach is the focus of this review paper. Figure 2 presents a schematic overview of an idealized molecular laser cooling experiment. Because many of these techniques were honed in the context of diatomic molecules, the interested reader should refer to the reviews by Hutzler et al. (2012); Tarbutt (2018); McCarron (2018); Fitch and Tarbutt (2021).

1.5.1. Forming closed cycling transitions

The photon scattering process is one in which molecules go through a series of photon absorption and spontaneous emission cycles that can be

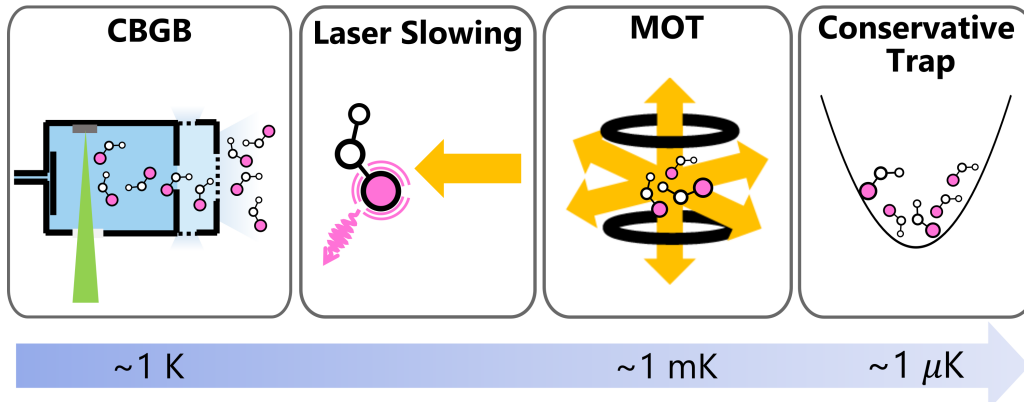


Figure 2: Overview of an idealized molecular laser cooling sequence. Molecules are produced in a cryogenic buffer-gas beam (CBGB) source, decelerated, trapped in a magneto-optical trap, and then transferred into a conservative trap for a particular science goal. Reproduced from Augenbraun (2020).

described as a Bernoulli sequence. Suppose we have applied laser repumpers such that a molecule has a probability p to decay to a state that is *not* addressed by laser light. The probability P_n for a molecule to experience n absorption-emission cycles is given by $P_n = (1 - p)^n$. The average number of photons scattered by molecules is $\bar{n} = \frac{1}{1-p}$. We often refer to this as the “photon budget,” and it sets the (exponential) scale for how many photons can be scattered before significant fractions of the population are lost. For example, if laser slowing requires 10,000 photon scattering events and we would like 90% of the initial population to remain after slowing, we require $p \approx 10^{-5}$. Clearly, understanding branching ratios as small as 1 part in 10^5 can be crucial to achieve efficient laser cooling.

A typical laser cooling experiment requires scattering many thousands of optical photons. To repeatedly scatter this number of photons without the molecules accumulating in states that do not couple to applied laser light (“dark states”), it is necessary to form a “closed cycling transition.” In a closed cycle, a molecule that is driven to an electronically excited state is guaranteed to decay back to the same state that it started in. In reality, no optical transition is fully closed and the molecule has a finite probability to decay to a state that is different from the initial state. Such a molecule needs to be “repumped” into the cycling transition. The higher the probability of decaying to other states, the more repumping transitions must be addressed.

This quickly becomes an experimental limitation, as each decay typically requires a separate laser to be added to the experiment. This points to the importance of selecting atoms and molecules whose branching ratios are favorable. The general guidelines for selecting molecules and transitions for laser cooling were first pointed out by Di Rosa (2004), who highlighted the need for (1) strong transitions, (2) highly diagonal vibrational branching, and (3) no intermediate (i.e., metastable electronic) states between the two states used for optical cycling.

The electronic transitions driven in laser cooling are typically electric dipole (E1) transitions. Since the dipole operator is odd under parity transformations, the parity of the excited and ground states must be opposite. As a result, selection rules for changes to the total angular momentum J are $\Delta J = 0, \pm 1$ (with $J' = 0$ to $J = 0$ forbidden). We can use these selection rules to our advantage by cycling from $J = 1$ to $J' = 0$, as originally recognized by Stuhl et al. (2008), which must decay back to $J = 1$, leading to rotational closure.

One consequence of driving from $J = 1$ to $J' = 0$ to attain rotational closure is the presence of dark states. This is a generic problem in the laser cooling of molecules, where the excited state often has the same number of sublevels (or fewer) than the ground state. This means that for any fixed laser polarization, dark states exist. Molecules that collect in these dark states can be returned to bright states in a number of different ways, most commonly using DC magnetic fields, polarization modulation, or microwave pulses (Berkeland and Boshier (2002)).

1.5.2. *Effects of multilevel systems on laser cooling*

For a system that can decay to multiple states, the prototypical two-level scattering rate equation is modified. For resonant light where all the transitions are driven with equal intensity, Williams et al. (2017) show that the maximum achievable scattering rate is modified to

$$R_{\text{scat}}^{\text{max}} = \frac{n_e}{n_g + n_e} \Gamma \quad (5)$$

where n_e is the number of excited states and n_g is the number of ground states. As an example, in CaF there are 12 Zeeman sublevels in the ground state, 4 in the excited state, and 12 in the $v=1$ ground state. Hence $n_e = 4$ and $n_g = 24$. If lasers are tuned to drive both $\tilde{X}(v=0)$ and $\tilde{X}(v=1)$ to the \tilde{A} state, the achievable scattering rate will reduce by a factor of about

4. This decrease in the scattering rate would significantly hinder the laser cooling of a molecule. A commonly employed technique to circumvent this limitation is to repump the molecules through a different excited state than the one used for the “main” transition. This approach is also crucial for polyatomic molecules as more states must be repumped in a laser cooling scheme.

With closed cycling transitions established, diatomic molecules have been laser slowed and cooled (Shuman et al. (2009, 2010); Barry et al. (2012); Zhelyazkova et al. (2014); Hemmerling et al. (2016); Truppe et al. (2017c); Lim et al. (2018)) and trapped in red-detuned magneto-optical traps (Hummon et al. (2013); Barry et al. (2014); McCarron et al. (2015); Norrgard et al. (2016); Steinecker et al. (2016); Chae et al. (2017); Truppe et al. (2017a); Anderegg et al. (2017); Williams et al. (2017); Collopy et al. (2018)) and blue-detuned magneto-optical traps (Bureau et al. (2022)), cooled to sub-Doppler temperatures (Truppe et al. (2017a); Cheuk et al. (2018); Caldwell et al. (2019); Ding et al. (2020)), and loaded into magnetic (Williams et al. (2018); McCarron et al. (2018)) and optical traps (Anderegg et al. (2018); Langin et al. (2021); Wu et al. (2021); Lu et al. (2022)) and tweezers (Anderegg et al. (2019); Lu et al. (2022); Holland et al. (2022); Bao et al. (2022)).

2. Molecular structure for laser cooling experiments

Compared to diatomic molecules, polyatomic molecules can have significantly more complex internal structures. Here, we review the structure of polyatomic molecules as is relevant to laser cooling and trapping experiments. We generally work within the Born-Oppenheimer approximation, separating the electronic, vibrational and rotational motions, but molecular physics beyond the Born-Oppenheimer approximation is also introduced as necessary to understand its impact on laser cooling and trapping experiments.

2.1. *Electronic structure*

For the molecules of interest to laser cooling experiments, the largest relevant energy scale corresponds to excitation of a valence electron that is used for optical cycling (changing the principle quantum number). Typical electronic excitation energies for several classes of molecules are in the visible region of the electromagnetic spectrum (400–800 nm). Understanding the origin and nature of these electronic states is needed to predict which molecules are favorable for laser cooling experiments.

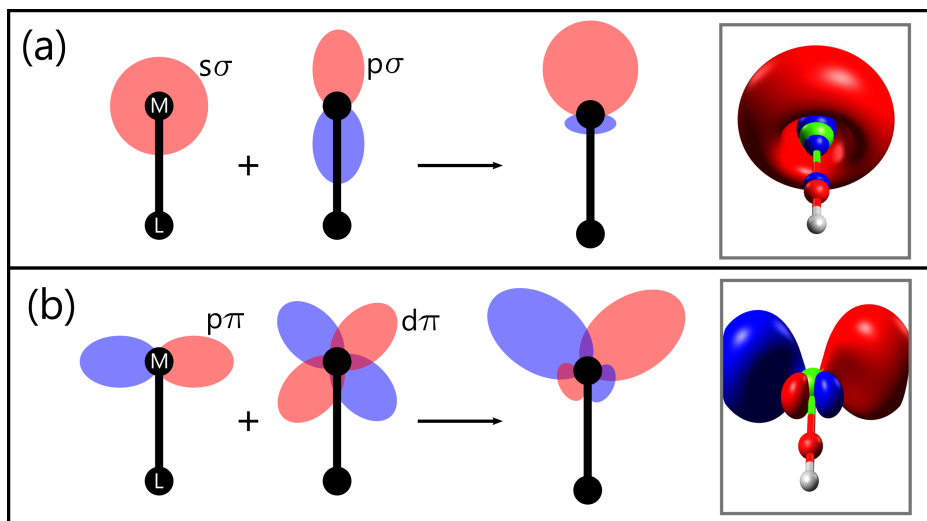


Figure 3: Illustration of orbital mixing reducing the interaction between valence electron and negatively charged ligand. (a) Mixing of $s\sigma$ and $p\sigma$ orbitals to generate the $\tilde{X}^2\Sigma^+$ state. (b) Mixing of $p\pi$ and $d\pi$ orbitals to generate the $\tilde{a}^2\Pi$ state. In both cases, the rightmost image shows quantum chemical calculations of the electronic distribution confirming this simple orbital mixing picture, using CaOH as an example. Reproduced from Augendrahn (2020).

We will focus, for the moment, on molecules in which an alkaline-earth atom, M , bonds to some electronegative ligand, L (e.g., F, OH, OCH_3 , SH, etc.), because these molecules are expected to have the structure desired for laser cooling (Kozyryev et al. (2016a); Augendrahn et al. (2020a); Isaev et al. (2017); Ivanov et al. (2019); Isaev and Berger (2016)). As explained by Ellis (2001), the alkaline-earth atoms tend to form ionically-bonded molecules due to their low ionization energies. Whether M transfers one or both of its valence electrons to the bonding partner depends on whether L can form singly or doubly charged anions. For the examples of L listed above, singly-charged anions form, so M retains one electron even after forming a bond.

The relevant structural details can largely be extracted from a simple picture involving just three ingredients: a positively charged metal ion, M^{2+} , an optically active “valence” electron near the metal, and a negatively charged ligand, L^- . The presence of an unpaired electron leads to low-lying, metal-centered electronic excitations that can be used for optical cycling and laser cooling. One would naively expect the unpaired electron to have dominant s orbital character in the electronic ground state. More detailed ligand-field

theory calculations (e.g., those by Rice et al. (1985); Allouche et al. (1993)) show that this is largely true, but also that the interaction with the negatively charged ligand deforms the valence electron to minimize electron-electron repulsion (Ellis (2001)). For example, in the ground state this deformation is realized via mixing of $s\sigma$ and $p\sigma$ orbitals on M , a process shown schematically in Fig. 3. The orbital notation will be described more in the next paragraph. It has been found that in CaF, the ground electronic state ($\tilde{X}^2\Sigma^+$) arises from a mixture of approximately 80% of the $4s\sigma$ orbital and about 20% of the $4p\sigma$ orbital, while the lowest electronic state $\tilde{A}^2\Pi$ is made up of about 70% $4p\pi$ and 25% $3d\pi$ character (Rice et al. (1985)). Similar values are found for Ba-containing monohalides (Allouche et al. (1993)) and larger monomethoxide species (Augenbraun et al. (2021b)).

An energy level diagram of the low-lying electronic states can be constructed from these ideas (Dick (2007); Ellis (2001)). The basic idea is to consider the Hamiltonian $\mathbf{H} = \mathbf{H}_{M^+} + \mathbf{H}_{L^-} + \mathbf{H}'$, where \mathbf{H}_{M^+} and \mathbf{H}_{L^-} describe the energy levels of the free ions and \mathbf{H}' describes the interaction between the optically active valence electron and the ligand (Rice et al. (1985); Allouche et al. (1993)). When the ligand is treated as a point charge perturbation, it has three qualitative effects on the spectrum (Dick (2007)):

1. It can shift the atomic ion's energy levels.
2. It can split the m_l components of each atomic nl state. We can think of this as arising from strong electrostatic forces along the bond, producing a Stark effect that resolves m_l components along the bond axis. As is typical for the Stark effect, we do not resolve $+m_l$ and $-m_l$ components, and therefore label states as $\lambda = |m_l| = 0, 1, 2, \dots$. States with $\lambda = 0, 1, 2, \dots$ are denoted by $\sigma, \pi, \delta, \dots$, respectively.¹
3. It can mix orbitals obeying the selection rule $\Delta m_l = 0$. This may seem innocuous at first, but is actually quite important because this effect means each molecular orbital is a linear combination of atomic ion orbitals. Not only does this greatly affect the ordering of molecular states, it also means the molecular parameters of a given state will appear as an “average” of the atomic states that it comprises.

Figure 4(i-iii) shows the development of the energy levels as these effects are sequentially added. This diagram also shows how we name electronic

¹We are using lower-case letters here because we are describing the single valence electron. Below, we will use capital letters to describe the total electronic state.

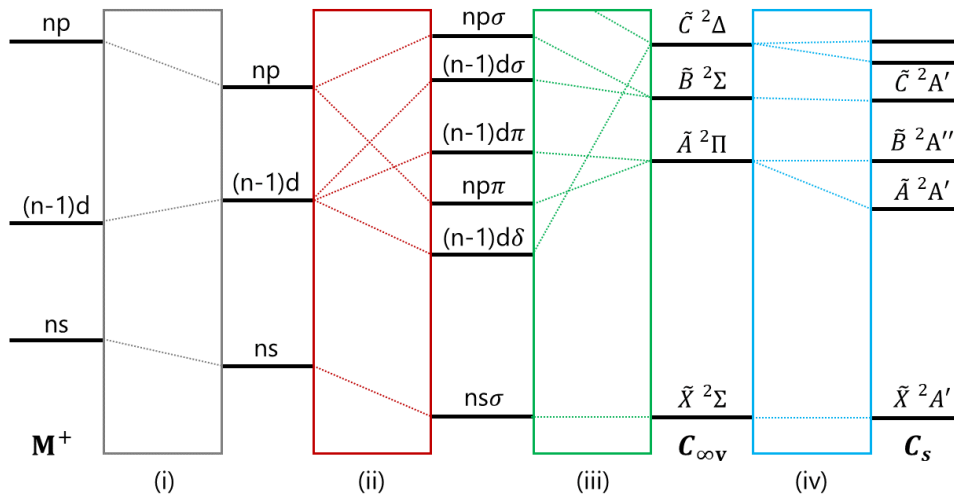


Figure 4: Correlation of low-lying electronic states from atomic ion (M^+) to linear ($C_{\infty v}$) and nonlinear (C_s) molecules. The labeled regions correspond to the following qualitative processes: (i) Shifting of atomic ion levels, (ii) Splitting of atomic m_l components, (iii) Mixing of energy levels with the same m_l , (iv) Cylindrical symmetry breaking due to a nonaxial ligand. Modeled after diagrams in Ellis (2001); Dick (2007).

states. For a linear molecule ($C_{\infty v}$ point group symmetry), we label electronic states by letters: \tilde{X} for the ground state, $\tilde{A}, \tilde{B}, \dots$ for the first, second, ..., electronically excited states, respectively. Note that (for historical reasons) the alphabetical ordering usually, but does not always, match the energetic ordering of energy levels.² In addition, because in most cases the electronic states can be identified by their electronic orbital angular momentum (Λ) and spin multiplicity ($2S + 1$), we use the labeling scheme $^{2S+1}\Lambda$. For states with definite projection of spin onto the molecular axis, we can also add a subscript (Ω) to specify the *total* angular momentum projection on the internuclear axis (see also discussion of angular momentum coupling below).

This description has so far assumed the ligand can be treated as a point charge, meaning the M^+L^- system has cylindrical symmetry about the $M-L$ axis. Such symmetry is exact only for linear molecules (diatomic or polyatomic). If ML is a nonlinear molecule but still retains some axial symmetry (e.g., MOCH_3) then the picture is largely unchanged except that there will be no formal distinction between the symmetries of degenerate electronic states (e.g., for C_{3v} symmetry, Π, Δ, \dots states are all classified as having E symmetry). If the ligand breaks the axial symmetry (e.g., MSH), then the orbital degeneracy described in steps (2) and (3) just above is no longer guaranteed, and degenerate electronic states can split. For example, a Π electronic state of CaOH will correlate to states of A' and A'' symmetry for CaSH , as shown in Fig. 4(iv). Figure 5 shows the clear role that asymmetry of the ligand has on slightly deforming the valence electron that remains localized on the metal optical cycling center. Despite the asymmetry, in all cases plotted the optical cycling properties are preserved.

2.2. Vibrational structure

During laser cooling of a polyatomic molecule, a number of vibrational states may be excited due to the lack of a perfectly closed cycling transition. These states are generally close to the bottom of the potential energy surface,

²Electronic states with multiplicity different from than the ground state are labeled by lower case letters $\tilde{a}, \tilde{b}, \dots$, usually in order of increasing energy.

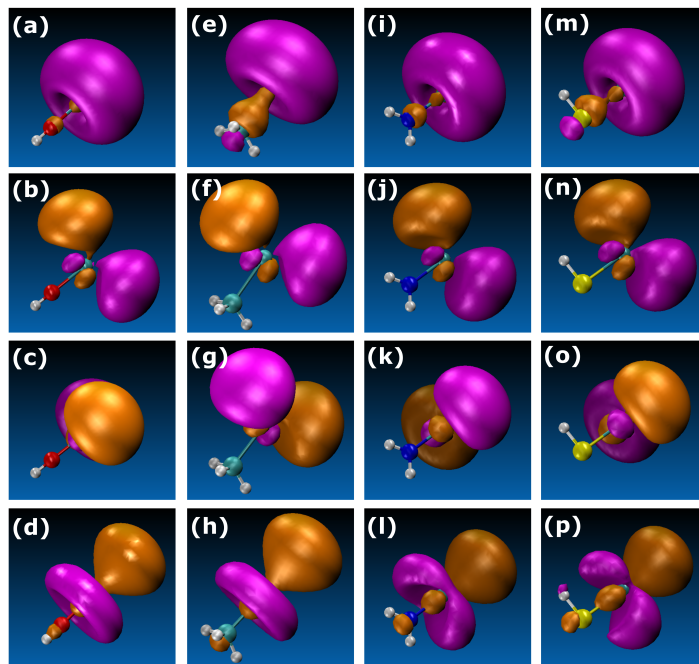


Figure 5: Molecular orbitals of the lowest several electronic states for Ca-containing molecules as symmetry is systematically lowered from $C_{\infty v}$ (CaOH) to C_{3v} (CaCH₃) to C_{2v} (CaNH₂) to C_s (CaSH). The distortion of the valence electron as a function of ligand asymmetry is clearly visible. Panels (a-d) show, respectively, the HOMO, LUMO, LUMO+1, and LUMO+2 for CaOH; (e-h) show these for CaCH₃; (i-l) for CaNH₂; and (m-p) for CaSH. Figure reproduced from Augenbraun et al. (2020a).

which can be Taylor expanded as

$$\begin{aligned}
V = V_0 &+ \frac{1}{2} \sum_{i=1}^{3N} \sum_{j=1}^{3N} \left(\frac{\partial^2 V}{\partial q_i \partial q_j} \right)_{q_i=q_j=0} q_i q_j \\
&+ \frac{1}{3!} \sum_i \sum_j \sum_k \left(\frac{\partial^3 V}{\partial q_i \partial q_j \partial q_k} \right)_0 q_i q_j q_k + \dots
\end{aligned} \tag{6}$$

Here we express the potential energy as a function of the $3N$ nuclear coordinates q_i , which describe the 3-dimensional motion of all N nuclei. To a good approximation, the low-lying vibrational states in this potential may be described within the harmonic approximation, in which case the vibrational Hamiltonian is (Demtröder (2003); Bernath (2017))

$$H_v = \sum_{i=1}^{3N-6(5)} \left(-\frac{\hbar^2}{2} \frac{\partial^2}{\partial Q_i^2} + \frac{1}{2} \lambda_i Q_i^2 \right) \tag{7}$$

where Q_i is a mass-weighted normal coordinate describing the i th normal mode of vibration and $\sqrt{\lambda_i}$ is the vibrational frequency of the mode. Notice that for a polyatomic molecule there are $3N - 6$ (or $3N - 5$ for a linear molecule) normal vibrational coordinates; the other $6(5)$ normal coordinates are taken up by the 3 translational and $3(2)$ rotational degrees of freedom of the molecule.

Vibrations along each of the normal coordinates are fully separable, so the vibrational wavefunction can be expressed as

$$\psi(Q_1, Q_2, \dots, Q_{3N-6}) = \prod_{i=1}^{3N-6} \psi_{v_i}(Q_i) \tag{8}$$

where $\psi_{v_i}(Q_i)$ is the simple harmonic oscillator wavefunction (Bernath (2017)) with vibrational quantum number v_i . The energy of the state in the harmonic approximation is

$$E_v = \sum_{i=1}^{3N-6} \hbar \omega_i \left(v_i + \frac{1}{2} \right) \tag{9}$$

Reintroducing the anharmonic terms in the potential energy surface has two effects. The first is to couple the harmonic oscillator eigenstates from Eq. 8, as discussed below. The second effect is to alter the state energies,

which can be expressed as (Demtröder (2003); Bernath (2017); Herzberg (1966))

$$G(v_1, v_2, \dots, v_p) = \sum_i \omega_i \left(v_i + \frac{d_i}{2} \right) + \sum_{j \leq i} x_{ij} \left(v_i + \frac{d_i}{2} \right) \left(v_j + \frac{d_j}{2} \right) + \sum_{j \leq i} g_{ij} \ell_i \ell_j + \dots \quad (10)$$

where ω_i is the frequency of the i th mode, d_i is its degeneracy, x_{ij} and g_{ij} are anharmonicity constants, and ℓ is a quantum number describing the vibrational angular momentum along the molecular axis.

2.2.1. Vibrational state notation

Linear triatomic molecules. Linear triatomic molecules, including the alkaline earth monohydroxides CaOH, SrOH, and YbOH, have 4 normal vibrational modes, one of which (the bending mode) is doubly degenerate. The vibrational state is labeled by $(v_1 v_2^\ell v_3)$, where v_1 is the quantum number for the symmetric stretching mode, v_2 describes the bending mode, v_3 describes the antisymmetric stretching mode, and ℓ gives the vibrational angular momentum in the bending mode. Note that this angular momentum arises because linear combinations of the degenerate bending vibrations along two perpendicular (linear) axes can be formed which have elliptical trajectories. This can be thought of as producing a nuclear orbital angular momentum about the molecular axis. Doubly degenerate bending modes such as this one are formally described by the 2D harmonic oscillator, and ℓ can take the values $v_2, v_2 - 2, \dots, -v_2 + 2, -v_2$ (see Bernath (2017)).

Larger polyatomic molecules. For larger molecules, labeling vibrational states as (v_1, v_2, \dots, v_N) becomes unwieldy. Instead, we use the notation i_{v_i} , where i labels the vibrational mode and v_i is the vibrational quantum number for that mode. Only modes with $v_i \neq 0$ are labeled, and i is enumerated from 1 to n , where n is the total number of modes. Typically, the modes are ordered first by the symmetry of the vibrational mode and then in order of decreasing energy, as described in Herzberg (1966). For example, in the symmetric top molecule CaOCH₃, the vibrational state 4_1 corresponds to one excitation of the 4th vibrational mode (Ca–O stretch), while $3_1 4_2$ corresponds to 2 excitations of the Ca–O stretch mode and one excitation of the O–C stretch mode (3rd vibrational mode). In this notation, unspecified vibrational modes are assumed to have $v_i = 0$.

2.2.2. Anharmonic coupling

As mentioned above, one effect of the anharmonic terms in the potential energy surface (Eq. 6) is to mix the harmonic oscillator wavefunctions, such that the eigenstates of the vibrational Hamiltonian are admixtures of different harmonic oscillator basis states. This effect is most prominent for vibrational states of the same symmetry that are nearby in energy, and is often referred to as *Fermi resonance*. The Fermi resonance interaction is described in detail in Hougen (1962).

One example of Fermi resonance occurs in CaOH, whose bending mode frequency is approximately half the stretching mode frequency. This means that, for example, the (100) and (02⁰0) states are nearly degenerate and strongly mixed by a cubic term in the potential energy surface, $V_{122} = k_{122}q_1q_2^2$, which mixes states with $|\Delta v_1| = 1$ and $|\Delta v_2| = 2$. Here k_{122} is an anharmonic force constant. One practical implication of this interaction is that excited electronic states that would decay to $\tilde{X}(100)$ can also decay to $\tilde{X}(02^{00})$ at an enhanced rate; this is important for understanding vibrational branching ratios in polyatomic molecules (see Sec. 2.4.2). In this example, (100) mixes with (02⁰0) but not (02²0) because states with different ℓ have different symmetry. For example, in a Σ electronic state, $\ell = 0$ vibrational levels have Σ symmetry, $\ell = 1$ vibrational levels have Π symmetry, and so on. For a more detailed discussion of symmetry in polyatomic molecules, see Bunker and Jensen (2006).

2.3. Rotational structure

The rotational structure of molecules can be described, to leading order, by a rigid rotor model. The Hamiltonian is $H_{\text{rot}} = \frac{R_a^2}{2I_a} + \frac{R_b^2}{2I_b} + \frac{R_c^2}{2I_c}$, where a, b, c denote the three principal axes in the molecular body-fixed frame, $I_a \leq I_b \leq I_c$ are their corresponding moments of inertia, and R_a, R_b, R_c are the corresponding projections of the molecule's rotational angular momentum. It is useful to introduce the molecular constants $A = (2I_a)^{-1}$, $B = (2I_b)^{-1}$, and $C = (2I_c)^{-1}$. The energy level structure resulting from this Hamiltonian depends on the relative values of I_a , I_b , and I_c . We describe each case in turn, initially neglecting the effects of electronic, nuclear, and vibrational angular momentum. In this scenario, the quantum number $N = J - S$ is equivalent to the rigid-body rotational angular momentum R . We will denote the rotational angular momentum by N to make the notation compatible with the more general case treated later.

2.3.1. Linear molecules

A linear molecule has $I_a = 0$ and $I_b = I_c$ so that $B = C$. All diatomic molecules, and a small but important class of polyatomic molecules including alkaline-earth hydroxides like CaOH and SrOH, are linear. In the limit that $I_a \rightarrow 0$, any angular momentum about the a -axis requires infinite energy, so we take $N_a = 0$. Then $H_{\text{rot}} = B(N_b^2 + N_c^2) = BN^2$. The energy levels of this Hamiltonian form a quadratic ladder with eigenvalues $E_N = BN(N + 1)$. Each N manifold contains $2N + 1$ degenerate states, distinguished by the quantum number $M \equiv N_Z$, the projection of N on the lab-fixed Z -axis.

2.3.2. Spherical top molecules

In the special case that $I_a = I_b = I_c$, so that $A = B = C$, the Hamiltonian also reduces to the form $H_{\text{rot}} = BN^2$, again with eigenvalues $E_N = BN(N + 1)$. In this case, however, the additional structure leads to a set of $(2N + 1)^2$ degenerate states, distinguished by independent quantum numbers M and $K \equiv N_a$. Spherical top molecules include species such as CH₄ (methane), SF₆ (sulfur hexafluoride), and C₆₀ (buckminsterfullerene), but to our knowledge no laser-coolable spherical top molecules have been proposed to date and we do not consider them further here.

2.3.3. Symmetric top molecules

A molecule with exactly two equal moments of inertia is classified as a symmetric top. This case is further subdivided into the prolate (“cigar-shaped”) symmetric top, where $I_a < I_b = I_c$, and the oblate (“pancake-shaped”) symmetric top, where $I_a = I_b < I_c$. We explicitly consider the prolate case first; in the oblate case, one must only substitute $a \rightarrow c$ and $A \rightarrow C$ in all formulas. Then the Hamiltonian is $H_{\text{rot}} = BN^2 + (A - B)K^2$, where as before $K \equiv N_a$. The energy levels are $E_{N,K} = BN(N + 1) + (A - B)K^2$, with the restriction that $K \leq N$. There are $2N + 1$ degenerate states with energy $E_{N,0}$, distinguished by M . When $K \neq 0$, there are $2(2N + 1)$ degenerate states distinguished by both M and the sign of $K = \pm|K|$. Examples of prolate symmetric top molecules include CH₃F (methyl fluoride) and the laser-coolable species CaOCH₃ (calcium monomethoxide). Examples of oblate molecules include C₆H₆ (benzene) and NH₃ (ammonia); to date, no oblate symmetric top molecules have been proposed for laser cooling. For molecules where $A \gg B$, typical of known laser-coolable molecules, there is a quadratic ladder of widely separated “ K -stacks,” each of which contains a quadratic ladder of more finely separated N states.

2.3.4. Asymmetric top molecules

In an asymmetric top molecule, all moments of inertia are unequal. The resulting energy level structure is quite complex, and no projection of N on the molecule-frame axes is a good quantum number. For each value of N , there are $2N + 1$ non-degenerate states. The degree of asymmetry can be characterized by the Ray's asymmetry parameter, $\kappa = \frac{2B-A-C}{A-C}$. In the prolate (oblate) symmetric top limit, $B = C(A)$, we obtain $\kappa = 1(-1)$. In the maximally asymmetric case, $B = (A + C)/2$, we obtain $\kappa = 0$. Eigenstates can be designated by labels $N_{K_a K_c}$, where K_a and K_c are the projections of N on the a -axis and c -axis in the limit that a molecule is deformed to the prolate and oblate symmetric top limits, respectively. In the general case, $-1 < \kappa < 1$, neither K_a nor K_c are rigorously good quantum numbers.

Laser-coolable asymmetric top molecules proposed in the literature to date (for example, CaSH, CaOCHDT, and SrOC₆H₅) are prolate ($\kappa < 0$), though there is no apparent reason that oblate molecules ($\kappa > 0$) are necessarily inconsistent with laser cooling. An example of an oblate asymmetric top molecule is C₄H₄N₂ (pyrimidine). In the case of an asymmetric top molecule near the prolate symmetric top limit, $\kappa \approx -1$, the energy level structure closely resembles that of a prolate symmetric top. A similar situation holds for asymmetric top molecules near the oblate limit.

2.3.5. Dependence on spin and electronic angular momenta

The ground states of proposed laser-coolable polyatomic molecules generally have vanishing electronic angular momentum, and can be described in a Hund's case (b) basis where N is a good quantum number. Corrections to the rotational structure described above occur due to electron spin, nuclear spin, and vibrational angular momentum (for example in the bending vibrational mode of a linear triatomic molecule). The last of these shifts the overall energy of the ladder of eigenstates but does not otherwise change the rotational energy progression.

Coupling of the electron spin and molecular rotation is generally more complicated. The spin-rotation Hamiltonian takes the general form

$$H_{\text{SR}} = \frac{1}{2} \sum_{\alpha, \beta} \epsilon_{\alpha\beta} (N_\alpha S_\beta + S_\beta N_\alpha), \quad (11)$$

where α, β takes values a, b, c and ϵ is a symmetric tensor described in, e.g., Hirota (1985). In a linear molecule, only the components $\epsilon_{bb} = \epsilon_{cc} \equiv \gamma$ take

nonzero values and the simpler form

$$H_{\text{SR}} = \gamma \mathbf{N} \cdot \mathbf{S} \quad (12)$$

is obtained. For linear molecules with $S = 1/2$, this term mixes adjacent N levels, and both N and S cease to be good quantum numbers, though $\vec{J} = \vec{N} + \vec{S}$ is preserved. When $\gamma \ll B$, as is typical of the alkaline-earth pseudohalides, the effect is to split N into a pair of states with $J = N \pm 1/2$.

The situation is more complicated for nonlinear molecules. In a symmetric top molecule, the spin-rotation Hamiltonian (neglecting contributions that can mix different values of Λ in a 2E state) reduces to

$$H_{\text{SR}} = \epsilon_{aa} N_a S_a + \frac{1}{4}(\epsilon_{aa} + \epsilon_{bb})(N_+ S_- + N_- S_+), \quad (13)$$

assuming the prolate case (see Hougen (1980)). The asymmetric top case is generically much more complicated, and spin-rotation interactions can mix states that differ in N by up to 1, and differ in K by up to 2 (Hirota (1985)). In alkaline-earth pseudohalides, the ground-state spin-rotation splittings are typically no larger than ~ 100 MHz at low N , and increase with larger N . In most laser-coolable molecules used so far, the size of the spin-rotation constant is dominated by a second-order perturbation via spin-orbit coupling rather than the direct coupling of electron spin and molecular rotation. Excited states with spin-rotation structure, for example the $\tilde{B}^2\Sigma^+$ state in MOH molecules, can have spin-rotation constants comparable to the rotational constant due to the closer proximity to electronic states with $\Delta\Lambda = \pm 1$. Because excited-state spin-rotation structure is large compared to the natural linewidth, and because the ground-state spin-rotation splittings are ~ 100 MHz or less, the spin-rotation structure is easily addressed with frequency sidebands added to the laser beam, e.g. using acousto-optic or electro-optic modulation.

In states with orbital angular momentum, for example a ${}^2\Pi_{1/2}$ electronic state of a linear molecule, electrostatic interactions couple the orbital angular momentum L to the internuclear axis and spin-orbit interactions couple L with S . In this case, N is not a good quantum number. The rotational energies follow a quadratic ladder in J as $H_{\text{rot}} = BJ(J+1)$, with each J value split into a pair of opposite-parity states by a Λ -doubling Hamiltonian, which arises from spin-orbit mixing with states of different Λ . In symmetric top and asymmetric top molecules, similar interactions split pairs of opposite-parity states in electronic manifolds with non-zero orbital angular momentum.

2.3.6. Hyperfine effects and nuclear spin statistics

In many of the polyatomic laser cooling experiments pursued to date, the valence electron responsible for optical cycling is localized on the spin-0 nucleus of an alkaline-earth (or alkaline-earth-like) metal atom, and a spin-0 oxygen nucleus serves as a “linker” to a ligand such as H and CH₃. As a result, the nuclei with non-zero spin are far from the optically active valence electron, and hyperfine interactions are on the order of only $\lesssim 1$ MHz in both the ground and excited electronic states. Hyperfine interactions therefore play a negligible role in laser cooling, though they might be important in single-quantum-state preparation and readout as needed for many applications (see Sec. 3.9).

Some applications, for example studying nuclear-spin-dependent parity violation (Norrgard et al. (2019a)) or nuclear magnetic quadrupole moments (Hutzler (2020)), require the optically active electron to be localized near a nucleus with spin $I > 0$. This complicates the structure by splitting each J level into $2I + 1$ states of distinct F levels. Generally, this should have no substantial effect on laser cooling as long as each F level is optically addressed by either spectral broadening or the addition of frequency sidebands to optical cycling lasers.

Another consequence of nuclear spins in polyatomic molecules stems from the connection between nuclear spin symmetry and molecular rotation that arises due to symmetry requirements on the total wavefunction, as described in Bunker and Jensen (2006). In the simplest case of a molecule composed of two identical atoms with vanishing nuclear spin, some rotational levels do not exist because the wave function must be even under exchange of the identical nuclei—for example, the ground $^3\Sigma_g^-$ manifold of $^{16}\text{O}_2$ only has odd J levels. Generically, rovibronic levels occur with a “statistical weight” that corresponds to the number of nuclear spin states that give the required totally symmetric state. For example, in CaOCH₃ the “para” nuclear spin configuration (in which two hydrogen nuclear spins are aligned) occurs in $K = 1, 2, 4, 5, \dots$ rotational states, but the “ortho” spin configuration (in which all nuclear spins are aligned) occurs in $K = 0, 3, \dots$ rotational states. Because of the weak hyperfine coupling in CaOCH₃, conversion between para and ortho configurations is highly suppressed; because of the lack of interconversion, the two nuclear spin configurations behave as though they were essentially independent species. Experimentally, laser cooling schemes for both nuclear spin isomers were demonstrated by Mitra et al. (2020) where

the isomer cooled was selected spectroscopically, by driving transitions out of either the $K = 0$ or $K = 1$ rotational state.

2.4. Transitions

In the following sections, we describe the properties and intensities of transitions between the various energy levels present in polyatomic molecules.

2.4.1. Electronic transitions

Transition intensities can be calculated from the square of the transition moment integral (Bernath (2017))

$$\mathbf{M} = \int \psi'(\mathbf{r}, \mathbf{R})^* \boldsymbol{\mu} \psi(\mathbf{r}, \mathbf{R}) d\tau, \quad (14)$$

where integration with respect to τ implies integrating over all electronic and nuclear coordinates, and single primes denote excited states. Invoking the BO approximation, we can write $\psi(\mathbf{r}, \mathbf{R}) = \psi_n(\mathbf{R})\psi_e(\mathbf{r}; \mathbf{R})$. Then the transition moment integral becomes

$$\mathbf{M} = \int \psi_{n'}(\mathbf{R})^* \left(\int \psi_{e'}^*(\mathbf{r}; \mathbf{R}) \boldsymbol{\mu} \psi_e(\mathbf{r}; \mathbf{R}) d\tau_e \right) \psi_n(\mathbf{R}) d\tau_n. \quad (15)$$

We have separated integration over all nuclear coordinates ($d\tau_n$) and electronic coordinates ($d\tau_e$). Let us now define an electronic transition dipole moment as $\mathcal{R}_{e'e}(\mathbf{R}) = \langle \psi_{e'} | \boldsymbol{\mu} | \psi_e \rangle$, and we explicitly denote its dependence on the nuclear coordinates. We can imagine expanding $\mathcal{R}_{e'e}(\mathbf{R})$ in a Taylor series about some value of \mathbf{R} and retaining only the first (constant) term, which we will denote by $\mathcal{R}_{e'e}^*$.³ This simplifies Eq. 15 and allows us to write

$$\mathbf{M} = \mathcal{R}_{e'e}^* \int \psi_{n'}(\mathbf{R})^* \psi_n(\mathbf{R}) d\tau_n. \quad (16)$$

The transition moment has factored into an electronic and nuclear portion, as would be expected from the BO approximation treatment. If we explicitly

³More details about the choice of point on which to center the expansion can be found in the textbook by Bernath (2017). Often, the value of $\mathcal{R}_{e'e}^*$ is inferred from measurements or $\mathcal{R}_{e'e}(\mathbf{R})$ can be found via *ab initio* calculations and used in conjunction with numerical vibrational wavefunctions to compute the necessary integral.

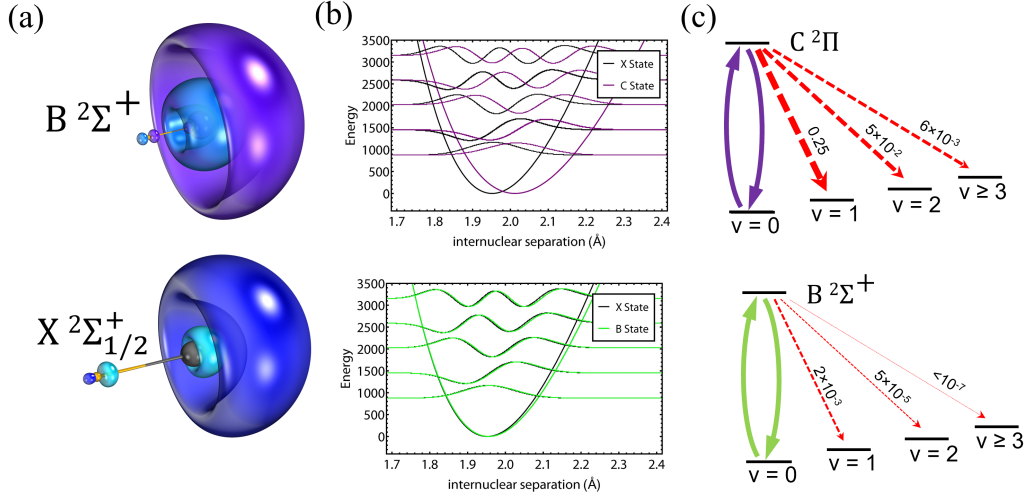


Figure 6: The Franck-Condon principle, as illustrated for diatomic molecules using CaF. (a) The $X^2\Sigma^+$ and $B^2\Sigma^+$ electronic orbitals of the prototypical laser cooling molecule CaF. Localization of the electron density near the Ca metal in both the ground and excited states leads to favorable Franck-Condon overlap. (b) Vibrational wavefunctions of CaF. (c) The corresponding vibrational decay strengths for the $X^2\Sigma^+ - B^2\Sigma^+$ and $X^2\Sigma^+ - C^2\Pi$ transition of CaF.

include both vibrational and rotational nuclear motions, we can write the intensities of rovibronic transitions as (Bernath (2017))

$$I_{(e'v'J') \rightarrow (evJ)} = \left| \mathcal{R}_{e''}^{e'} \right|^2 q_{v' \rightarrow v} S_{J''}^{J'}, \quad (17)$$

where $\mathcal{R}_{e''}^{e'}$ is the electronic transition dipole moment between electronic states e' and e , $q_{v' \rightarrow v''}$ is a Franck-Condon factor (FCF) between vibrational states v' and v , and $S_{J''}^{J'}$ is a Hönl-London factor between states J' and J . We can interpret this factorization as stating that the intrinsic strength of some transition is set by $\left| \mathcal{R}_{e''}^{e'} \right|^2$ while the distribution of that intensity among vibrational and rotational lines are set by $q_{v' \rightarrow v''}$ and $S_{J''}^{J'}$.

2.4.2. Vibrational transitions

Unlike rotational transitions, where angular momentum conservation rigorously constrains the allowed decay channels, in vibrational transitions no selection rules are absolute. Instead, vibrational branching is governed in the Born-Oppenheimer approximation by the overlap of the nuclear wave func-

tions of the initial and final vibronic states, as characterized by the Franck-Condon Factor,

$$q_{v' \rightarrow v''} = \left| \int \psi_{e,v'}^* \psi_{g,v} d\tau_n \right|^2. \quad (18)$$

where v' denotes a vibrational state in the excited electronic manifold e , and v denotes a vibrational state in the ground electronic manifold g . If the Franck-Condon factors of an electronic transition are “diagonal” then $q_{v' \rightarrow v''} \approx \delta_{v',v''}$; in other words, a vibrational level $e(v')$ decays (almost) only to $g(v)$. Geometrically, this will occur when all bond lengths, bond angles, and vibrational constants are approximately identical between the ground and excited electronic states. In practice, off-diagonal FCFs are more sensitive to small fractional changes in bond lengths compared to similarly small fractional changes in harmonic constants. This can be understood from a simple model of wave function overlap between displaced 1D harmonic oscillators with distinct harmonic constants. An example of this, for the diatomic molecule CaF, is shown in Fig. 6.

The vibrational branching ratios from a given vibronic excited state are proportional to the FCFs, but contain an additional factor of $\omega_{v',v}^3$:

$$b_{v' \rightarrow v} = \frac{q_{v' \rightarrow v} \omega_{v',v}^3}{\sum_v q_{v' \rightarrow v} \omega_{v',v}^3}. \quad (19)$$

Thus, transitions to lower-lying vibrational states are slightly favored, relative to what one might expect from considering only the FCF. In practice, the VBRs and FCFs are quantitatively similar, but only the VBR is important for determining and achieving a nearly-closed optical cycle.

In the Born-Oppenheimer (BO) approximation, the symmetry of a vibrational state is conserved in a vibronic transition. For example, in linear molecules like CaOH and SrOH, $|\ell|$ would not be expected to change. In practice, non-BO perturbations induce weak $|\ell|$ -changing transitions at the level of $\sim 10^{-3}$ vibrational branching probability; see Sec. 2.5 for details.

2.4.3. Measuring vibrational branching ratios

Vibrational branching ratios can be measured in any of several ways. The simplest method conceptually is to add repumping lasers (lasers that address vibrational loss channels and return them to the set of bright states) one at a time and observe the total fluorescence collected. To determine the diagonal vibrational branching ratio, one can measure the fluorescence induced when

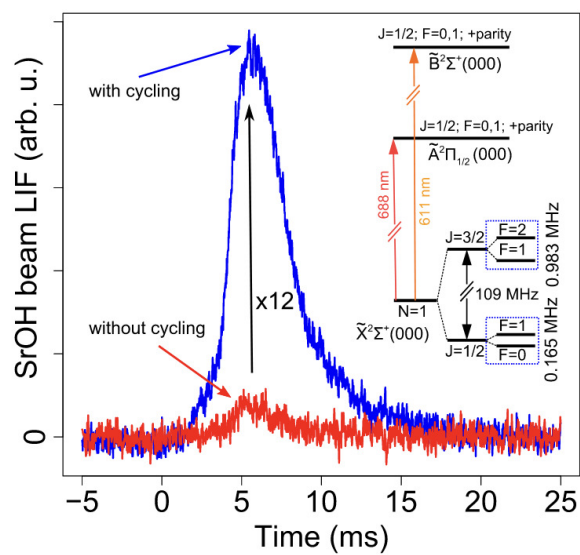


Figure 7: Demonstration of optical cycling with the polyatomic molecule SrOH. Molecular beam fluorescence with (blue) and without (red) addressing both spin-rotation components of the optical cycling rovibronic transition. When both spin-rotation components are addressed, population cycles between the ground $N = 1$ and excited $J' = 1/2$ manifolds, and repeated photon scattering increases the detected fluorescence by over an order of magnitude. Reproduced from Kozyryev et al. (2016b).

addressing all spin-rotation and hyperfine components of a rotationally-closed vibronic transition, and then compare this to the fluorescence induced when only a single quantum state is addressed (for which typically ~ 1 photon is scattered before populating an unaddressed quantum state, depending only on theoretically well-known rotational branching ratios). See Fig. 7 for an example in SrOH. In a similar manner, observing the fluorescence collected when repumping v in an optical cycle, as opposed to exhausting a lossy optical cycle without repumping v , reveals the probability that v is populated among all possible loss channels. By sequentially adding repumpers, in principle all excited vibrational branching ratios can be determined in this way. In practice, this method may be suitable to measure vibrational branching ratios in a long-lived trap (e.g., a MOT), but it is impractical in a molecular beam for VBRs smaller than $\sim 1\%$ because molecules exit the fluorescence region before exhausting a highly closed optical cycle.

An improved method to measure vibrational branching ratios below $\sim 1\%$ is to optically cycle ~ 100 photons in an “interaction region,” e.g. by addressing the diagonal vibronic transition and dominant one or two repumping pathways, and to measure the fraction of molecular population that is recovered to low-lying states when repumping a state v in a “cleanup region” (between the interaction region and fluorescence detection region). If recovery of $\sim 1\%$ of the molecular population can be resolved after $\sim 10^2$ photons are scattered in the interaction region, then vibrational branching ratios of $\sim 10^{-4}$ can be measured. This method was used by Baum et al. (2021) to determine an optical cycling scheme for CaOH with approximately 5×10^3 photons scattered per molecule.

A major limitation of the methods described above is that a vibrational branching ratio can only be measured for a state with known high-resolution repumping transitions. Most polyatomic molecules that might be of interest for future laser-cooling experiments have little preexisting spectroscopic data, especially in excited vibrational states. Therefore, an alternative method should be used to screen a potential laser-coolable molecule for favorable VBRs without requiring high-resolution spectroscopy of up to a dozen vibrational states.

The standard approach to measure VBRs without directly repumping vibrationally excited states is dispersed laser-induced fluorescence (DLIF). See Fig. 8 for a typical experimental configuration. Molecules in a molecular beam are driven to an excited state of interest, e , and subsequently fluoresce to the vibronic ground states $\{v_i\}$ with probabilities $\{P_i\}$. The fluorescence

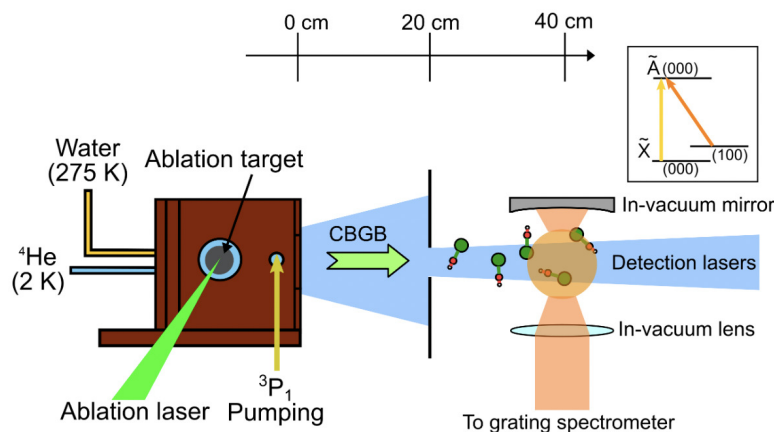


Figure 8: Dispersed laser-induced fluorescence apparatus, reproduced from Zhang et al. (2021). CaOH and YbOH molecules are produced in a CBGB via ablation of a metal precursor in the presence of water vapor. 40 cm downstream, molecules are excited via an optical cycle with 50–100 photons scattered per molecule on average, increasing the fluorescence yield. Fluorescence is collimated by an in-vacuum lens and directed toward a Czerny-Turner monochromator, which disperses light emitted in different vibronic transitions (generally separated by many nm in wavelength) onto different regions of an EMCCD camera.

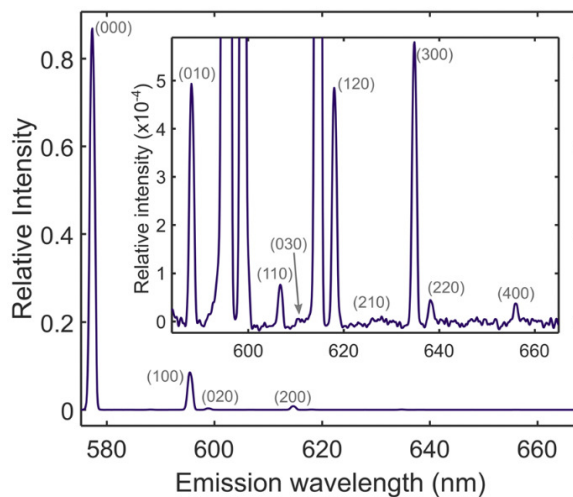


Figure 9: Dispersed fluorescence measurements of YbOH $\tilde{A}(000)$, showing 89% probability of decay on the diagonal vibronic transition, with progressively weaker decays to higher-lying vibrational states. Decays with strength as small as $2(1) \times 10^{-5}$ relative probability can be measured due to the increased fluorescence yield arising from optical cycling excitation. Reproduced from Zhang et al. (2021).

is collected and focused into a spectrometer, in which a diffraction grating is used to spatially disperse the fluorescence wavelengths. The light is then imaged onto an EMCCD, producing an image that shows the relative intensity of each decay feature. Example data are shown for emission from the $\tilde{A}(000)$ state of YbOH in Fig. 9.

With $\sim 10^4$ ablation pulses, vibronic decays with relative probabilities of $10^{-2} - 10^{-3}$ may be detected. By optically cycling molecules in the detection region, up to 100 photons may be scattered per molecule, directly increasing the number of fluorescence photons collected. In cases where the detection sensitivity is limited by camera read-noise or clock-induced-charge, the sensitivity of the measurement is increased proportionally to the number of photons scattered per molecule. In this way, branching ratios on the order of 10^{-5} have been measured for CaOH, YbOH, and SrOH by Zhang et al. (2021); Lasner et al. (2022). The unambiguous assignment of weak decays is greatly aided by high-quality theoretical predictions, which must account for perturbations like those described in Sec. 2.5.

DLIF measurements of VBRs are a powerful method to directly observe all decay channels (inside an observed wavelength range) without requiring high-resolution spectroscopy for optical pumping and repumping of many vibrational states. It is especially important for measuring vibrational branching ratios of polyatomic molecules, where numerous vibrational states may have VBRs around $10^{-5} - 10^{-4}$, a level that is weak in an absolute sense but sufficiently strong to require repumping during radiative slowing and magneto-optical trapping. For a polyatomic molecule with many vibrational modes, it is not necessarily clear in the absence of measurements what the dominant loss channel will be for an optical cycle scattering many more than ~ 100 photons per molecule. This makes a brute-force search for vibrational repumpers inefficient in all but the exceptional cases where the molecule is extensively well-understood from the outset.

2.4.4. Repumping transition spectroscopy

Even in the best-studied laser-coolable molecules such as CaOH and SrOH, the vibrational states that become populated after a molecule has scattered around 10^4 photons have not all been fully analyzed in the literature. It is thus necessary to conduct spectroscopic searches for repumping pathways. These measurements are often conducted in one of two ways: fluorescence in a molecular beam, or absorption in a cryogenic buffer-gas cell.

When repumper spectroscopy is conducted using laser-induced fluores-

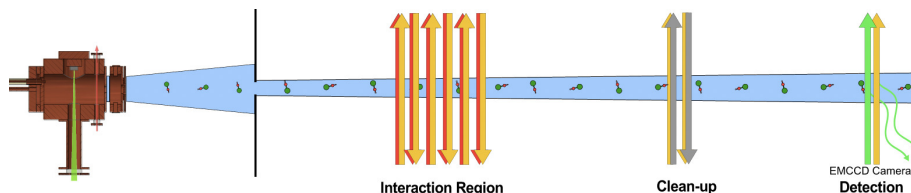


Figure 10: Beamline configuration for pump-repump spectroscopy of vibrationally excited states. An upstream interaction populates vibrationally excited states either through optical cycling or direct off-diagonal excitation. A clean-up region recovers population into a detected state (or set of states), which is excited by a known laser transition to produce fluorescence that is imaged onto an EMCCD camera. When a laser in the interaction region is scanned over an excited state with the clean-up lasers off or out of resonance, a dip in detected fluorescence is observed. This enables the discovery of excited-state repumping pathways. When a laser in the clean-up region is scanned over a repumping transition, detected fluorescence is partially recovered.

cence from a molecular beam (see Fig. 10), a vibrationally excited state can be prepared either by optically cycling until vibrational dark states are populated, or by direct off-diagonal excitation that decays preferentially to the vibrational state of interest in the ground electronic manifold. Due to the rotationally-closed nature of the transition used for optical cycling, often only the $N = 1$ level of the target vibrational state is populated. (Additional rotational levels may be populated in nonlinear polyatomic molecules where the rotational selection rules are slightly relaxed; see Tab. 1.) The frequency of a laser in a downstream “clean-up” region can then be scanned to repump population into (often lower-lying) detectable states, which are excited in a region even farther downstream. Fluorescence in the detection region is observed on a PMT or EMCCD camera. When the frequency of the repumping laser passes through a resonance, an increase in detected population will be observed. Since CBGBs sometimes do not efficiently thermalize the molecular vibrational distribution, in some cases a molecular beam may have sufficient natural population of a vibrationally excited state to detect, provided the correct repumping frequency is addressed in the clean-up region. The same geometry shown in Fig. 10 can also be used to search for excited vibrational states in the electronically excited manifold by scanning the frequency of a laser in the interaction region and observing a dip in the detected population of low-lying vibrational states.

This pump-repump method is best-suited to discovering the frequency of *specific* rovibronic transitions, since in practice at most a few states can be

simultaneously detected in the downstream region. This means that, for a given experimental configuration, only a few transitions (including the “laser cooling transition”) in the clean-up region can produce a spectroscopic signal, dramatically simplifying the data analysis. A corresponding disadvantage, however, is that the signal is spectroscopically sparse, and a good initial estimate of the repumping frequency is required. This estimate can be made either from the observed decay wavelengths obtained via DLIF, or by high-quality theoretical predictions (e.g., made by extrapolating from the known positions of lower-lying vibrational states). Repumper frequency uncertainties obtained by high-resolution DLIF measurements are typically on the order of 5 cm^{-1} , but can be improved by using a diffraction grating with higher line density or by narrowing the width of the entrance slit to the spectrometer.

A related technique can be used to locate repumping transitions after a MOT has been achieved. Namely, one can apply laser light near a suspected repumping transition in the MOT region, with all other trapping laser beams on. While scanning the frequency of the (unknown) repumping laser, one monitors the MOT lifetime. When a resonance is reached, the lifetime of the MOT should increase. This is analogous to the pump-repump method but with an interaction time of tens or even hundreds of ms, which would be impractical in a molecular beam.

An alternative approach to identifying vibrational repumpers is high-sensitivity absorption measurements inside a buffer gas cell (Pilgram (2023)). Frequency-modulated (FM) absorption spectroscopy has been used to observe the weak $\Delta v = -2$ repumping transition for states as high as (300) in YbOH. Unlike the pump-repump spectroscopy described above, all thermally populated rotational states will be probed in this way. This may be desirable in order to make a full spectroscopic assignment of the molecular transitions and constants in a vibronic transition, or to more quickly locate a spectroscopically active frequency region (since a denser “forest” of lines appears, compared with the signal in pump-repump measurements). On the other hand, the spectrum must be fully assigned in order to identify which transitions are connected to the laser cooling state. Aside from these broader considerations, the experimental signal-to-noise ratio may favor either the pump-repump or high-sensitivity absorption measurements depending on factors like the vibrational quenching efficiency in the buffer gas cell, the degree of scattered light suppression in the downstream fluorescence region, the strengths of the probed transitions, and other technical

factors.

2.4.5. Designing an optical cycle

With known vibrational branching ratios (e.g., from high-resolution DLIF measurements), one must carefully design the optical cycle. Several factors are important:

- The number of lasers should be minimized, to reduce cost and experimental complexity
- The excited state that is coupled to the ground vibrational state—e.g., (000) in an MOH molecule—should not be coupled to any other vibrational states if possible, so as to maximize the photon scattering rate and optical forces (see Sec. 1.5.2)
- Lasers should be at convenient optical wavelengths and available at high power
- Optical transitions should be strong (e.g., $\Delta v = -1$ repumpers) to increase the optical pumping or repumping rates for fixed laser powers
- Decays to states without existing spectroscopy should be eliminated where possible

Not all of these factors are mutually compatible, and some balancing is required (e.g., the number of lasers is generally minimized when only a single excited state is used). Typically, only one or two “diagonal enough” excited states are available to choose from for the dominant excitation, and one of these may result in significantly fewer states populated after the $\sim 10^4$ photon scattering events required for magneto-optical trapping. For example, in SrOH, both $\tilde{A}(000)$ and $\tilde{B}(000)$ appear to have reasonably diagonal VBRs, but high-resolution DLIF measurements show that $\tilde{B}(000)$ populates (03¹0), (12⁰0), (13¹0), and (05¹0) at the $\sim 10^{-4}$ level; none of these are significantly populated by $\tilde{A}(000)$, as demonstrated in Lasner et al. (2022). Therefore, many additional repumpers would need to be added to scatter 10^4 photons primarily through $\tilde{B}(000)$, as compared to scattering the same number of photons through $\tilde{A}(000)$. For this reason, an optical cycle coupling $\tilde{A}(000) \leftarrow \tilde{X}(000)$ is favored. Because vibrationally excited states are populated only after approximately 20 photons are scattered through $\tilde{A}(000)$, the $\tilde{B}(000)$ state may be used as a repumping pathway without limiting the

optical cycle to less than 1.5×10^4 photons scattered. Wherever possible, the optical cycle proposed in Lasner et al. (2022) favors repumping through the \tilde{B} manifold due to the much more inexpensive and convenient high-power sum-frequency generation (SFG) sources around 630–650 nm compared with 690–710 nm. The only exception is that the (02²0) state cannot be repumped through \tilde{B} due to a near-vanishing transition strength, and is instead coupled to $\tilde{A}(100)$. Wherever possible, the strongest transition that decreases vibrational quantum numbers from the ground to excited state is chosen, under the constraint that $\tilde{A}(000)$ may not be coupled strongly to any state except $\tilde{X}(000)$. The resulting optical cycle is shown in Fig. 11, along with the optical cycle used to magneto-optically trap CaOH.

To model the number of scattered photons before loss to unaddressed vibrational states occurs, it is useful to construct an absorbing Markov chain model similar to that described in Baum et al. (2021): the states of the Markov chain represent vibrational levels in the electronic ground manifold. For a given optical cycling scheme, the transition probabilities from a state v are given by the VBRs of the excited state to which v is coupled. Each step of the Markov chain represents a single photon scatter. Unaddressed vibrational states “transition” only to themselves, and are absorbing states in the Markov chain. In this model, it is straightforward to calculate many properties of interest to laser cooling, including the average number of scattered photons before an absorbing (i.e., dark vibrational) state is reached, how many times each transient state is visited on average, and the distribution of population among dark states.

2.4.6. Rotational transitions

Rotational transitions follow a generally well-behaved set of selection rules governed by angular momentum algebra. Unless otherwise stated, in this section we consider only electric dipole (E1) transitions. Higher-order transitions (e.g. M1, E2, etc.) are significantly weaker and are typically irrelevant for molecular laser cooling.

The general formula for generating a closed cycling transition in molecules was first proposed by Stuhl et al. (2008), and relies on rotational and parity selection rules ($\Delta J = 0, \pm 1$; $\Delta p = \pm 1$; $J = 0 \rightarrow J' = 0$ forbidden). The key observation was that, while a traditional “type-I” $J \rightarrow J + 1$ transition cannot be rotationally closed (since a rotational level with $J + 2$ necessarily exists in the ground state), driving the “type-II” $J = 1 \rightarrow J' = 0$ transition (or its closest analogue within the molecule of choice) forms a closed tran-

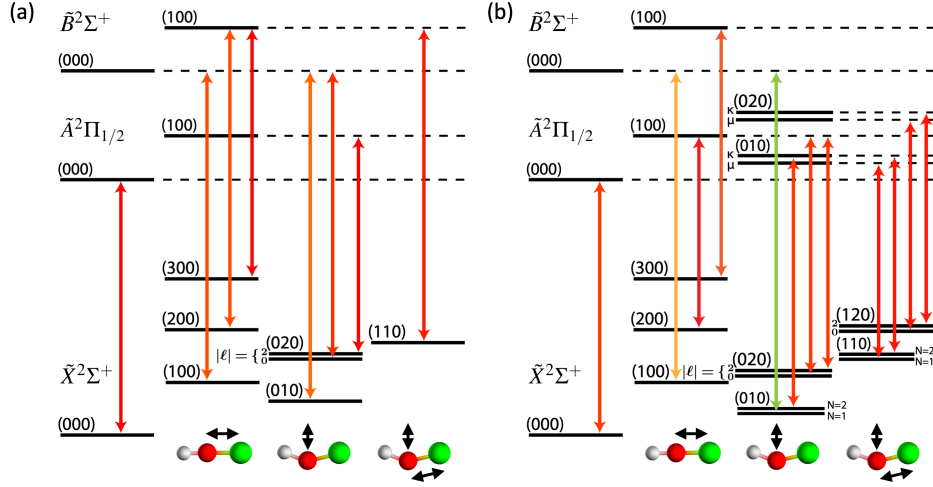


Figure 11: (a) Optical cycling scheme proposed for laser cooling and trapping SrOH, reproduced from Lasner et al. (2022). (b) Optical cycling scheme used to produce a MOT of CaOH.

sition. One consequence of this choice of transition is that there are more ground states than excited states, $m_J > m'_J$, meaning that there will be dark states regardless of the laser polarization chosen. These can be remixed with magnetic fields or polarization modulation (Berkeland and Boshier (2002)).

All polyatomic molecules that have been directly laser cooled (and most polyatomics proposed for laser cooling) have a single valence electron and therefore have spin-doublet ground states ($S = 1/2$). In this case, the rotational angular momentum N couples to the electron spin to form a total angular momentum quantum number J , which takes half-integer values.⁴ In such a system, the electric dipole selection rules $\Delta J = 0, \pm 1$ and $J = 0 \nrightarrow J' = 0$ always apply, as well as the requirement that the parity of the state changes, $\Delta p = \pm 1$. In this case, the excited state used to achieve rotational closure is no longer $J' = 0$ but $J' = 1/2$.

In addition to the universal selection rules on J and parity, other selection rules exist for specific molecular geometries and angular momentum coupling cases. These are summarized in Table 1. The selection rules are sorted by

⁴Here we ignore hyperfine degrees of freedom, which are often unresolved in polyatomic molecules, though the selection rules discussed below can be easily generalized to include hyperfine structure.

Geometry	Transition axis	Basis*	Selection rules*
Linear	\parallel	b \rightarrow b	$\Delta\Lambda = 0; \Delta\ell = 0; \Delta N = 0, \pm 1$
Linear	\perp	b \rightarrow a	$\Delta\Lambda = \pm 1; \Delta\ell = 0$
STM	\parallel	b \rightarrow b	$\Delta K = 0; \Delta N = 0, \pm 1$
STM	\perp	b \rightarrow a	$\Delta K_R = 0; \Delta K = \pm 1$
ATM	a type	b \rightarrow b	$\Delta K_a = 0; \Delta K_c = \pm 1; \Delta N = 0, \pm 1^{**}$
ATM	b type	b \rightarrow b	$\Delta K_a = \pm 1; \Delta K_c = \pm 1; \Delta N = 0, \pm 1^{**}$
ATM	c type	b \rightarrow b	$\Delta K_a = \pm 1; \Delta K_c = 0; \Delta N = 0, \pm 1^{**}$

Table 1: Summary of the main selection rules discussed in this review. All transitions follow the selection rules $\Delta J = 0, \pm 1$ and $\Delta p = \pm 1$ in addition to those listed. Also note that at least one angular momentum quantum number must change, so transitions with $\Delta K = \Delta N = \Delta J = 0$ (or analogous) are forbidden.

*Note that the selection rules described here apply only when the states are exactly described by the basis listed; in many real scenarios the selection rules are only approximate.

** $\Delta N = 2$ transitions may be allowed in ATMs where the electronic angular momentum is not fully quenched.

molecule geometry, as well as the axis along which the transition dipole moment is induced. For molecules with cylindrical symmetry, transitions can be either parallel (\parallel) or perpendicular (\perp), meaning the transition dipole moment is induced either along the principal molecular axis or perpendicular to it, respectively. For asymmetric top molecules, a transition can be induced along any of the three molecular axes, as described further below. Finally, different selection rules apply depending on the coupling of angular momenta within each electronic state involved. Typically, in nondegenerate states with zero electronic angular momentum Hund’s case (b) applies, where both N and J are good quantum numbers. However, degenerate states with electronic angular momentum $\Lambda \neq 0$ are typically described by Hund’s case (a), where the electron spin is strongly coupled to the molecular axis and N is no longer a good quantum number.

Rotational transition strengths are described by the Hönl-London factors $S_J^{J'}$ in eqn. 17. They can be calculated using angular momentum algebra by taking matrix elements of the dipole operator (see, e.g., Hirota (1985)), or looked up in tables.

Linear molecules. In nondegenerate vibrational states ($\ell = 0$) of ${}^2\Sigma^+$ linear polyatomic molecules like CaOH, SrOH, and YbOH, a closed optical cycling transition is formed by driving the ${}^PQ_{21}(J = 1/2)$ and $P_1(J = 3/2)$

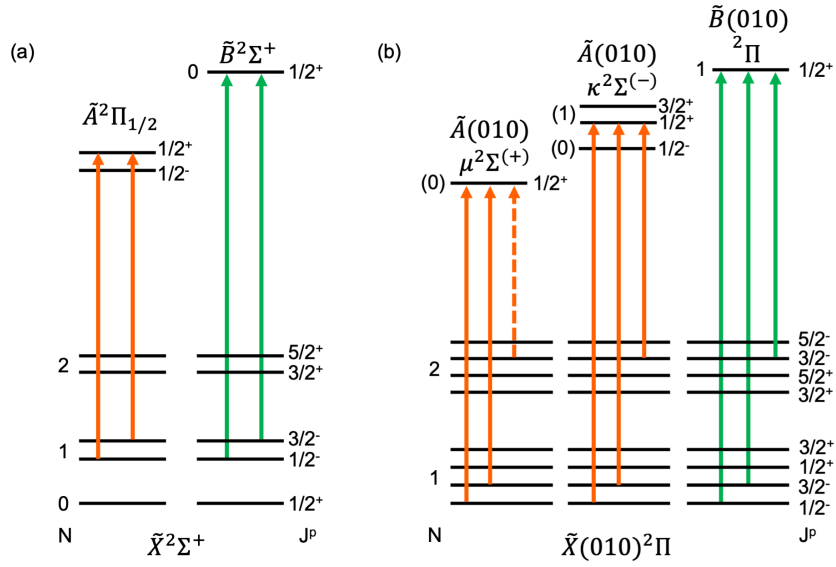


Figure 12: Closed cycling transitions in alkaline-earth monohydroxides (e.g. CaOH) for laser cooling on the $\tilde{X}^2\Sigma^+ \rightarrow \tilde{A}^2\Pi_{1/2}$ and $\tilde{X}^2\Sigma^+ \rightarrow \tilde{B}^2\Sigma^+$ electronic transitions. (a) For nondegenerate ($\ell = 0$) vibrational levels of the ground state, two laser frequencies are required to address the $J = 1/2^-$ and $J = 3/2^-$ levels of the $N = 1$ rotational state. (b) For repumping the $\tilde{X}(010)$ bending mode, which has vibrational angular momentum $|\ell| = 1$, an additional color addressing the $N = 2, J = 3/2^-$ state is required, regardless of which excited state is chosen. The dashed line refers to a transition which is allowed only when the excited state does not adhere to the case (b) limit, i.e. when N is not a good quantum number.

transitions, which address both spin-rotation components of the $\tilde{X}^2\Sigma^+(N = 1^-)$ ground state and excite them to either the $\tilde{A}^2\Pi_{1/2}(J' = 1/2^+)$ or $\tilde{B}^2\Sigma^+(N' = 0, J' = 1/2^+)$ state (Fig. 12a). The key ingredient for achieving rotational closure in this scheme is not the specific electronic state but the fact that it have a well-resolved $J' = 1/2^+$ level. In this case the transition is guaranteed to be closed by the E1 selection rules $\Delta J = 0, \pm 1$ and $\Delta p = \pm 1$.

The inclusion of hyperfine structure threatens to void these selection rules because the $(J' = 1/2, F = 1^+)$ level of the excited state may, in principle, decay to the $(N = 3, J = 5/2, F = 2^-)$ ground state level. However, this requires that the hyperfine interaction mix the $N = 1$ and $N = 3$ states. The mixing fraction is on the order of $\sim c^2/(10B)^2 \sim 10^{-10}$ for CaOH, where c is the dipolar hyperfine constant and B is the rotational constant. While this decay mechanism is negligible for CaOH and alkaline-earth monohydroxides with similar structure, it may be of some significance for species with large hyperfine structure, e.g., with a nuclear spin on the optical cycling center (see, e.g., Pilgram et al. (2021)).

In degenerate vibrational states ($\ell \neq 0$) rotational closure is complicated by the appearance of parity doublets in the ground state (Fig. 12b). In this case, the excited $J' = 1/2^+$ state can not only decay to $N = 1^-$ as before, but also to the $N = 2, J = 3/2^-$ sublevel. For the linear polyatomic molecules which have been laser cooled to date, the most important cases are $\ell = 1$ and $\ell = 2$. For example, in CaOH, YbOH, and SrOH, the $\tilde{X}(01^1_0)$ and $\tilde{X}(02^2_0)$ states typically require repumping at or above the 10^{-4} level (Zhang et al. (2021); Lasner et al. (2022)). As shown in Fig. 12, $\ell = 1$ states require both an $N = 1^-$ and an $N = 2^-$ repumping laser. Unlike the spin-rotation splitting between the $J = 1/2$ and $J = 3/2$ states in $N = 1$, which are typically spaced by $\sim 10 - 100$ MHz and can be addressed with rf modulation (e.g. AOMs or EOMs), the $N = 1$ and $N = 2$ repumpers in $\ell = 1$ bending modes are split by 10s of GHz in the alkaline-earth monohydroxides, meaning that either two separate lasers or high frequency EOMs need to be used to bridge the gap. The $\ell = 2$ states, meanwhile, require just a single repumping laser, which addresses the $N = 2, J = 3/2^-$ state.

For $\ell \neq 0$ bending modes, the excited state used for repumping also merits careful consideration. The primary concern is that many candidate states are best described by a Hund's case (b) basis, meaning that both N' and J' are good quantum numbers. Accordingly, while the $N = 1^-$ ground state levels can always be repumped through the excited $J' = 1/2^+$

state, in some cases repumping of $N = 2^-$ is forbidden by an approximate $\Delta N = 0, \pm 1$ selection rule. For example, in the laser cooling scheme used for CaOH by Vilas et al. (2022), $\tilde{X}(01^1 0)(N = 1^-)$ is repumped through the $\tilde{B}^2\Sigma^+(000)(N' = 0, J' = 1/2^+)$ state, but $N = 2^-$ is not because of ΔN selection rules. Instead, the $N = 2, J = 3/2^+$ state is repumped through the $\tilde{A}(010)$ electronic manifold, which has two components $\mu^2\Sigma^{(+)}$ and $\kappa^2\Sigma^{(-)}$ (Fig. 12b; this state is described in detail in Li and Coxon (1995)). These states are intermediate between case (a) and case (b), so ΔN selection rules are somewhat weakly enforced; however, the $\kappa^2\Sigma^{(-)}$ is the best candidate for $N = 2^-$ repumping because its $J' = 1/2^+$ state has dominantly $N' = 1$ character, while the $\mu^2\Sigma^{(+)}$ ($J' = 1/2^+$) state has predominantly $N' = 0$ character. In CaOH, the $\mu^2\Sigma^{(+)}$ ($J' = 1/2^+$) state has only a $\sim 7\%$ transition strength to $N = 2^-$, while the $\kappa^2\Sigma^{(-)}$ ($J' = 1/2^+$) state connects in approximately equal proportion to $N = 1^-$ and $N = 2^-$ in the $\ell = 1$ bending modes.

In practice, it is often necessary to repump degenerate bending modes using transitions that do not satisfy the $\Delta\ell = 0$ selection rule (see section 2.4.5). In this case, rotational transition strengths are challenging to calculate because they may be altered by vibronic perturbations. These must be considered on a molecule-by-molecule basis. For repumping the $\ell = 1$ bending modes in CaOH, it is empirically known that repumping on the $\tilde{X}^2\Sigma^+(010)(N = 1^-) \rightarrow \tilde{B}^2\Sigma^+(000)(N' = 0, J' = 1/2^+)$ transition is sufficiently strong (Baum et al. (2020, 2021); Vilas et al. (2022)). However, in CaOH the $N = 2^-$ states are repumped using $\Delta\ell = 0$ transitions (Vilas et al. (2022)).

Symmetric top molecules. The rotational cycling transitions for 2A_1 symmetric top molecules (STMs) (e.g. CaOCH₃ or YbOCH₃) are shown in Fig. 13. In addition to the J and parity selection rules discussed above, there are also K selection rules for STMs.

For parallel transitions between two nondegenerate electronic states (e.g. $\tilde{X}^2A_1 \rightarrow \tilde{B}^2A_1$), the selection rule $\Delta K = 0$ holds. It is useful to divide the molecule into “ K stacks”, each of which is well isolated during optical cycling. A canonical $N = 1^- \rightarrow N' = 0^+$ cycling transition can therefore be formed in the $K = 0$ stack, while cycling in the $K = 1$ stack requires an additional $N = 2$ repumping laser, as shown in Fig. 13b.

For perpendicular transitions between a nondegenerate and a degenerate electronic state (e.g. $\tilde{X}^2A_1 \rightarrow \tilde{A}^2E$), the photon adds one unit of electronic

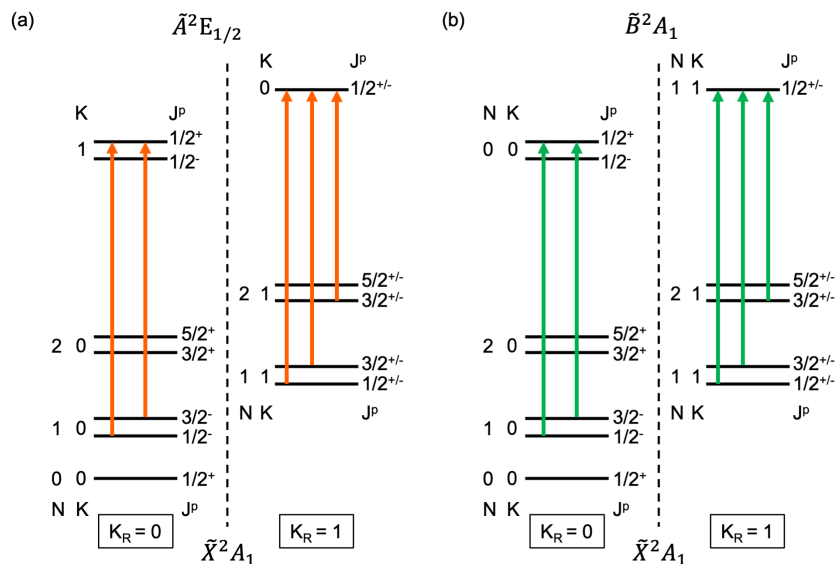


Figure 13: Rotationally closed cycling transitions for symmetric top molecules with structure similar to CaOCH_3 on the (a) $\tilde{X}^2A_1 \rightarrow \tilde{A}^2E$ and (b) $\tilde{X}^2A_1 \rightarrow \tilde{B}^2A_1$ electronic transitions. Cycling transitions exist within both the $K_R = 0$ stack and the $K_R = 1$ stack, though in the latter case an $N = 2$ rotational repumping laser is required.

angular momentum (Λ) about the molecular axis, while the rigid body rotation of the molecule (i.e. K_R , the projection of R onto the molecular axis) is unchanged. Therefore $\Delta K = \Delta K_R + \Delta \Lambda = \pm 1$, but $\Delta K_R = 0$.⁵ In this case we can instead divide the structure into isolated “ K_R stacks”, noting that $K = K_R$ in the nondegenerate ground state. A closed $N = 1^- \rightarrow J' = 1/2^+$ cycling transition can be found in the $K_R = 0$ stack, while cycling in the $K_R = 1$ stack requires an $N = 2$ repumping laser because each rotational level contains parity doublets (Fig. 13a). Note that the degenerate excited state is typically well described by a Hund’s case (a) basis, so N' is not a good quantum number. See Herzberg (1966); Brown (1971); Cerny et al. (1993); Brazier and Bernath (1989) for additional details on rotational selection rules

⁵Note that the electronic angular momentum is quenched in symmetric top molecules, so Λ is not necessarily an integer. Instead, the orbital angular momentum about the symmetry axis is labeled by ζ_e , and both it and K_R are only approximate quantum numbers. Nonetheless, the selection rules discussed above based on K_R stacks are expected to hold in general, though the K_R notation is simply a convenience for molecules where $\zeta_e \approx 1$ (see Brazier and Bernath (1989)).

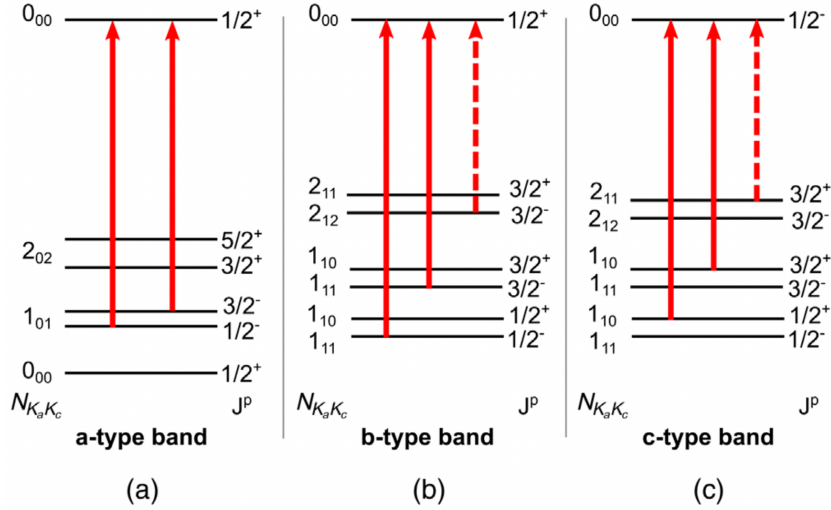


Figure 14: Rotationally closed cycling transitions for a , b , and c -type bands in asymmetric top molecules, as described in the text. Dashed lines correspond to transitions that are allowed in ATMs with unquenched electronic angular momentum, which is expected to be true for molecular geometries near the symmetric-top limit. Reproduced from Augenbraun et al. (2020a).

and K_R stacks in STMs.

The selection rules described above have been tested in experiments with CaOCH_3 (Mitra et al. (2020)), where ~ 120 photons were scattered in the $K_R = 0$ stack and ~ 30 photons were scattered in the $K_R = 1$ stack. It is empirically unknown whether the K_R selection rules hold beyond this number of photons.

Asymmetric top molecules. In asymmetric top molecules (ATMs), there are three types of electronic transitions to consider, corresponding to induced dipole moments along either the a , b , or c principal axis of the molecule. These are analogous to parallel and perpendicular transitions in linear molecules or STMs, where parallel transitions become a (c)-axis transitions for prolate (oblate) molecules, and the other two axes play the role of perpendicular transitions. Each transition axis has its own selection rules, shown in Tab. 1, and closed cycling transitions for each transition type are shown in Fig 14. The transition dipole moment μ will in general have a projection onto each of the principal axes and inherit some of each of the selection rules (Augenbraun et al. (2020a)). It is therefore advisable to choose molecules whose transition dipole moments are well aligned with the molec-

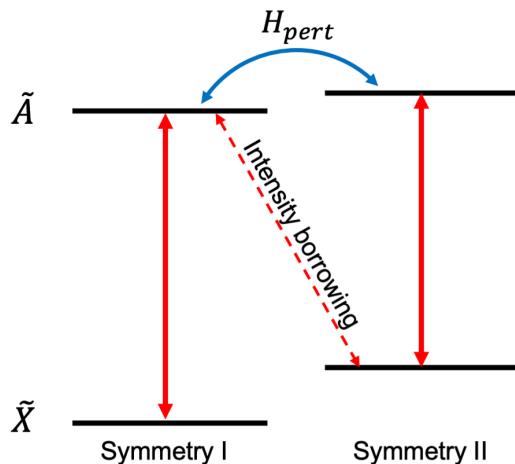


Figure 15: Schematic illustration of how perturbations among electronically excited states can lead to an “intensity borrowing” effect that induces nominally forbidden transitions (or increases the intensities of transitions that were expected to be very weak).

ular axis to limit the number of rotational states that require repumping.

2.5. Perturbations

We have thus far described the energy eigenstates of polyatomic molecules using a basis of well-defined quantum numbers. These, in turn, led to strict selection rules governing vibrational and rotational branching. In real molecules, however, there are mechanisms that perturbatively couple these basis states, e.g. via mixing of electronic and vibrational angular momentum. The result is an effect known as “intensity borrowing”: nominally forbidden transitions become allowed because the energy eigenstates of the molecule contain a small admixture of basis states with different quantum numbers and/or symmetry. The effect is illustrated schematically in Fig. 15. While these effects are typically small ($\sim 10^{-3}$ level or below), they can become important when forming cycling transitions capable of scattering many thousands of photons, or when certain vibronic levels of electronically excited states have energy gaps that are “accidentally” small.

While perturbations can take many forms and must in general be considered on a molecule-to-molecule basis, below we will discuss a few known effects for molecules presently being laser cooled or proposed for laser cooling.

The Renner-Teller (RT) effect describes vibronic mixing between the electronic angular momentum Λ and the vibrational angular momentum ℓ in

linear polyatomic molecules with degenerate vibrational modes. In particular, it allows Λ and ℓ to change while conserving the total spinless angular momentum projection $K = \Lambda + \ell$. The physical origin of this effect is that bending vibrations reduce the cylindrical symmetry of the molecule and can therefore break the degeneracy of the in-plane and out-of-plane electronic orbitals in states with $\Lambda > 0$. See Hirota (1985) for a detailed description of this interaction.

The Renner-Teller effect is responsible for vibrational branching that violates the $\Delta\ell = 0$ selection rule in linear polyatomic molecules, as previously studied in detail for CaOH, SrOH, BaOH, and YbOH (Baum et al. (2021); Zhang et al. (2021); Lasner et al. (2022); Kinsey-Nielsen et al. (1986)). In these molecules, there are two important types of RT-induced branching. The first is $\Delta\ell = \pm 1$ branching enabled by first-order RT coupling, which mixes states according to the selection rule $\Delta\Lambda = -\Delta\ell = \pm 1$. This enables direct vibronic coupling between the $\tilde{A}^2\Pi(000)$ and $\tilde{B}^2\Sigma^+(01^10)$ states in alkaline earth monohydroxides, thereby allowing $\tilde{A}(000)$ to decay directly to $\ell = 1$ ground states (e.g. $\tilde{X}(01^10)$) via intensity borrowing from the $\tilde{B}(01^10)$ state. Likewise, $\tilde{B}(000)$ can decay to $\tilde{X}(01^10)$ via RT coupling with $\tilde{A}(01^10)$. This coupling typically contributes at the $\sim 10^{-3}$ to 10^{-4} range in the alkaline earth monohydroxides (Baum et al. (2021); Zhang et al. (2021); Lasner et al. (2022)). A smaller effect mixes $\tilde{A}(000)$ and $\tilde{A}(01^10)$ directly via contributions from both first-order RT and spin-orbit coupling, but it is not discussed further here. See Baum et al. (2021); Zhang et al. (2021) for more details.

The second effect of RT mixing is $\Delta\ell = \pm 2$ branching induced by second-order RT coupling, which mixes states according to the selection rule $\Delta\Lambda = -\Delta\ell = \pm 2$. This term directly couples $\tilde{A}^2\Pi(000)$ to $\tilde{A}^2\Pi(02^20)$, as it can mix the $|\Lambda = 1, \ell = 0\rangle$ and $|\Lambda = -1, \ell = 2\rangle$ components of the \tilde{A} state. Observed decays to $\tilde{X}(02^20)$ and $\tilde{X}(12^20)$ in alkaline earth monohydroxides are attributed to this mechanism (Baum et al. (2021); Zhang et al. (2021); Lasner et al. (2022); Vilas et al. (2022)).

An analogous interaction, called the (pseudo-)Jahn-Teller (JT) effect, is possible in nonlinear symmetric top molecules. A detailed review of Jahn-Teller physics is provided by Barckholtz and Miller (1998). For the purposes of laser-coolable polyatomic molecules such as CaOCH₃ or YbOCH₃, we can regard the (pseudo-)JT effect in the 2E state of a nonlinear molecule as analogous to the RT effect in a $^2\Pi$ linear molecule. This effect can lead to mixing between a 2E and 2A_1 electronic state which alters the vibrational

structure of the 2E state and changes the vibronic emission intensities associated with spontaneous emission from this state. In a molecule such as CaOCH_3 or YbOCH_3 , the first electronically excited state ($\tilde{A}{}^2E$) is affected by mixing with the $\tilde{B}{}^2A_1$ level. Especially due to second-order spin-orbit–vibronic coupling, this interaction can dramatically increase the intensity of decays to vibrational bending modes that would have been symmetry-forbidden within the BO approximation. Experimentally, these decays have been observed in CaOCH_3 (Augenbraun (2020)) and in YbOCH_3 (Augenbraun et al. (2021b)). In both cases, it was possible to model the intensity of decay to vibrational bending modes on the basis of quantum chemical predictions of the JT parameters provided by Paul et al. (2019). In both cases, the nominally symmetry-forbidden decays were significantly stronger than decays to symmetry-allowed levels of the same vibrational mode, directly indicating the role that vibronic coupling plays in this process.

These observations point to two important considerations in the selection of laser-coolable nonlinear molecules. First, one must consider beyond-BO-approximation effects when deciding whether simple estimates of FCFs are justified in selecting a molecule for future experimentation. Second, experimental measurements of vibrational branching ratios are crucial to identify weak decays that violate expectations based on molecular symmetry. See Sec. 2.4.3 for details on such measurements.

3. Experimental techniques

3.1. Cryogenic buffer-gas beams

Almost all applications of laser-cooled molecules benefit from long interaction times, achieved either through a trap (enabling, in principle, arbitrarily long hold times) or a molecular beam propagating over a large distance (tens of centimeters to a few meters, enabling probe times of ~ 1 – 100 ms). In both cases, a large flux of initially slow molecules is essential. In order to trap molecules, any motion at the time of production must be removed in a manner whose difficulty typically scales with the initial momentum or kinetic energy, whereas for a fixed beam line the interaction time is inversely proportional to the beam velocity.

An additional requirement for a practical molecular source is a low rotational temperature. Rotationally excited states of small molecules like CaF and SrOH obtain significant thermal population at temperatures of ~ 1 K,

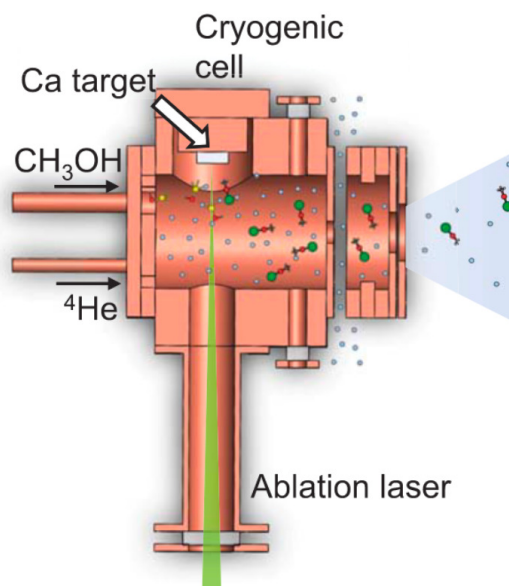


Figure 16: A representative cryogenic buffer gas cell, modified from Mitra et al. (2020). Hot reagent CH_3OH (methanol) gas is introduced via a capillary, and cold ^4He buffer gas is introduced via a second capillary. A pulsed Nd:YAG laser ablates a “target” of Ca metal, which reacts with methanol to form CaOCH_3 in the first-stage cell. Additional windows at the downstream end of the first-stage cell may be used to monitor molecular production via optical absorption measurements. The helium thermalizes the molecules and entrains them through a hole in the front of the cell. A second-stage cell, stood off from the first stage to lower the buffer gas density, reduces the forward velocity of the molecular beam. Buffer gas and molecules are extracted through the front of the second-stage cell.

and the population in any single quantum state at room temperature is suppressed by orders of magnitude compared to the low-temperature limit. This problem grows exponentially for large asymmetric top molecules, with multiple rotational modes that have small rotational constants (owing to the large moments of inertia).

Buffer-gas cooling in closed cells was developed by the atomic hydrogen community in the late 1970s/early 1980s. Early examples with molecules include the De Lucia group, which studied CO molecules (and, later, polyatomic molecules) in the presence of a ~ 4 K He buffer gas, as in Messer and De Lucia (1984); Willey et al. (1988); Mengel and De Lucia (2000). The Doyle group pioneered the use of buffer-gas cooling to load atoms and molecules into (superconducting) magnetic traps in Doyle et al. (1995); Wein-

stein et al. (1998); Campbell et al. (2007); Doret et al. (2009). The first molecular beam source generated from buffer-gas cells was developed in the Doyle group in collaboration with Prof. David DeMille, as described in Maxwell et al. (2005b). Hydrodynamic cryogenic buffer-gas beams (CBGBs) were created by Patterson and Doyle (2007) and developed by both the Doyle and DeMille groups and the Hinds/Tarbutt groups. Reviews by Hutzler et al. (2012); Barry et al. (2011) discuss the key features of such sources, which include low forward velocities and hydrodynamic enhancement effects that led to beams several orders of magnitude brighter than previous realizations.

A primary benefit of a CBGB (beyond the low velocity and high flux) is that it allows the experiment to separate molecule *production* (occurring in a cryogenic region with poor optical access) from molecule *manipulation* (usually occurring in a room-temperature, ultra-high vacuum region). The CBGB was a key technological development that enabled direct laser cooling of molecules, as supersonic beams produce velocities so high as to make the deceleration of molecules to trappable velocities extremely difficult.

A CBGB source typically consists of four nested regions. The innermost region is a “buffer gas cell,” usually made of high-purity copper and cooled to $\sim 1 - 4$ K. A representative example is shown in Fig. 16. There, stable reagent molecules (methanol) are introduced into the cell via a hot capillary, while Ca metal is ablated via a pulsed Nd:YAG laser (typically with $\sim 10-40$ mJ/pulse). The ablated atoms and methanol gas react to form CaOCH_3 . Simultaneously, He buffer gas is flowed through a second capillary that pre-cools the He gas before it enters the cell. Inside the cell, the He thermalizes with the cold walls of the cell and collisions between molecules and He atoms cool the molecules. The flow of helium entrains molecules through a hole in the front of the cell (typically $\sim 3-7$ mm diameter). The helium and molecules then flow into a lower-density “second-stage cell” that is stood off from the first stage of the buffer gas cell with a small gap for buffer gas to escape. This lowers the buffer gas density in the second-stage cell and reduces the forward velocity of molecules, at the expense of some reduction in the molecular extraction (typically a factor of order unity). Molecules then emerge from the second cell with forward velocities in the range of $\sim 40-200$ m/s, depending on the molecular mass, cell temperature, and buffer gas flow rate.

A number of variations on the buffer gas cell are used, depending on experimental requirements and the molecular species of interest. To produce cold beams of stable molecules such as ammonia or formaldehyde, no ablation is necessary (Buuren et al. (2009)). On the other hand, even complex radical

molecules can be produced directly from ablation of pressed-powder pellets (or “targets”) of stable constituents, without reagent gases. For example, a mixture of SrH₂ and naphthol powders produces SrO-naphthyl radicals (Mitra et al. (2022)). Because of the versatility in molecular production methods, a wide variety of polyatomic molecules including both radical (Augenbraun et al. (2020b); Baum et al. (2020); Mitra et al. (2020); Zhu et al. (2022); Mitra et al. (2022) and non-radical Maxwell et al. (2005a); Buuren et al. (2009); Herschbach (2009); Sawyer et al. (2011); Eibenberger et al. (2017); Spaun et al. (2016); Satterthwaite et al. (2019); Patterson and Doyle (2013); Piskorski (2014)) species can be created in a CBGB. Molecules as large as Nile red (C₂₀H₁₈N₂O₂) have been produced and spectroscopically studied in a cryogenic buffer gas cell without forming helium-molecule clusters (Piskorski et al. (2014)).

Both helium and neon buffer gas are commonly used in CBGBs, with neon requiring cell temperatures above approximately 16 K to maintain a suitable vapor pressure. Depending on the requirements for molecular flux and the initial beam velocity, the second-stage cell may be omitted. The lowest forward velocities can be achieved by cooling the second stage with a He-3 pot at temperatures around or below 1 K (Augenbraun et al. (2021a)). In that work, the heat loads arising from ablation and gas flows, in the range of tens to hundreds of mW, made it impractical to cool the first-stage cell using a He-3 refrigerator. Nevertheless, by cooling the second-stage alone, beams of Yb (Ca) with peak forward velocities as low as about 20 m/s (40 m/s) have been observed by Augenbraun (2020); Augenbraun et al. (2021a); Sawaoka et al. (2022).

Surrounding the buffer gas cell is a cold box, usually constructed of high-purity copper and held at ~ 4 K by a pulse tube cryocooler to serve as a cryopump. When helium buffer gas is used, charcoal sorbs are thermally anchored to the 4 K box in order to achieve adequate helium (cryo)pumping speeds; other buffer gasses, such as neon, are efficiently cryopumped directly using copper surfaces held at 4 K.

The cryopumping box is contained within another box, typically made of aluminum or copper, held at ~ 50 K by the first stage of a pulse tube cryocooler. This box shields the cryopumping box and buffer gas cell from room-temperature black body radiation. The radiation shields are housed within a vacuum chamber at $\sim 10^{-7}$ Torr or better.

We summarize several important molecular beam parameters under typical conditions in Tab. 2. Experiments seeking to trap molecules usually

Parameter	Typical range
Forward velocity	40–200 m/s
Solid angle FWHM	0.2–1 sr
Rotational temperature	1–4 K
Brightness	10^8 - 10^{11} sr ⁻¹ pulse ⁻¹
Ablation repetition rate	1–50 Hz
Ablation energy	10–40 mJ
Buffer gas flow rates	2–40 sccm

Table 2: Representative operating and performance parameters of molecular CBGBs.

operate toward the lower range of buffer gas flow rates, ablation energy, and ablation repetition rate, to enable lower temperatures and forward molecular beam velocities at the expense of beam brightness and experimental duty cycle.

3.2. Optical cycling

The key ingredient to laser cooling is the near-closure of an optical cycle, so as to approximate an ideal two-level system, as depicted in Fig. 17. A molecule initially in its ground state absorbs a photon with energy $\hbar\omega$, which excites the molecule to a higher quantum level and imparts a momentum recoil $p_{\text{recoil}} = \hbar k$. The molecular state subsequently spontaneously decays, ideally back to the ground state, emitting a photon in a random direction. By using optical cycling, the molecule’s external motion can be controlled through various cooling schemes such as Doppler or polarization gradient cooling, Λ -enhanced grey molasses, etc. In real molecules, an optical cycle consists of many “ground” states (which are generally in the ground electronic state, but excited vibrationally or rotationally) and many excited states (which are electronically, vibrationally, and/or rotationally excited). Thus, any chosen pair of ground and excited states will fail to form a closed optical cycle.

However, by careful selection of a group of ground states and excited states (manifolds), a nearly-closed optical cycle can be formed. For example, in molecules like CaOH and SrOH, parity and angular momentum selection rules ensure that the excited $J^P = 1/2^+$ states in the lowest-lying excited electronic state $\tilde{A}^2\Pi_{1/2}$ can *only* decay to the $N^P = 1^-$ rotational manifolds in the ground electronic state $\tilde{X}^2\Sigma^+$. Each $J^P = 1/2^+$ state contains four

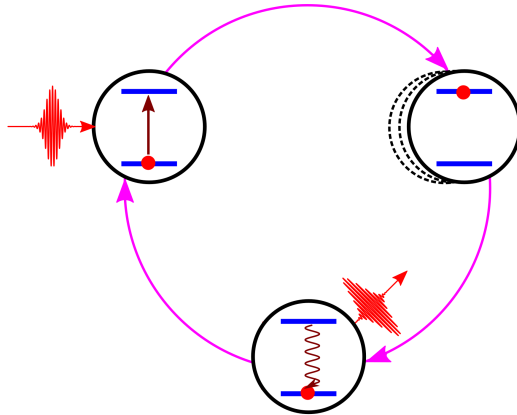


Figure 17: Optical cycle for an ideal two-level system, reproduced from Augendraun et al. (2020a). Three phenomena repeat up to tens of thousands of times: (1) A photon is absorbed, driving a molecule from the ground to excited state and imparting a momentum recoil to the molecule, (2) subsequently, a photon is spontaneously emitted in a random direction, and (3) the molecule returns to its ground state.

optically unresolved hyperfine levels, while each $N^P = 1^-$ manifold contains a $J = 1/2$ manifold and a $J = 3/2$ manifold, which are split from each other by spin-rotation splittings of $\sim 10\text{--}100$ MHz that are easily spanned with optical frequency modulation techniques. These $J = 1/2$ and $J = 3/2$ manifolds contain 4 and 8 hyperfine states, respectively. This nearly-closed molecular cycling transition contains 12 ground and 4 excited states. A scheme to achieve a rotationally and vibrationally closed optical cycle (and eventually laser cooling) of a polyatomic molecule was first discussed by Kozyryev et al. (2015, 2016b) using the example of SrOH.

For any practical application of optical cycling or laser cooling, it is necessary to add repumping lasers to also address excited vibrational states of the ground electronic manifold, as when the molecule decays from the electronically excited state there are no selection rules on the vibrational quantum number. How many vibrational repumpers are required depends on the vibrational branching ratios (VBRs) and on the optical cycling scheme chosen, see Sec. 2.4.5. The exact optical cycling scheme required for a particular application depends on the details of the molecular structure. For example, the optical cycle used to laser cool the symmetric top molecule CaOCH_3 , (with C_{3v} symmetry) is depicted in Mitra et al. (2020). Similarly, an overview of

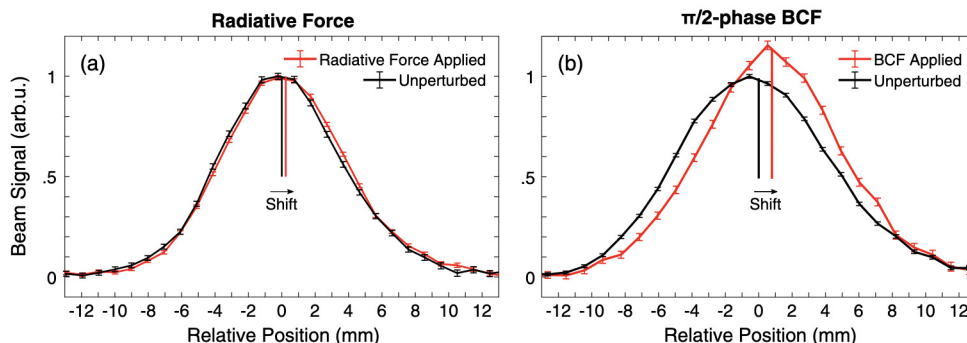


Figure 18: Comparison of molecular beam deflection via radiation pressure force (left) and bichromatic force (right) in SrOH, reproduced from Kozyryev et al. (2018). Under these conditions, the bichromatic force is greater by a factor of 3.7, as seen by the shift in the position of the molecular beam.

the optical cycles required to achieve optical cycling with respect to the rotational structure in asymmetric tops are shown in Augendraun et al. (2020a).

3.3. Optical forces

The radiative force on a molecule is determined by the momentum recoil, p_{recoil} , and the scattering rate γ , as $F_{\text{recoil}} = p_{\text{recoil}}\gamma$. Thus to achieve large optical forces, it is important to maximize the scattering rate by judicious selection of optical cycling transitions and saturation of all laser powers. The first demonstration of the radiation pressure force on a polyatomic molecule was performed with SrOH, with a single vibrational repumper, scattering ~ 100 photons per molecule in a single direction orthogonal to the molecular beam propagation axis. In this experiment, Kozyryev et al. (2016b) observed a resultant 0.2° deflection of the molecular beam. This work served as an initial proof of principle that polyatomic molecules could experience significant optical forces in a practical experimental configuration, and thus that direct laser cooling of polyatomic molecules should be possible. Extending optical cycling to $\sim 10^4$ photon scattering events would allow for radiation pressure slowing of molecular beams and capture into a magneto-optical trap.

The magnitude of the radiation pressure force is determined by the spontaneous decay rate, Γ , of the excited state. For a saturated two-level system, the force is $F_{\text{recoil}} = \hbar k\Gamma/2$. Larger optical forces can be applied using a coherent process, sometimes in combination with magnetic or electric field interactions, enabling many units p_{recoil} of momentum transfer per photon

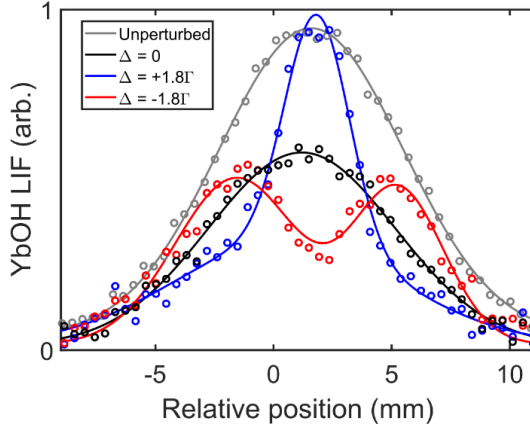


Figure 19: Spatial distribution of a YbOH molecular beam along the transverse direction, in the presence of Sisyphus heating ($\Delta = -1.8\Gamma$) and cooling ($\Delta = +1.8\Gamma$). In the cooling configuration, the on-axis flux is increased compared to an unperturbed beam. The double-peaked structure in the heating configuration arises from a balancing effect between Sisyphus heating and conventional Doppler cooling. Reproduced from Augenbraun et al. (2020b).

scattered. This approach was demonstrated for SrOH using the bichromatic force, in which two phase-locked laser beams (at different frequencies) pass through the molecular beam transversely and are retroreflected. Due to the presence of two laser frequencies, beat notes are formed and by tuning the distance between the molecular beam and retroreflecting mirror, the relative phase of the counterpropagating beats can be controlled. The resulting light field induces alternating cycles of stimulated absorption of a photon travelling in one direction, and stimulated emission of a photon travelling in the opposite direction. For a fixed detuning δ between frequency components, the maximum force is set by $F_{\text{BCF}} = \hbar k \delta / \pi$, which can vastly exceed F_{recoil} at large δ . Bichromatic force deflection was demonstrated using SrOH by Kozyryev et al. (2018). Calculations show that by employing four laser frequencies in a four-level system, which consists of two coupled two-level subsystems in bichromatic force configurations, large optical molasses forces should also be possible, as simulated by Wenz et al. (2020).

3.4. Transverse cooling

A more efficient method of imparting forces to polyatomic molecules, for a fixed number of scattered photons, is Sisyphus cooling. Specifically, magnetically-assisted transverse 1D Sisyphus cooling has been demonstrated

for SrOH, YbOH, and CaOCH₃ (Kozyryev et al. (2017); Augenbraun et al. (2020b); Mitra et al. (2020)). In all cases, the experimental configuration was very similar to that shown in Fig. 10, except that the lasers in the interaction region were partially overlapped with their retroreflections to form a standing wave. The bright molecular states (i.e., those addressed by the laser) are AC Stark shifted at the antinodes of the standing wave, but not at the nodes where the laser intensity vanishes. As a molecule in a bright state traverses the standing wave along the direction orthogonal to the primarily molecular beam direction, it gains or loses kinetic energy, depending on whether the laser detuning is red- or blue-detuned, respectively. To transversely cool a molecular beam, therefore, blue-detuned light is used. A molecule is preferentially likely to be optically pumped at higher laser intensities, and has a probability of order unity to populate a dark state, whose energy is unaffected by the laser light. As the molecule then traverses the region of the standing wave node, the bright and dark states come to near degeneracy and are mixed by magnetic fields, converting the dark state to a bright state with non-zero probability. The molecule is then free to “ride up” the potential hill again (in the blue-detuned configuration), losing more energy. The energy loss per photon scatter is limited only by the depth of the AC Stark shift, which is in turn limited by available laser power. At high laser intensities, therefore, Sisyphus cooling can be far more efficient per photon scatter at removing energy than conventional Doppler cooling.

The effect of Sisyphus cooling (or heating) can be observed by the reduced (or increased) thermal expansion of the molecular beam along the standing wave axis, as it propagates far downstream. An example of the effect of Sisyphus cooling on YbOH molecules, reported by Augenbraun et al. (2020b), is shown in Fig. 19. The authors also demonstrated Doppler cooling of the YbOH molecular beam, although the Sisyphus laser cooling produced a colder sample and was more efficient at cooling molecules on a per-photon basis. In future experiments, Doppler or sub-Doppler cooling could be used to increase the flux in molecular beam experiments or the loading efficiency into magneto-optical traps, as advocated by Alauze et al. (2021).

3.5. *Molecular deceleration*

Common trapping techniques used in laser cooling experiments generally have capture velocities that are considerably lower than the forward velocities of molecular beams, even those produced in CBGBs. Molecular MOTs, in particular, can typically only trap molecules with speeds below ~ 15 m/s

(Tarbutt and Steimle (2015); Williams et al. (2017); Langin and DeMille (2022)), while the forward velocities of molecular beams produced by CBGBs fall in the range of ~ 50 m/s to several 100 m/s (Hutzler et al. (2012)). Under certain optimized conditions, CBGBs with output velocities as low as 30 m/s–50 m/s have been observed for species such as CaF or CaOH; see Augenbraun et al. (2021a); Lu (2014). For heavier species, like YbOH, peak beam velocities as low as 20 m/s can be achieved, as shown in Augenbraun (2020). The molecules must be slowed as they travel from the beam source to the trap to a velocity at or below the capture velocity of the chosen trapping method. Significant work has been devoted to the slowing of atomic beams since the initial demonstration of slowing a beam of sodium atoms in 1981 by Phillips and Metcalf (1982). These efforts have helped guide recent efforts in slowing of molecular beams.

Slowing of atoms is often based on the radiation pressure forces due to a laser beam counterpropagating to the flow of atoms in an atomic beam. This laser addresses a closed electronic transition to continuously scatter photons. Importantly, as the atomic beam is slowed, the transition frequency of the cycling transition is shifted due to a gradually changing Doppler shift. This Doppler shift must be compensated during slowing, and three principal methods to accomplish this have been demonstrated with atoms. Two of these techniques, white-light slowing (Zhu et al. (1991)) and chirped slowing (Ertmer et al. (1985)) have been successfully extended to diatomic molecules (Barry et al. (2012); Zhelyazkova et al. (2014); Hemmerling et al. (2016); Yeo et al. (2015); Truppe et al. (2017a)). In white-light slowing, the slowing light is frequency-broadened to create “white light” that covers the full range of the Doppler shift, whereas in chirped slowing, the frequency of the slowing light is narrow-band but rapidly shifted, or “chirped” to match the changing Doppler shift as the particles decelerate. Zeeman slowing (Phillips and Metcalf (1982)) is one of the most efficient and popular techniques used for atoms. This method uses the Zeeman shifts induced by a spatially varying magnetic field to compensate for the changing Doppler shift, keeping the laser light resonant with atoms as they are slowed. The type of transitions that are typically used for laser cooling of molecules, namely transitions in which $J' \geq J$, makes it challenging to adapt Zeeman slowing to molecules, although this approach is potentially viable and being pursued by Petzold et al. (2018a,b). The review paper by Fitch and Tarbutt (2021) provides a comprehensive overview of laser deceleration of diatomic molecules.

3.5.1. Radiative slowing

Due to the presence of many rotational and vibrational degrees of freedom, beams of polyatomic molecules are generally more difficult to decelerate than are atoms or diatomic molecules. Radiative slowing requires scattering of thousands of photons per atom/molecule, which is difficult to achieve for polyatomic molecules due to vibrational branching, as described previously. While sufficient optical cycling for radiative slowing has been achieved for diatomic molecules by repumping just 1 or 2 vibrational stretching modes, a much larger number of vibrational modes must be addressed for polyatomic molecules. By choosing to work with polyatomic molecules that have favorable VBRs, it is possible to use a reasonable number of laser wavelengths to scatter sufficiently many photons to achieve radiative slowing of a molecular beam, e.g., to the capture velocity of a magneto-optical trap. White-light slowing was demonstrated for CaOH molecules, as reported by Vilas et al. (2022) and reviewed in detail below.

In order to achieve radiative slowing of any species, a photon cycling scheme capable of scattering the required number of photons must first be established. Assuming a molecular mass of m , an initial beam velocity of v_{beam} , and wavenumber k for the scattered photons, the number of photons needed for slowing is of order $n_{\text{slowing}} \sim v_{\text{beam}}/v_{\text{recoil}} = mv_{\text{beam}}/\hbar k$. For smaller polyatomic molecules, typical values of n_{slowing} are of order $\sim 10^4$. Radiative slowing of a polyatomic molecule therefore will typically require repumping enough rovibrational decays to limit branching to dark states to the $\sim 10^{-4}$ level. Considering CaOH and using the values $m_{\text{CaOH}} = 57$ amu, $v_{\text{beam}} = 140$ m/s, and $k = 2\pi/(626 \text{ nm})$, the number of photons required for slowing is $n_{\text{slowing}} \sim 12,500$. The electronic transition chosen for cycling in CaOH is the $\tilde{A}^2\Pi_{1/2}(000)(J' = 1/2, p' = +) \leftarrow \tilde{X}^2\Sigma^+(000)(N = 1, p = -)$ transition, which is both rotationally closed and has favorable vibrational branching ratios: by repumping spontaneous decay to 11 rovibrational states, an average of $\sim 12,000$ photons are scattered per molecule before a $1/e$ fraction of the molecules has decayed to unaddressed dark states. In other words, about a $1/e$ fraction of the molecules in the molecular beam will, in principle, scatter enough photons to be slowed to zero velocity. A diagram for the corresponding optical cycling scheme is shown in Fig. 11. In the slowing of CaOH molecules, all 11 transitions were addressed by separate repumping laser beams that were overlapped and coaligned with the main slowing laser beam counterpropagating to the molecular beam. This required combining a

total of 12 lasers of different wavelengths varying from 566 nm to 651 nm into a single beam, which was accomplished using a series of dichroic beamsplitters. The overlapped beams were passed through an electro-optic modulator (EOM) that produced a frequency-broadened spectrum able to address all velocity classes between about 0 m/s and ~ 140 m/s (the initial velocity of the molecular beam).

The primary slowing force came from driving the $\tilde{A}^2\Pi_{1/2}(J' = 1/2, p' = +) \leftarrow \tilde{X}^2\Sigma^+(N = 1, p = -)$ transition. As will be discussed in Sec. 3.6, this is a type-II transition, characterized by the existence of dark states in the ground state manifold. For any chosen polarization of the slowing light, there exist dark states into which a molecule may be optically pumped; after such an optical pumping event, that molecule will stop scattering photons from the slowing light. These dark states must be destabilized for continued photon scattering during slowing. In the experiment described by Vilas et al. (2022), this was achieved by switching the polarization of the slowing light between two orthogonal polarizations. Crucially, the dark states of the two polarizations are distinct, so continued photon scattering can be achieved. The photon scattering rate achieved for CaOH molecules in the deceleration scheme was observed to be around 1–2 MHz, similar to that achieved for diatomic molecules.

Figure 20(a) shows a characteristic velocity profile for an unslowed beam of CaOH molecules, as well as the velocity profile of the molecular beam following slowing. While the population of molecules with initial velocities below 50 m/s is negligible, the slowed distribution shows significant accumulation of molecules at velocities as low as 10–20 m/s. Time-resolved measurements of the molecular beam with and without slowing light applied are shown in Fig. 20(b). Here, slowing of the molecular beam is evident from the late arrival of a significant portion of the slowed beam, as compared to the unslowed beam. Finally, we note that, while a large number of different laser frequencies was used to address the various vibrational repumping transitions, the total slowing power (~ 2.5 W) is similar to that used for diatomic molecules. This is because most of the repumping laser beams contained relatively low power (10–100 mW).

3.5.2. Zeeman-Sisyphus deceleration

Despite the success of radiative slowing for CaOH molecules, the large number of photons that must be scattered off of each molecule to be slowed makes the method difficult to implement in general. Larger molecules, or

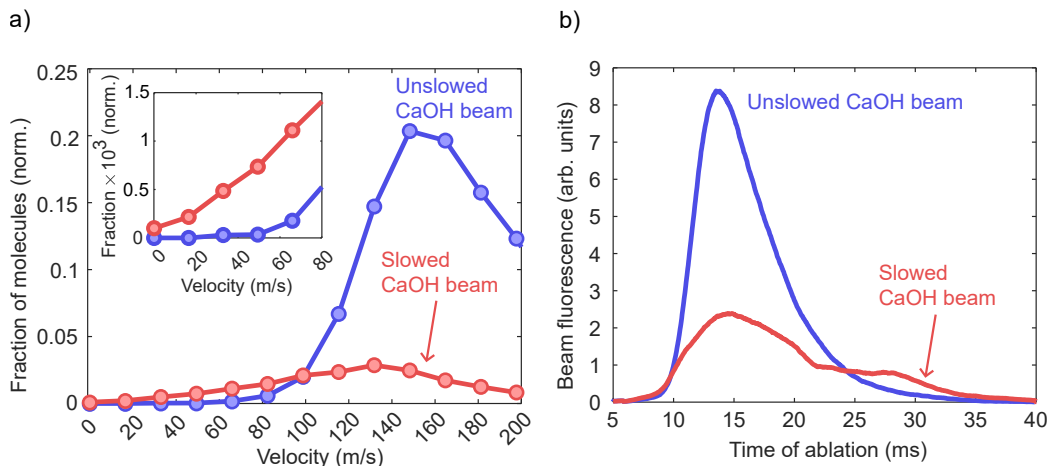


Figure 20: (a) Fraction of molecules detected as a function of velocity for both an unsloved (blue) and sloved (red) beam of CaOH molecules. Populations are detected by a Doppler-sensitive fluorescence signal. Inset: Accumulation of population at low velocities when slowing light is applied. (b) Time-resolved laser-induced fluorescence from unsloved (blue) and sloved (red) beams of CaOH molecules.

molecules with more complex level structure, may have insufficiently diagonal FCFs to support such a photon budget. For this reason, it is desirable to develop other methods of molecular beam deceleration that do not depend on the radiation pressure force. The alkaline-earth-containing polyatomic molecules that we have focused on are polar radicals, implying that interactions with either electric or magnetic fields can lead to energy-level shifts that could be used to manipulate molecular motion.

One example of such a method that has been experimentally demonstrated for laser-coolable polyatomic molecules is Zeeman-Sisyphus (ZS) deceleration. In a ZS decelerator, originally proposed by Comparat (2014) and expanded on by Fitch and Tarbutt (2016), one leverages the large energy shifts induced by Tesla-scale magnetic fields. The principle of the ZS decelerator is depicted in Fig. 21. The deceleration scheme is highly reminiscent of the process used by Lu (2014) to slow and load CaF molecules into a magnetic trap. In brief, molecules in a weak-field-seeking (WFS) state are incident on a region of increasing magnetic field magnitude and decelerate as they climb the potential. Near the magnetic field maximum, the molecules are optically pumped through an electronically excited state to a strong-field-seeking (SFS) state and continue to decelerate as they exit the

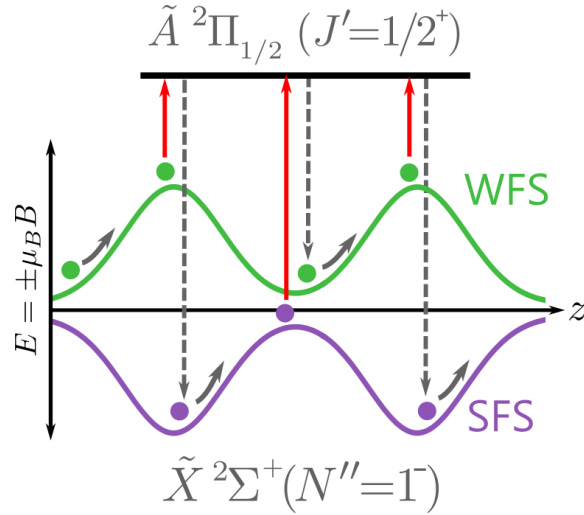


Figure 21: Overview of the Zeeman-Sisyphus deceleration scheme. Molecules enter the magnetic field region in a weak-field-seeking state and decelerate as they travel toward the peak magnetic field. At the peak magnetic field, molecules are optically pumped to a strong-field-seeking (SFS) state and continue to decelerate. Near the field minimum, molecules are pumped back to the weak-field-seeking (WFS) state and the process can be repeated for additional deceleration.

high-field region. In this way, an energy $\Delta E_{\text{stage}} \approx 2\mu_B \mathcal{B}_{\text{max}}$ can be removed from molecules passing through each deceleration stage, where μ_B is the Bohr magneton and \mathcal{B}_{max} is the maximum magnetic field in the high-field region. This process can be repeated to remove additional energy. Furthermore, the deceleration applies to all molecules regardless of their arrival time, and thus is effective for continuous (or long-pulsed) molecular beams. Because a fixed *energy* is removed in each stage, the decelerator will slow to rest $1\mu_B$ molecules of any mass produced at or below the same threshold temperature.

ZS deceleration was first tested experimentally using CaOH molecules by Augenbraun et al. (2021a). The experimental setup comprised a set of superconducting coils, shown in Fig. 22. Our particular decelerator comprises two magnets with $\mathcal{B}_{\text{max}} \approx 2.8$ T, leading to $\Delta E_{\text{stage}} \approx 3.8$ K. The total energy removal for two stages (~ 7.6 K) is therefore well matched to CBGBs, which can have typical kinetic energies $E_{\text{kin}} \lesssim 8$ K. There is some overhead associated with superconducting coils (principally the use of a cryocooler). Nonetheless, the use of superconducting coils leads to a number of technical advantages as compared to permanent magnet designs. First and foremost,

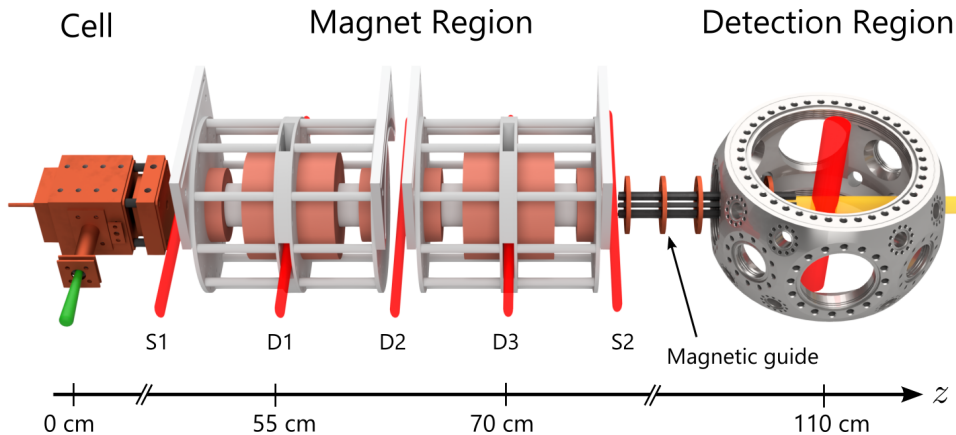


Figure 22: Schematic of the Zeeman-Sisyphus decelerator (not to scale). Molecules are produced in a two-stage cryogenic buffer-gas beam. They travel through two superconducting magnets in Helmholtz configuration and are optically pumped in three deceleration pumping regions (D1, D2, D3) by transverse laser beams at 626 nm. State-preparation regions (S1 and S2) pump molecules into WFS states in order to populate magnetically guidable states. Molecules are detected via laser-induced fluorescence.

stronger magnetic fields can be achieved over a larger bore. The superconducting design is necessary to achieve peak fields $\mathcal{B}_{\max} \lesssim 4$ T over bores a few cm in diameter. That is, a superconducting coil can simultaneously enable greater deceleration per stage and larger spatial acceptances. Second, the cryogenic apparatus required to support the superconducting coils naturally leads to excellent vacuum due to high-speed cryopumping. Third, superconducting coils can easily be designed with transverse optical access in order to drive laser transitions only at particular positions along the solenoids. Performing optical pumping in a spatially selective way eliminates concerns about “accidental” resonances along the slowing path (which could lead to population loss) and minimizes Zeeman broadening (which reduces the laser power requirements).

The results of ZS deceleration of CaOH under optimal optical pumping performance in all pumping regions is shown in Fig. 23 (Augenbraun et al. (2021a)). Compared to the unperturbed molecular beam, when the optical pumping light is applied the fraction of slow molecules rises to 24(3)% below 20 m/s and 3.5(5)% below 10 m/s. The fraction of slow molecules is therefore enhanced by at least two orders of magnitude following deceleration. Based on the calibration of the fluorescence collection and the estimated number of

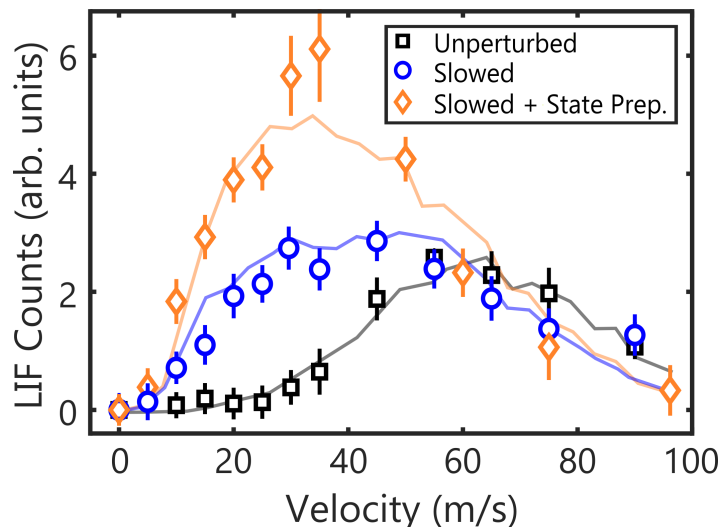


Figure 23: CaOH velocity distributions with (blue circles) and without (black squares) Zeeman-Sisyphus deceleration applied. Also shown (orange diamonds) is the velocity distribution when all molecules are pumped into WFS states in region S1 as they enter the decelerator. Solid lines are the results of Monte Carlo trajectory simulations that take into account the three-dimensional field profile inside the decelerator.

molecules in the unperturbed beam, this means that approximately 3×10^4 molecules per pulse are found in velocity classes capturable by traps (e.g., MOT or magnetic). The solid lines in Fig. 23 are the results of Monte Carlo simulations that take as input experimentally measured laser parameters and accurate, three-dimensional magnetic field profiles for both the superconducting coils and the magnetic guide. We find excellent agreement between the simulations and experimental results, indicating that the details of the slowing process are modeled accurately.

Based on measurements of the optical pumping into higher-lying vibrational states, it was found that fewer than 10 photons were scattered per molecule in the optical pumping steps to decelerate a CaOH molecule near the peak of the distribution by $\Delta v_f \approx 35$ m/s. By contrast, the radiative force due to 10 scattered photons would slow a CaOH molecule by just $\Delta v_f \approx 0.1$ m/s. This clearly indicates the promise of ZS deceleration to slow molecules for which radiation pressure force slowing would be impractically difficult due to a limitation on the number of photon scattering events that can be realized. More recently, ZS deceleration has been extended to the complex polyatomic molecule YbOH by Sawaoka et al. (2022). Again

molecules with velocities below 20 m/s were produced.

3.6. Magneto-optical trapping

The magneto-optical trap (MOT) is an essential tool in atomic physics and, in particular, a key ingredient for producing ultracold samples of atoms with sufficiently high numbers (and densities) to be useful for subsequent science experiments. In brief, MOTs are based on radiation forces from six orthogonal laser beams, combined with a quadrupole magnetic field to tune the lasers into/out of resonance depending on position (Phillips (1998); Chu (1998)). By choosing the polarization appropriately, the trapped particles can be made to scatter photons preferentially from lasers that push them toward the center of the trap. This results in simultaneous trapping and rapid cooling to temperatures near the Doppler limit. An essential challenge in realizing MOTs for molecules is that they rely on the ability to cycle a large number of photons, typically at scattering rates of at least ~ 100 kHz. Nonetheless, over the past decade magneto-optical trapping has been achieved for a number of diatomic molecules. In this section, we describe recent developments in extending magneto-optical trapping to polyatomic molecules, particularly the recent demonstration of a MOT for CaOH. The following discussion is based on the same experiment that was discussed in section 3.5.1 on radiative slowing of CaOH.

The CaOH MOT used the same rotationally-closed cycling transition as was used for laser slowing, i.e., $\tilde{A}^2\Pi_{1/2}(000)(J' = 1/2, p' = +) \leftarrow \tilde{X}^2\Sigma^+(000)(N = 1, p = -)$. The photon cycling scheme discussed in Sec. 3.5.1 allows CaOH molecules to scatter $\sim 12,000$ photons in the MOT before $1/e$ of the population remains in bright states. In the experiment, the 11 repumping lasers that were used for slowing also covered the volume of the MOT; the same laser beams were used for both slowing and the MOT. Most of the repumping lasers used to achieve radiative slowing and a MOT for CaOH did not require much laser power, see Fig. 25(b). While laser power requirements in laser cooling experiments with polyatomic molecules will generally depend on the exact photon cycling scheme used for the given molecule, the observed powers needed for CaOH provide a preliminary indication of the technical requirements for laser systems in laser cooling of polyatomic molecules.

Coupling of the electron spin and rotational degrees of freedom splits the $\tilde{X}^2\Sigma^+(000)(N = 1)$ level into two spin-rotation (SR) components spaced by ~ 52 MHz, with total angular momenta of $J = 1/2$ and $J = 3/2$. To address both SR components in the MOT, the MOT laser light includes two frequency

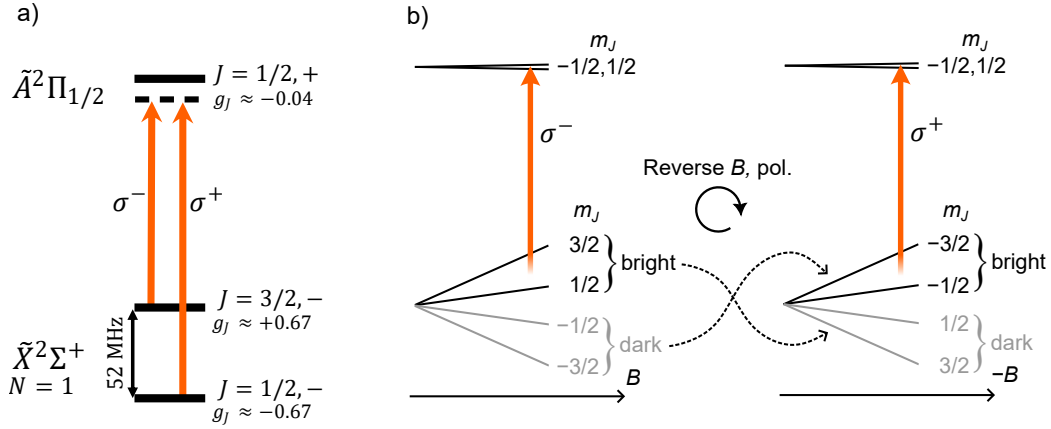


Figure 24: Overview of the CaOH laser cooling and RF MOT scheme. (a) The level structure of the main cycling transition used in the CaOH MOT, and the polarization configuration of the two frequency components of the MOT light. Since the $J = 1/2$ and $J = 3/2$ components have g -factors of opposite sign, each component is addressed with opposite polarization. Reproduced from Vilas et al. (2022). (b) The magnetic sublevels of the $J = 3/2 \leftarrow J' = 1/2$ transition for the two configurations of the RF MOT. Magnetic dark states of each configuration are indicated.

components separated by the SR splitting, as shown in Fig. 24(a). The small hyperfine splittings in $\tilde{X}^2\Sigma^+(000)(N = 1)$ of ~ 1 MHz were unresolved by the MOT light, so additional laser frequencies were not required to address hyperfine sublevels.

The transitions addressed in the CaOH MOT, $J' = 1/2 \leftarrow J = 1/2$ and $J' = 1/2 \leftarrow J = 3/2$, are both type-II transitions, characterized by $J' \leq J$. A defining characteristic of type-II MOTs is the presence of magnetic dark states, which arise because the ground state has more sublevels than the excited state. (A detailed description of the physics of type-II MOTs, and their comparison to type-I MOTs, was given by Tarbutt (2015); Tarbutt and Steimle (2015).) As described in Sec. 3.5.1, these dark states must be destabilized in order to generate trapping forces in the MOT, which derive from repeated photon scattering. A common strategy to achieve this dark-state remixing is to rapidly switch the polarization of the MOT light while simultaneously alternating the direction of the magnetic field gradient. The switching occurs at a rate similar to the rate at which molecules pump into dark states, typically 1 – 2 MHz, leading to the moniker radio-frequency (RF) MOT (Norrsgard et al. (2016)). Figure 24(b) illustrates the situation

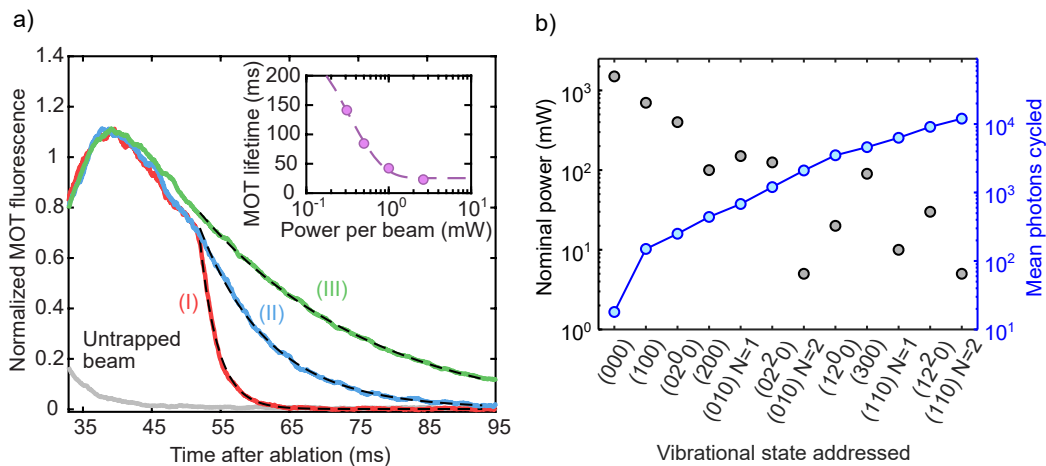


Figure 25: (a) Fluorescence signal from the CaOH MOT as a function of time after the molecules were produced. In the three curves (I), (II), and (III), different repumpers were turned off at ~ 50 ms to limit the average number of scattered photons per molecule to 1200, 4600, and 12,000, respectively. Dotted lines are exponential fits to extract lifetimes, of 2.60(3) ms, 10.1(2) ms, and 25.7(6) ms for (I)-(III). Inset: MOT lifetime as a function of MOT beam power. (b) Laser power required by each of the repumping lasers (denoted by the ground vibrational state addressed) used in the CaOH photon cycling scheme. Reproduced from Vilas et al. (2022).

for CaOH, showing how the RF switching destabilizes dark states to provide a trapping force and allows for continuous scattering from the laser beams that provide a restoring force toward the center of the MOT. A separate approach, known as a dual-frequency MOT, has been used for diatomic molecules and is likely to be possible for polyatomic molecules (Tarbutt and Steimle (2015); Truppe et al. (2017b); Ding et al. (2020)).

Vilas et al. (2022) produced an RF MOT of CaOH molecules containing $2.0(5) \times 10^4$ molecules trapped at a peak density of $n = 3.0(8) \times 10^8 \text{ cm}^{-3}$. The temperature of the molecules ($T = 870(50) \mu\text{K}$), the damping constant ($\beta = 455(85) \text{ s}^{-1}$), and oscillation frequency ($\omega = 2\pi \times 59(4) \text{ Hz}$), were all comparable to values characteristic of MOTs of diatomic molecules.⁶ The lifetime of the CaOH MOT was limited by photon scattering causing population to accumulate in rovibrational states that are not addressed by the

⁶Here, the damping constant β and oscillation frequency ω result from the common approximation of the MOT forces as a damped harmonic oscillator, $F/m = -\beta v - \omega^2 r$, where v and r are the velocity and position in the trap, respectively.

photon cycling scheme, as shown in Fig. 24(a). The maximum achieved lifetime was ~ 150 ms, similar to the timescale observed for diatomic molecules but much shorter than the lifetimes that can be realized in atomic MOTs. The characteristic damping time of the CaOH MOT—the time to compress the captured cloud of molecules—was an order of magnitude shorter than the lifetime, enabling full cooling and compression before the trapped molecules were lost to vibrational dark states.

The temperature of the CaOH MOT was relatively high compared to the Doppler limit (around $150 \mu\text{K}$), a situation that is common in type-II MOTs. This prevents direct loading from the MOT into conservative traps, such as optical traps, which have relatively low trap depths. The elevated temperature arises from polarization-gradient forces due to the presence of dark states in type-II transitions; we discuss these forces in more detail in Sec. 3.7.

3.7. Sub-Doppler cooling

As discussed in Sec. 3.6, dark states present in the optical cycling scheme of molecular MOTs can lead to relatively high temperatures for the trapped molecules. A variety of techniques have been developed to cool the molecules to lower temperatures, and many of these have been applied to polyatomic molecules. We discuss these methods here, using CaOH as a representative test case.

3.7.1. Grey molasses

As mentioned previously the temperature limitation in the MOT is due to a Sisyphus-like heating effect. This can be turned into a cooling effect by detuning the cooling light to the blue of resonance. Because photon cycling is achieved on an $F \rightarrow F$ and $F \rightarrow F - 1$ transition, dark states are present. This means the ground state manifold has both bright and dark states. The bright states, when blue detuned, are shifted above the dark state and are sinusoidally modulated due to the AC stark shift, Fig. 26(a). An atom or molecule in the ground state will move across this spatially varying potential, undergoing motional coupling from the dark state to be bright state. The atom or molecule then moves up the potential hill and is driven to the excited state where it will then decay back into the dark state. This cycle repeats, each time cooling the particle by an energy proportional to the amplitude of the AC stark modulation. This is commonly referred to as grey molasses cooling as it is a mix of a bright and dark molasses.

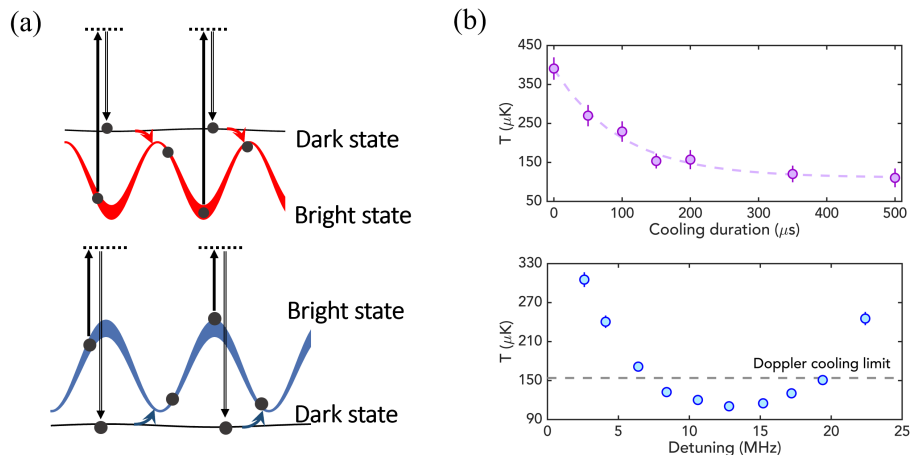


Figure 26: (a) Illustration of the grey molasses effect. Molecules are optically pumped into dark states near the antinodes of an intensity standing wave and then transit from dark to bright states near the standing wave’s nodes. (b) Grey molasses cooling of CaOH. Top: Temperature as a function of cooling duration Bottom: Temperature as a function of sub-Doppler detuning Δ_{SD} . Reproduced from Vilas et al. (2022).

Grey molasses cooling was first successfully demonstrated in molecules by Truppe et al. (2017c), who focused on the molecule CaF. This cooling method was extended to polyatomic molecules by Vilas et al. (2022), who used CaOH. It was found that, in the CaOH experiment, optimal cooling occurs at a detuning of 13 MHz (see Fig. 26(b)). The temperature increases for higher detuning due the cooling light being red-detuned relative to the $J = 1/2$ state. The observed (exponential) timescale for cooling is less than about 0.5 ms, indicating that the cooling is relatively rapid.

3.7.2. Λ -enhanced grey molasses

Standard grey molasses is often limited to temperatures $\sim 100 \mu\text{K}$ and more advanced schemes are required to reach lower temperatures. Two such techniques that have been successfully demonstrated in ultracold molecules are Λ -enhanced grey molasses (Cheuk et al. (2018); Langin et al. (2021)) and single frequency (SF) cooling (Caldwell et al. (2019)). Both techniques rely on creating velocity-dependent dark states.

Λ -enhanced grey molasses cooling combines grey molasses with velocity selective coherent population trapping (VSCPT) (Aspect et al. (1988)). The VSCPT mechanism relies on the creation of coherent dark states present in

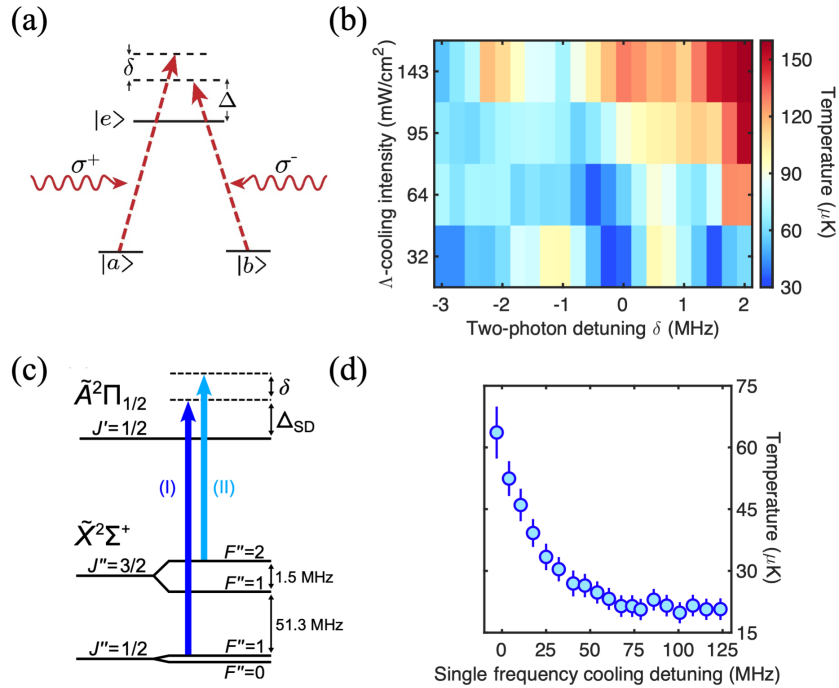


Figure 27: (a) Simple picture of the level structure used in Λ -enhanced grey molasses cooling. Ground states $|a\rangle$ and $|b\rangle$ are coupled to excited state $|e\rangle$ with single-photon detuning Δ and two-photon detuning δ . (b) Temperature vs. two-photon detuning and cooling intensity for Λ -enhanced grey molasses cooling of CaOH . (c) Level scheme used in Λ -enhanced grey molasses and single-frequency cooling. Λ -enhanced cooling uses both frequencies, while only laser (I) is used for single-frequency cooling. (d) Temperature vs. detuning for single-frequency cooling of CaOH . Reproduced from Cheuk et al. (2018) and Hallas et al. (2022).

multi-level systems, as shown in Fig. 27(a). With counter-propagating circularly polarized laser beams, a superposition of two states (called $|a\rangle$ and $|b\rangle$ for generality) can be formed where the transition amplitudes destructively interfere to form a dark state. The dark state does not persist to large non-zero velocities because in that case the two beams are not at the same frequency (due to opposite Doppler shifts). While VSCPT cooling can reach sub-recoil temperatures in atoms, it is slow and inefficient, relying on random walks to cool toward zero velocity. However, by combining VSCPT cooling with grey molasses, the cooling no longer relies solely on a random walk, as the grey molasses provides a restoring force towards zero velocity and the VSCPT effect traps the atoms or molecules near zero velocity. However, the

presence of grey molasses forces reduces the extent to which the zero-velocity state is “dark,” raising the minimum temperature achievable by this type of cooling. This Λ -enhanced grey molasses cooling method was first demonstrated on the D1 lines of alkali atoms (Grier et al. (2013)) and later in CaF molecules (Cheuk et al. (2018)).

Λ -enhanced grey molasses cooling can be naturally extended to polyatomic molecules. In CaOH, this was achieved by coupling two hyperfine levels in the $\tilde{X}^2\Sigma^+(N = 1)$ manifold to the $\tilde{A}^2\Pi_{1/2}(J' = 1/2)$ excited state (Hallas et al. (2022)). Specifically, the $\tilde{X}^2\Sigma^+(J = 3/2, F = 2)$ and $\tilde{X}^2\Sigma^+(J = 1/2)$ levels are addressed with σ^- and σ^+ polarization, respectively. Both frequency components are blue-detuned by a common amount Δ_{SD} of about 12 MHz, and the two-photon detuning δ is varied.

The dependence of Λ -enhanced grey molasses cooling on both δ and I_{SD} is shown in Fig. 27(b). The lowest measured temperature, $T_{\text{min}} = 34 \mu\text{K}$, occurs at $\delta \approx 0$ MHz. A second, slightly higher local temperature minimum is observed at $\delta \approx 1.5$ MHz, which corresponds to the two-photon resonance for the Λ -system consisting of $\tilde{X}^2\Sigma^+(J = 3/2, F = 1)$ and $\tilde{X}^2\Sigma^+(J = 1/2)$. At higher intensities, the temperature is minimized at increasingly negative δ because of the AC Stark shifts of the hyperfine levels coupled in the Λ -enhanced grey molasses: for higher intensities, the levels move further apart, and smaller δ is required to satisfy the two-photon resonance condition.

3.7.3. Single-frequency cooling

A primary limitation of Λ -enhanced grey molasses cooling is the fact that the dark states are destabilized by off-resonant scattering from the two laser frequencies interacting with nearby states. Single-frequency cooling solves this by creating dark states with a single laser frequency at large detuning, reducing this effect. This cooling method was first demonstrated for molecules by Caldwell et al. (2019), who used CaF molecules in their experiment.

Single-frequency cooling can also be implemented in polyatomic molecules, as was shown with CaOH by Hallas et al. (2022). By applying light blue-detuned by an amount Δ_{SD} (about 70 MHz) from the $\tilde{A}^2\Pi_{1/2}(J = 1/2) \leftarrow \tilde{X}^2\Sigma^+(N = 1, J = 1/2)$ transition, a minimum temperature $T_{\text{min}} = 20 \mu\text{K}$ was realized (Fig. 27(c-d)). The cooling was observed to be insensitive to detuning above a certain value ($\Delta_{\text{SD}} \approx 70$ MHz), Fig. 27(d). This insensitivity is beneficial for cooling molecules into an ODT, where trap-induced light

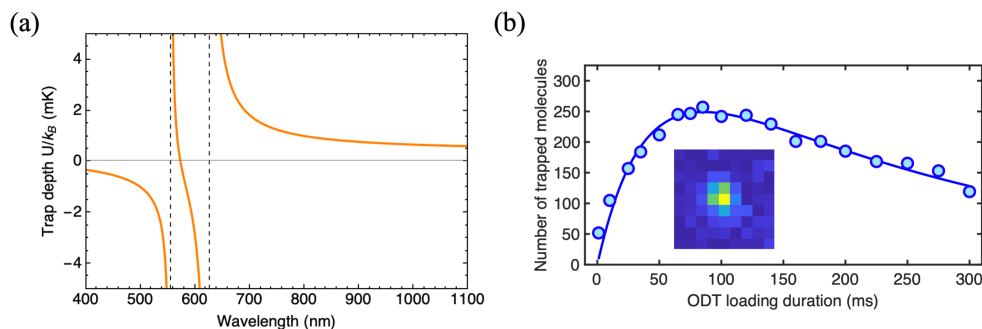


Figure 28: (a) Trap depth vs. wavelength for an optical dipole trap (ODT) of CaOH generated from a 13 W laser with a $25 \mu\text{m}$ waist. (b) Loading of CaOH molecules into an ODT. Reproduced from Hallas et al. (2022)

shifts can affect the cooling efficiency.

3.8. Optical trapping

Due to the availability of high-power fiber lasers, optical trapping has become a popular method to trap ultracold atoms and diatomic molecules. Optical trapping has several key advantages, including the ability to trap atoms and molecules irrespective of their internal state, and the ability to greatly increase phase space density due to the small trap volume. However, laser cooling of molecules inside an optical trap can be hindered by a variety of effects, including differential AC Stark shifts. Optical dipole traps consist of tightly focused Gaussian beams, which in combination with the induced Stark shift on the molecules, creates a harmonic confining potential for the molecules. This potential is wavelength-dependent, and the dependence can be quite complicated due to the many levels present in molecules. In the limit of large detuning from an electronic transition, the strength of the trapping potential is inversely proportional to the detuning. Caldwell and Tarbutt (2020) provide details on calculating Stark shifts for molecules in trapping laser fields. The trap depth as a function of wavelength for the polyatomic molecule CaOH, in the large-detuning limit, is shown in Fig. 28(a).

Optical trapping of directly laser-cooled molecules was first demonstrated with CaF (Anderegg et al. (2018)). To efficiently load molecules into the optical dipole trap, the molecules must be cooled into the trap. This was accomplished with CaF by overlapping a far detuned 1064 nm laser with the cloud of molecules during grey molasses cooling. As the molecules traversed the optical trapping light, the grey molasses cooled the molecules, loading

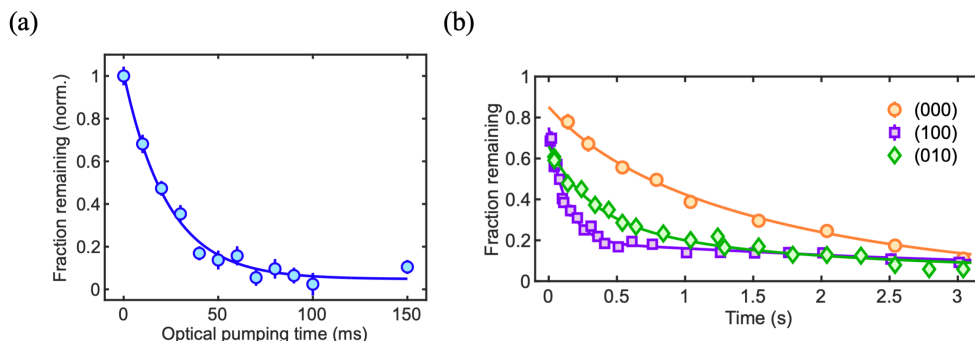


Figure 29: (a) Optical pumping of optically trapped CaOH molecules into the $\tilde{X}(010)$ bending vibrational mode via single frequency cooling with the $\tilde{X}(010)$ repumping laser removed. (b) Lifetime of optically trapped CaOH molecules in the $\tilde{X}(000)$, $\tilde{X}(010)$, and $\tilde{X}(100)$ vibrational levels. The solid curves are fits to a rate equation model capturing blackbody excitation and radiative decay along with vacuum losses. Reproduced from Hallas et al. (2022)

them into the trap and increasing their density. Using Λ -enhanced grey molasses, the transfer efficiency into the ODT was greatly improved (Cheuk et al. (2018)).

Optical trapping of CaOH was demonstrated in much the same fashion (Hallas et al. (2022)). Figure 28(b) shows the loading of CaOH molecules into an ODT from the single-frequency grey molasses cloud. ODT loading is relatively inefficient, typically transferring only 1 – 10% of the molecules from the molasses. This could be improved by employing new cooling and trapping techniques, such as blue-detuned optical traps (Lu et al. (2022)) and blue-detuned MOTs (Jarvis et al. (2018)), where molecules may be directly loaded from the MOT. Recent work by Bureau et al. (2022) has demonstrated the advantages of a blue-detuned MOT for the diatomic radical YO. The additional substructure present in polyatomic species has not been found to hinder the optical trapping process in any significant way. Generically, however, the increased density of states in larger polyatomic molecules may increase the likelihood of unwanted excitations, e.g. due to “accidental” resonances or via Raman or multi-photon processes.

Along with trapping of CaOH molecules in the $\tilde{X}(000)$ vibrational ground state, Hallas et al. (2022) demonstrated trapping of CaOH in the excited $\tilde{X}(010)$ bending vibrational state and the $\tilde{X}(100)$ stretching vibrational level. Trapped molecules were optically pumped into these states by applying a

single-frequency molasses while turning off the corresponding vibrational re-pumping laser. For the $\tilde{X}(010)$ bending mode the optical pumping requires 1200 photon scattering events before the average molecule vibrationally decays, corresponding to an optical pumping timescale of 23 ms (Fig. 29(a)). Optical pumping into the $\tilde{X}(100)$ stretching mode was much faster due to the large branching ratio to this state ($\sim 5\%$). Fig. 29(b) shows measurements of the lifetime of CaOH molecules trapped in each of the $\tilde{X}(000)$, $\tilde{X}(010)$, and $\tilde{X}(100)$ states. It was found that the ground state lifetime was limited primarily by room-temperature blackbody excitation to excited vibrational levels and by imperfect vacuum, while the excited state lifetimes were shorter due to spontaneous, radiative decay back to the vibrational ground state (Hallas et al. (2022)). The lifetimes of all three states could be improved by cooling the surrounding environment to reduce blackbody radiation-induced losses.

3.9. Preparation and coherent control of single quantum states

Following sub-Doppler cooling and ODT loading, the trapped molecular population is distributed over multiple hyperfine sublevels. The many internal states present in polyatomic molecules complicate the task of transferring this population into a single quantum state. An optical pumping sequence for CaOH, shown in Fig. 30(a), is used to populate a single quantum state in the $\tilde{X}^2\Sigma^+(010)(N = 1^-)$ vibrational bending mode. This bending mode is of interest because it is precisely the state proposed for use in various quantum computation or precision measurement experiments (Kozyryev and Hutzler (2017); Yu et al. (2019)). Following optical pumping into the bending mode as described in the previous section, the molecular population is spread across twelve hyperfine states. To prepare the molecules in a single quantum state, a microwave-optical pumping sequence is employed; microwave transitions allow hyperfine splittings below the linewidth of optical transitions to be resolved, while optical excitation provides the dissipation necessary for single state preparation. In CaOH, molecules can be prepared in the $(N = 1, J = 1/2^-, F = 0)$ state using the following sequence. Microwaves are first used to drive population from the $(N = 1, J = 3/2^-)$ state to the $(N = 2, J = 3/2^-)$ level. A small electric field is applied to mix states of opposite parity and thereby lend transition strength to this nominally forbidden transition. An optical transition then drives population from $(N = 2, J = 3/2^-)$ to the excited $\tilde{A}(010)\kappa^2\Sigma^{(-)}(J = 1/2^+)$ electronic

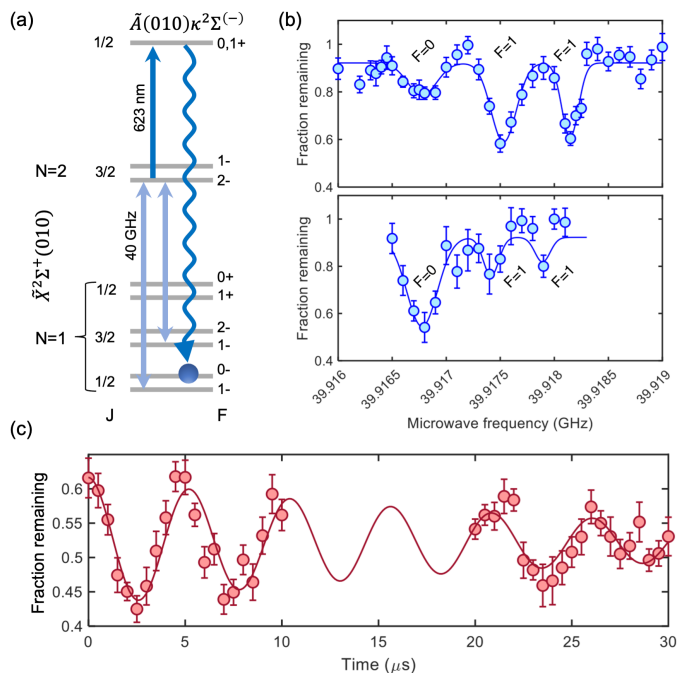


Figure 30: Demonstrations of coherent control of CaOH molecules. (a) Level diagram showing the microwave/optical pumping steps used to transfer population to a single quantum state. (b) Microwave spectroscopy showing $F = 0$ and $F = 1$ population before and after optical pumping into $F = 0$. (c) Coherent Rabi oscillations driven with 40 GHz microwaves between the $N = 1$ and $N = 2$ levels of optically trapped CaOH molecules in the $\tilde{X}(010)$ bending mode. Panel (a) is adapted from Anderegg et al. (2023).

state, which decays to the $F = 0$ (the target state) and $F = 1$ levels of the $(N = 1, J = 1/2^+)$ manifold. This sequence is then repeated, but with the microwaves driving population in $(N = 1, J = 1/2^+, F = 1)$ to $(N = 2, J = 3/2^-)$, where molecules are again optically excited and pumped into the target $F = 0$ state. Spectroscopy scans of the $(N = 1, J = 1/2^+)$, $F = 0$ and $F = 1$ states before and after optical pumping are plotted in Fig. 30(b), showing that the population of the $F = 0$ state is greatly enhanced. The population in the $F = 0$ state can then be transferred to the desired target state and any remaining molecules that were not successfully transferred can be pushed out of the trap using resonant laser light. Rabi oscillations between states can also be driven, as shown in Fig. 30(c). In CaOH, hyperfine splittings are approximately 1 MHz, meaning that Rabi frequencies <1 MHz are necessary in order to avoid off-resonant excitation.

4. Outlook and challenges

4.1. Toward larger molecules

One of the underlying trends in the quest to laser cool polyatomic molecules has been a drive to control increasingly large and complex molecules. Nearly from the first proposals to laser cool polyatomic molecules, by both Isaev and Berger (2016) and Kozyryev et al. (2016a), authors were identifying molecules with five or more atoms that appeared to have FCFs sufficiently diagonal to admit direct laser cooling. These proposals relied critically on the concept eventually dubbed an “optical cycling center,” such as the MO (M=Ca,Sr,Yb, etc.) moiety that has formed the core of the laser cooling experiments described throughout this review.

More recently, theoretical work has identified an even wider range of aromatic molecules that can be adorned with optical cycling centers, including phenols (and derivatives; Dickerson et al. (2021a); Ivanov et al. (2020a)), polycyclic arenes (Dickerson et al. (2021b)), and fully saturated hydrocarbons (Dickerson et al. (2022)). Remarkably, Dickerson et al. (2021a) were even able to show that substitutions around a cyclic hydrocarbon could be used to *tune* the FCFs of the metal-centered excitations using simple principles from organic chemistry—a capability that is only possible in large polyatomic species. Experimental verification of these theoretical predictions has been obtained by Zhu et al. (2022); Mitra et al. (2022); Augenbraun et al. (2022); Lao et al. (2022), who have synthesized both phenol and naphthol derivatives adorned with Ca- and Sr-based optical cycling centers and shown that these molecules indeed have the properties desired of laser-coolable species (namely diagonal FCFs and localized metal-centered electronic excitations).

Figure 31 compares the DLIF spectra for three Ca-containing molecules of increasing complexity: CaOH, CaOCH₃, and CaOC₁₀H₇ (based on measurements reported by Zhang et al. (2021); Augenbraun (2020); Mitra et al. (2022)). Despite the fact that CaOC₁₀H₇ contains over an order of magnitude more vibrational modes than CaOH, the gross structure of their DLIF spectra is largely similar. In all cases, the Ca-O stretching mode is the dominant off-diagonal decay channel. CaOC₁₀H₇ shows some activity in a handful of additional modes at the $\sim 0.1 - 1\%$ level, indicating that achieving optical cycling will be more challenging— but not necessary prohibitive.

The laser cooling and full quantum control of larger molecules (containing a dozen or more atoms) is at the very frontier of the the field, so much so that ideas of what to do with them are just beginning to be explored. Funda-

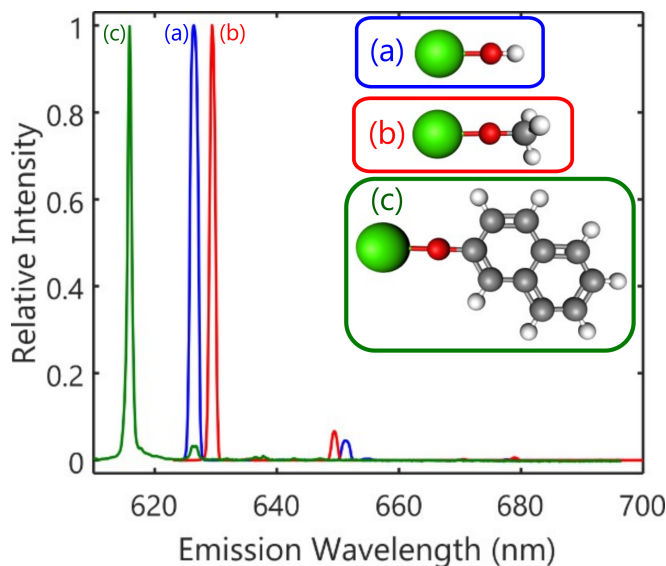


Figure 31: Comparison of DLIF spectra following excitation of (a) CaOH, (b) CaOCH₃, and (c) CaOC₁₀H₇ to the \tilde{A} excited state. Spectra (a) and (b) were recorded using fluorescence from a molecular beam, and spectrum (c) was recorded by collecting fluorescence from inside a buffer-gas cell. The diagonal fluorescence features are normalized to unity.

mentally, the larger number of atoms in the molecule, the larger the number of vibrational modes and hyperfine states. The concept of “internal motion” also starts to enter, e.g. a spinning ligand. Such modes can naturally be used to store quantum information, but exactly how this can be done and how useful this will be has not been fully explored. With a large enough molecule, one may be able to completely separate the laser cooling and readout section of the molecule (through an “optical cycling center”) from the physics end, perhaps containing an exotic atom such as a heavy radioactive species. Thus, one might be able to realize a “configurable” molecular framework that allows targeted substitution of scientifically interesting components.

4.2. Other molecular motifs

To date, all laser-cooled polyatomic molecules are of the form MOR, in which an alkaline-earth-like metal hosting a localized valence electron is bonded to a linker oxygen atom and electronegative radical. However, other molecular structures may also be suitable for laser cooling. Closely related to MOR molecules are other ML molecules, where L is an electronegative ligand such as NC, SH, or CH₃ (Norrsgard et al. (2019b); Augenbraun et al.

(2020a)). We describe two more dramatic departures from the MOR model, which appear to be favorable for future laser cooling experiments.

First, polyatomic molecules could be functionalized with multiple optical cycling centers, for example the linear molecules SrCCSr and YbCCCa, or asymmetric top molecules consisting of two metals linked by a benzene ring (O'Rourke and Hutzler (2019); Ivanov et al. (2020b)). These systems are expected to exhibit enhanced scattering rates due to the presence of two optical cycling centers, and offer separation of functions between distinct metals (for example, precision measurement localized on a Yb atom, and co-magnetometry localized on a Ca atom). Symmetric molecules like SrCCSr possess a structure analogous to Sr₂, which is a leading candidate for a molecular clock with applications to precision measurement (Zelevinsky et al. (2008)).

Second, polyatomic molecules with multivalent optical cycling centers, for example AlSH, should also be possible (Yu et al. (2023)), in a manner analogous to diatomic molecules like AlF, AlCl, TlF, BH, and CH (Hofsass et al. (2021); Daniel et al. (2021); Grasdijk et al. (2021); Hendricks et al. (2014); Schnaubelt et al. (2021)). Although the generalization from MF to MOH molecules has been highly successful for alkaline-earth-like metals (e.g., M=Ca,Sr,Yb), calculations show that for p-block metals (e.g., M=Al,Si,P), MOH molecules are bent and undergo a large bond angle deflection upon electronic excitation. This phenomenon can be mitigated with the use of a different linker atom like S or Se despite their lower bond polarity, due to reduced bond repulsion. Thus by careful tuning of the competition between bond repulsion and bond polarity, optical cycling of polyatomic molecules also appears feasible for species with p-block metals. Generalization of optical cycling to other structures may also be possible, but remains so far unexplored.

4.3. Challenges and possibilities for other polyatomic molecules

As larger and more complex molecular species are explored, new difficulties and limitations of quantum state control are likely to arise. Larger polyatomic molecules offer richer internal structures, a promising prospect for encoding qudits (higher dimensional analogues of qubits), and unique rovibrational modes, a potential platform to use for searches for fundamental symmetry violations. However, controlling these structures will potentially be more difficult than is the case for small polyatomic species. Several open

questions remain. For example, in the case of ATMs identified by Augendraun et al. (2020a), it is generally the case that the excited electronic states have large and anisotropic g -factors; it will be necessary to understand how that structure affects the magnetic-field-dependent forces that are necessary in a MOT. In addition, nonlinear molecules are subject to many symmetry-breaking effects such as the Jahn-Teller effect and other vibronic couplings, and it will be necessary to understand the extent to which these features affect the rovibrational selection rules that aided laser-based control of smaller and higher symmetry species.

Other challenges may arise in the quest to gain quantum-state control over larger species. From a practical standpoint, because buffer-gas cooling techniques are generally most applicable at temperatures above about 0.5 K, large molecules will be distributed over a substantially larger number of internal states. Moreover, the energy levels in large molecules are separated by smaller intervals, which generically complicates the task of achieving coherent control of these molecules. With smaller spacings, Rabi frequencies must be reduced in order to suppress off-resonant excitation and unwanted state transfer. In quantum simulation/quantum information processing applications, for example, reduced Rabi frequencies may become an impediment to high-speed gate operations. To complicate the problem, the larger number of states in these complex polyatomic molecules lead to more pathways present for blackbody excitations and spontaneous decay, limiting the coherence times of experiments.

There may also be fundamental challenges due to the complex level structure of large polyatomic molecules. For example, larger molecules are potentially more susceptible to non-radiative loss channels that may interrupt optical cycling (Bixon and Jortner (1968)). We present here a simple model that, while speculative, conveys our sense of the structural questions that must be understood in order to achieve laser cooling of increasingly large polyatomic molecules. The essential details follow the treatment provided by Uzer and Miller (1991). Readers should also consult the excellent, and highly pedagogical, overview of intramolecular vibrational energy redistribution presented by Nesbitt and Field (1996). Our model begins with the observation that the density of vibrational states at some energy above the absolute ground state grows very rapidly with molecule size, especially for molecules that contain low-frequency ($\nu \lesssim 100 \text{ cm}^{-1}$) vibrational modes. In many cases, laser cooling transitions involve excitation to an excited electronic state \tilde{A} with energy below the dissociation threshold of the ground electronic state

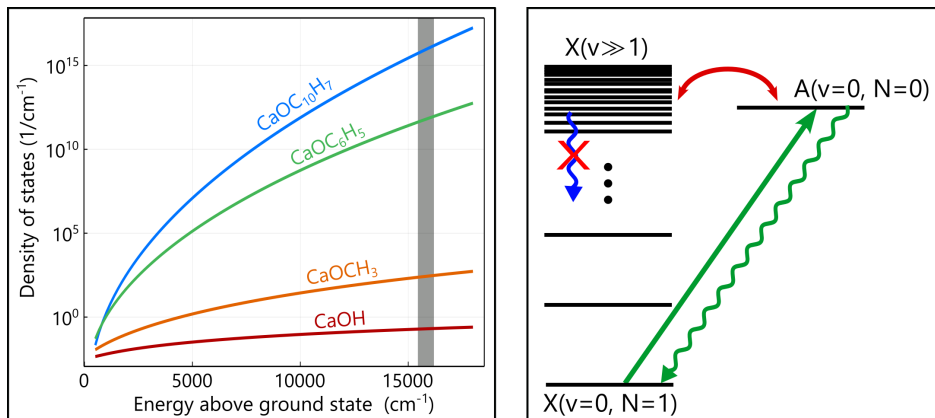


Figure 32: (Left) Density of states as a function of energy above the absolute ground state $\tilde{X}(v=0)$ for CaOR molecules with ligands of increasing size. The vertical gray band indicates the typical energy range of the $\tilde{A} \leftarrow \tilde{X}$ electronic transition in these species. (Right) Schematic diagram highlighting the levels important to our hypothesized loss mechanism.

\tilde{X} , meaning that \tilde{A} is embedded in a dense manifold of highly-excited vibrational levels of \tilde{X} . See Fig. 32 for calculations of the density of vibrational states for molecules of the form CaOR obtained using the method presented in Haarhoff (1964). For ligands, R, such as C₆H₅ or C₁₀H₇, the density of vibrational states at the location of the $\tilde{A}(v=0)$ level can be as large as 10¹¹ or 10¹⁵ states per cm⁻¹, respectively. For CaOC₆H₅ (CaOC₁₀H₇) this means there are around 10⁸ (10¹²) dark states within the frequency range spanned by the natural linewidth of a typical bright state (~ 30 MHz).

Consider a near-resonant excitation that transfers molecular population from a ground rovibronic state $|\phi_0\rangle$ (in practice a single rotational level of the $\tilde{X}(v=0)$ manifold) to a “bright” rovibronic excited state $|\phi_b\rangle$ that has natural lifetime τ_b (typically a single rotational level of the $A(v=0)$ or $\tilde{B}(v=0)$ manifolds). If $|\phi_b\rangle$ were an energy eigenstate, the only time evolution that would occur following excitation is decay back to $|\phi_0\rangle$ at a rate $\Gamma_b = 1/\tau_b$. If, however, $|\phi_b\rangle$ is coupled via some vibronic interaction to the highly-excited levels of \tilde{X} via a matrix element V_{bd} , then $|\phi_b\rangle$ is not an energy eigenstate; the energy eigenstates can be expressed as

$$|\psi_n\rangle = a_{bn}|\phi_b\rangle + \sum_{j=1}^N a_{d_j n}|\phi_{d_j}\rangle. \quad (20)$$

Thus, laser excitation that selectively targets $|\phi_b\rangle$ actually populates numerous energy eigenstates, meaning the excited state that is prepared will evolve in time and lead to population building up in the dark manifold $\{|\phi_d\rangle\}$ with a characteristic timescale τ_{bd} . Because the states in $\{|\phi_d\rangle\}$ are very closely spaced, the timescale for population to return to $|\phi_b\rangle$ (τ_{return}) may be very long. Under conditions where $\tau_{bd} \ll \tau_b$ (so that leakage to the dark manifold occurs more rapidly than photon emission) and $\tau_{\text{return}} \gg \tau_b$ (so that population remains in the dark manifold over many natural lifetimes), this process will appear to cause loss from the laser cooling experiment. The timescale during which population is primarily found in the dark manifold limits the achievable photon scattering rate, directly impeding optical cycling and laser cooling. Under a crude estimate based on Fermi's golden rule, if τ_{bd} is to compete with spontaneous emission (for a typical excited-state lifetime of about 30 ns), we must require

$$\frac{1}{\tau_{bd}} \approx 2\pi \langle V^2 \rangle \rho, \quad (21)$$

where $\sqrt{\langle V^2 \rangle}$ is the root-mean-squared coupling matrix element between the bright and dark manifolds and ρ is the density of states. For a molecule with vibrational density of states $\rho \approx 10^{14}$ per cm^{-1} , an average coupling matrix element as small as $\sqrt{\langle V^2 \rangle} \sim 10^{-9} \text{ cm}^{-1}$ would be sufficient to satisfy this condition. It is not currently clear whether coupling matrix elements of this magnitude are present in the large CaOR molecules being proposed for laser cooling applications. It is also possible that the average coupling matrix element could be tuned through judicious molecular design choices that reduce interaction between the metal-centered valence electron and the portion(s) of the molecule that contribute most to the vibrational density of states. It is critical that new theoretical and experimental studies be pursued to study these questions.

5. Conclusion

In this review, we have described how the field of ultracold polyatomic molecules is poised to impact many of the frontiers in modern atomic, molecular, and optical physics. Recent experimental results have shown that much of the toolbox developed for ultracold atoms can be applied to molecules with equal success. As we have described, the control of polyatomic molecules depends on a careful understanding of their internal structure. However, the class of molecules that has garnered the most experimental attention

(alkaline-earth psuedohalides) share a set of common features such as diagonal FCFs and manageable rotational selection rules, that points toward a generic way to “design” laser-coolable molecules with diverse geometries, atomic constituents, and responses to external fields. The breadth of molecular species and structures that appear amenable to laser cooling is extremely large, and continues to grow as researchers explore increasingly complex systems.

6. Acknowledgments

We gratefully acknowledge valuable comments from Profs. David DeMille, Nicholas Hutzler, Michael Tarbutt, and Jun Ye, as well as Parul Aggarwal and Calder Miller. We also thank Prof. Robert W. Field and Bryan Changala for insightful input on IVR coupling mechanisms in larger molecules. The work described in this paper that was conducted within the Doyle group was supported by the AFOSR, the NSF, and the Heising-Simons Foundation.

References

- ACME Collaboration. Improved limit on the electric dipole moment of the electron. *Nature*, 562:355–360, 2018. doi: 10.1038/s41586-018-0599-8.
- X. Alauze, J. Lim, M. A. Trigatzis, S. Swarbrick, F. J. Collings, N. J. Fitch, B. E. Sauer, and M. R. Tarbutt. An ultracold molecular beam for testing fundamental physics. *Quantum Science and Technology*, 6(4):044005, July 2021. doi: 10.1088/2058-9565/ac107e. URL <https://doi.org/10.1088/2058-9565/ac107e>.
- V. V. Albert, J. P. Covey, and J. Preskill. Robust encoding of a qubit in a molecule. *Phys. Rev. X*, 10(3):031050, 2020. URL <https://doi.org/10.1103/PhysRevX.10.031050>.
- A. Allouche, G. Wannous, and M. Aubert-Frécon. A ligand-field approach for the low-lying states of Ca, Sr and Ba monohalides. *Chemical Physics*, 170(1):11–22, 1993. URL [https://doi.org/10.1016/0301-0104\(93\)80087-p](https://doi.org/10.1016/0301-0104(93)80087-p).

- L. Anderegg, B. L. Augenbraun, E. Chae, B. Hemmerling, N. R. Hutzler, A. Ravi, A. L. Collopy, J. Ye, W. Ketterle, and J. M. Doyle. Radio frequency magneto-optical trapping of CaF with high density. *Phys. Rev. Lett.*, 119:103201, 2017. URL <https://doi.org/10.1103/PhysRevLett.119.103201>.
- L. Anderegg, B. L. Augenbraun, Y. Bao, S. Burchesky, L. W. Cheuk, W. Ketterle, and J. M. Doyle. Laser cooling of optically trapped molecules. *Nature Phys.*, 14(9):890–893, 2018. URL <https://doi.org/10.1038/s41567-018-0191-z>.
- L. Anderegg, L. W. Cheuk, Y. Bao, S. Burchesky, W. Ketterle, K.-K. Ni, and J. M. Doyle. An optical tweezer array of ultracold molecules. *Science*, 365(6458):1156–1158, sep 2019. doi: 10.1126/science.aax1265.
- L. Anderegg, S. Burchesky, Y. Bao, S. S. Yu, T. Karman, E. Chae, K.-K. Ni, W. Ketterle, and J. M. Doyle. Observation of microwave shielding of ultracold molecules. *Science*, 373(6556):779–782, Aug. 2021. doi: 10.1126/science.abg9502. URL <https://doi.org/10.1126/science.abg9502>.
- L. Anderegg, N. B. Vilas, C. Hallas, P. Robichaud, A. Jadbabaie, J. M. Doyle, and N. R. Hutzler. Quantum control of trapped polyatomic molecules for eedm searches. 2023. doi: 10.48550/ARXIV.2301.08656. URL <https://arxiv.org/abs/2301.08656>.
- A. André, D. DeMille, J. M. Doyle, M. D. Lukin, S. E. Maxwell, P. Rabl, R. J. Schoelkopf, and P. Zoller. A coherent all-electrical interface between polar molecules and mesoscopic superconducting resonators. *Nature Physics*, 2(9):636–642, Aug. 2006. doi: 10.1038/nphys386. URL <https://doi.org/10.1038/nphys386>.
- A. Aspect, E. Arimondo, R. Kaiser, N. Vansteenkiste, and C. Cohen-Tannoudji. Laser cooling below the one-photon recoil energy by velocity-selective coherent population trapping. *Phys. Rev. Lett.*, 61:826–829, Aug 1988. doi: 10.1103/PhysRevLett.61.826. URL <https://link.aps.org/doi/10.1103/PhysRevLett.61.826>.
- B. L. Augenbraun. *Methods for Direct Laser Cooling of Polyatomic Molecules*. PhD thesis, Harvard University, 2020.

- B. L. Augenbraun, J. M. Doyle, T. Zelevinsky, and I. Kozyryev. Molecular asymmetry and optical cycling: Laser cooling asymmetric top molecules. *Phys. Rev. X*, 10(3), 2020a. URL <https://doi.org/10.1103/PhysRevX.10.031022>.
- B. L. Augenbraun, Z. D. Lasner, A. Frenett, H. Sawaoka, C. Miller, T. C. Steimle, and J. M. Doyle. Laser-cooled polyatomic molecules for improved electron electric dipole moment searches. *New J. Phys.*, 22:022003, 2020b. URL <https://doi.org/10.1088/1367-2630/ab687b>.
- B. L. Augenbraun, A. Frenett, H. Sawaoka, C. Hallas, N. B. Vilas, A. Nasir, Z. D. Lasner, and J. M. Doyle. Zeeman-Sisyphus Deceleration of Molecular Beams. 2021a. doi: 10.1103/PhysRevLett.127.263002.
- B. L. Augenbraun, Z. D. Lasner, A. Frenett, H. Sawaoka, A. T. Le, J. M. Doyle, and T. C. Steimle. Observation and laser spectroscopy of ytterbium monomethoxide, YbOCH₃. *Phys. Rev. A*, 103(2):022814, 2021b. URL <https://doi.org/10.1103/physreva.103.022814>.
- B. L. Augenbraun, S. Burchesky, A. Winnicki, and J. M. Doyle. High-resolution laser spectroscopy of a functionalized aromatic molecule. *The Journal of Physical Chemistry Letters*, 13(46):10771–10777, Nov. 2022. doi: 10.1021/acs.jpcllett.2c03041. URL <https://doi.org/10.1021/acs.jpcllett.2c03041>.
- L. D. Augustovičová and J. L. Bohn. Ultracold collisions of polyatomic molecules: CaOH. *New Journal of Physics*, 21(10):103022, Oct. 2019. doi: 10.1088/1367-2630/ab4720. URL <https://doi.org/10.1088/1367-2630/ab4720>.
- N. Balakrishnan. Perspective: Ultracold molecules and the dawn of cold controlled chemistry. *J. Chem. Phys.*, 145(15):150901, 2016. URL <https://doi.org/10.1063/1.4964096>.
- Y. Bao, S. S. Yu, L. Anderegg, E. Chae, W. Ketterle, K.-K. Ni, and J. M. Doyle. Dipolar spin-exchange and entanglement between molecules in an optical tweezer array. *arXiv:2211.09780*, 2022.
- T. A. Barckholtz and T. A. Miller. Quantitative insights about molecules exhibiting Jahn-Teller and related effects. *Int. Rev. Phys. Chem.*, 17(4): 435–524, 1998. doi: 10.1080/014423598230036.

- D. Barredo, S. de Léséleuc, V. Lienhard, T. Lahaye, and A. Browaeys. An atom-by-atom assembler of defect-free arbitrary two-dimensional atomic arrays. *Science*, 354(6315):1021–1023, 2016. URL <https://doi.org/10.1126/science.aah3778>.
- J. Barry, D. McCarron, E. Norrgard, M. Steinecker, and D. DeMille. Magneto-optical trapping of a diatomic molecule. *Nature*, 512:286–289, 2014. URL <https://doi.org/10.1038/nature13634>.
- J. F. Barry, E. S. Shuman, and D. DeMille. A bright, slow cryogenic molecular beam source for free radicals. *Phys. Chem. Chem. Phys.*, 13(42):18936, 2011. URL <https://doi.org/10.1039/C1CP20335E>.
- J. F. Barry, E. S. Shuman, E. B. Norrgard, and D. DeMille. Laser radiation pressure slowing of a molecular beam. *Phys. Rev. Lett.*, 108(10):103002, 2012. URL <https://doi.org/10.1103/PhysRevLett.108.103002>.
- L. Baum, N. B. Vilas, C. Hallas, B. L. Augenbraun, S. Raval, D. Mitra, and J. M. Doyle. 1D Magneto-Optical Trap of Polyatomic Molecules. *Phys. Rev. Lett.*, 124:133201, Mar 2020. URL <https://link.aps.org/doi/10.1103/PhysRevLett.124.133201>.
- L. Baum, N. B. Vilas, C. Hallas, B. L. Augenbraun, S. Raval, D. Mitra, and J. M. Doyle. Establishing a nearly closed cycling transition in a polyatomic molecule. *Phys. Rev. A*, 103(4):043111, 2021. URL <https://doi.org/10.1103/physreva.103.043111>.
- R. Bause, A. Schindewolf, R. Tao, M. Duda, X.-Y. Chen, G. Quéméner, T. Karman, A. Christianen, I. Bloch, and X.-Y. Luo. Collisions of ultracold molecules in bright and dark optical dipole traps. *Phys. Rev. Research*, 3:033013, Jul 2021. doi: 10.1103/PhysRevResearch.3.033013. URL <https://link.aps.org/doi/10.1103/PhysRevResearch.3.033013>.
- R. Bause, A. Christianen, A. Schindewolf, I. Bloch, and X.-Y. Luo. Ultracold sticky collisions: Theoretical and experimental status. *arXiv:2211.10223*, 2022.
- D. J. Berkeland and M. G. Boshier. Destabilization of dark states and optical spectroscopy in Zeeman-degenerate atomic systems. *Phys. Rev. A*, 65(3):033413, 2002. URL <https://doi.org/10.1103/PhysRevA.65.033413>.

- P. F. Bernath. *Spectra of Atoms and Molecules*. OUP, 2017.
- M. Bixon and J. Jortner. Intramolecular radiationless transitions. *The Journal of Chemical Physics*, 48(2):715–726, Jan. 1968. doi: 10.1063/1.1668703. URL <https://doi.org/10.1063/1.1668703>.
- J. L. Bohn, A. M. Rey, and J. Ye. Cold molecules: Progress in quantum engineering of chemistry and quantum matter. *Science*, 357(6355):1002–1010, 2017. URL <https://doi.org/10.1126/science.aam6299>.
- C. R. Brazier and P. F. Bernath. The $\tilde{A}^2E - \tilde{X}^2A_1$ transition of monomethyl calcium: A rotational analysis. *J. Chem. Phys.*, 91(8):4548–4554, 1989. doi: 10.1063/1.456742.
- M. Brouard, D. H. Parker, and S. Y. T. van de Meerakker. Taming molecular collisions using electric and magnetic fields. *Chem. Soc. Rev.*, 43(21):7279–7294, 2014. doi: 10.1039/c4cs00150h. URL <https://doi.org/10.1039/c4cs00150h>.
- J. Brown. Rotational energy levels of symmetric top molecules in 2E states. *Molecular Physics*, 20:817–834, 1 1971. ISSN 0026-8976. doi: 10.1080/00268977100100801. URL <http://www.tandfonline.com/doi/abs/10.1080/00268977100100801>.
- P. R. Bunker and P. Jensen. *Molecular symmetry and spectroscopy*. NRC Research Press, 2006.
- J. J. Bureau, P. Aggarwal, K. Mehling, and J. Ye. Blue-detuned magneto-optical trap of molecules. *arXiv:2212.07472*, 2022.
- L. D. V. Buuren, C. Sommer, M. Motsch, S. Pohle, M. Schenk, J. Bayerl, P. W. Pinkse, and G. Rempe. Electrostatic extraction of cold molecules from a cryogenic reservoir. *Physical Review Letters*, 102:2–5, 2009. ISSN 00319007. doi: 10.1103/PhysRevLett.102.033001. Ref. 17 in Nick’s beam paper.
- W. B. Cairncross, D. N. Gresh, M. Grau, K. C. Cossel, T. S. Roussy, Y. Ni, Y. Zhou, J. Ye, and E. A. Cornell. A precision measurement of the electron’s electric dipole moment using trapped molecular ions. *Phys. Rev. Lett.*, 119:153001, 2017.

- W. B. Cairncross, J. T. Zhang, L. R. B. Picard, Y. Yu, K. Wang, and K.-K. Ni. Assembly of a rovibrational ground state molecule in an optical tweezer. *Phys. Rev. Lett.*, 126:123402, Mar 2021. URL <https://link.aps.org/doi/10.1103/PhysRevLett.126.123402>.
- L. Caldwell and M. R. Tarbutt. Sideband cooling of molecules in optical traps. *Phys. Rev. Research*, 2:013251, Mar 2020. doi: 10.1103/PhysRevResearch.2.013251. URL <https://link.aps.org/doi/10.1103/PhysRevResearch.2.013251>.
- L. Caldwell, J. A. Devlin, H. J. Williams, N. J. Fitch, E. A. Hinds, B. E. Sauer, and M. R. Tarbutt. Deep laser cooling and efficient magnetic compression of molecules. *Phys. Rev. Lett.*, 123(3):033202, 2019. URL <https://doi.org/10.1103/PhysRevLett.123.033202>.
- W. C. Campbell, E. Tsikata, H.-I. Lu, L. D. van Buuren, and J. M. Doyle. Magnetic Trapping and Zeeman Relaxation of NH ($X^3\Sigma^-$). *Phys. Rev. Lett.*, 98:213001, May 2007. URL <https://link.aps.org/doi/10.1103/PhysRevLett.98.213001>.
- L. D. Carr, D. DeMille, R. V. Krems, and J. Ye. Cold and ultracold molecules: Science, technology and applications. *New J. Phys.*, 11(5):055049, 2009. URL <https://doi.org/10.1088/1367-2630/11/5/055049>.
- T. M. Cerny, X. Q. Tan, J. M. Williamson, E. S. J. Robles, A. M. Ellis, and T. A. Miller. High resolution electronic spectroscopy of ZnCH₃ and CdCH₃. *The Journal of Chemical Physics*, 99(12):9376–9388, Dec. 1993. doi: 10.1063/1.465521. URL <https://doi.org/10.1063/1.465521>.
- E. Chae, L. Anderegg, B. L. Augenbraun, A. Ravi, B. Hemmerling, N. R. Hutzler, A. L. Collopy, J. Ye, W. Ketterle, and J. M. Doyle. One-dimensional magneto-optical compression of a cold CaF molecular beam. *New Journal of Physics*, 19(3):033035, mar 2017. doi: 10.1088/1367-2630/aa6470.
- L. W. Cheuk, L. Anderegg, B. L. Augenbraun, Y. Bao, S. Burchesky, W. Ketterle, and J. M. Doyle. Λ -enhanced imaging of molecules in an optical trap. *Phys. Rev. Lett.*, 121:083201, 2018. doi: 10.1103/PhysRevLett.121.083201. URL <https://link.aps.org/doi/10.1103/PhysRevLett.121.083201>.

- L. W. Cheuk, L. Anderegg, Y. Bao, S. Burchesky, S. S. Yu, W. Ketterle, K.-K. Ni, and J. M. Doyle. Observation of Collisions between Two Ultracold Ground-State CaF Molecules. *Phys. Rev. Lett.*, 125:043401, Jul 2020. URL <https://link.aps.org/doi/10.1103/PhysRevLett.125.043401>.
- L. Chomaz, I. Ferrier-Barbut, F. Ferlaino, B. Laburthe-Tolra, B. L. Lev, and T. Pfau. Dipolar physics: a review of experiments with magnetic quantum gases. *Reports on Progress in Physics*, 86(2):026401, 2023. doi: 10.1088/1361-6633/aca814. URL <https://doi.org/10.1088/1361-6633/aca814>.
- S. Chu. The manipulation of neutral particles. *Rev. Mod. Phys.*, 70(3):685, 1998. URL <https://doi.org/10.1103/RevModPhys.70.685>.
- A. L. Collopy, S. Ding, Y. Wu, I. A. Finneran, L. Anderegg, B. L. Augenbraun, J. M. Doyle, and J. Ye. 3-D magneto-optical trap of yttrium monoxide. *Phys. Rev. Lett.*, 121(21):213201, 2018. URL <https://doi.org/10.1103/PhysRevLett.121.213201>.
- D. Comparat. Molecular cooling via sisyphus processes. *Phys. Rev. A*, 89:043410, Apr 2014. doi: 10.1103/PhysRevA.89.043410. URL <https://link.aps.org/doi/10.1103/PhysRevA.89.043410>.
- D. Cory, R. Laflamme, E. Knill, L. Viola, T. Havel, N. Boulant, G. Boutis, E. Fortunato, S. Lloyd, R. Martinez, C. Negrevergne, M. Pravia, Y. Sharf, G. Teklemariam, Y. Weinstein, and W. Zurek. NMR based quantum information processing: Achievements and prospects. *Fortschritte der Physik*, 48(9-11):875–907, 2000. doi: [https://doi.org/10.1002/1521-3978\(200009\)48:9/11<875::AID-PROP875>3.0.CO;2-V](https://doi.org/10.1002/1521-3978(200009)48:9/11<875::AID-PROP875>3.0.CO;2-V).
- A. Cournol et al. A new experiment to test parity symmetry in cold chiral molecules using vibrational spectroscopy. *Quantum Electron.*, 49(3):288–292, 2019. doi: 10.1070/qel16880.
- J. R. Daniel, C. Wang, K. Rodriguez, B. Hemmerling, T. N. Lewis, C. Bardeen, A. Teplukhin, and B. K. Kendrick. Spectroscopy on the $A^1\Pi \leftarrow X^1\Sigma^+$ transition of buffer-gas-cooled AlCl. *Physical Review A*, 104:012801, 7 2021. ISSN 24699934. doi: 10.1103/PHYSREVA.104.012801/FIGURES/6/MEDIUM. URL <https://journals.aps.org/pra/abstract/10.1103/PhysRevA.104.012801>.

- D. DeMille. Quantum computation with trapped polar molecules. *Phys. Rev. Lett.*, 88(6):067901, 2002. doi: 10.1103/physrevlett.88.067901.
- D. DeMille, S. B. Cahn, D. Murphree, D. A. Rahmlow, and M. G. Kozlov. Using molecules to measure nuclear spin-dependent parity violation. *Phys. Rev. Lett.*, 100:023003, Jan 2008. doi: 10.1103/PhysRevLett.100.023003. URL <https://link.aps.org/doi/10.1103/PhysRevLett.100.023003>.
- W. Demtröder. *Molecular Physics: Theoretical Principles and Experimental Methods*. Weinheim: Wiley-VCH Verlag, 2003.
- M. Di Rosa. Laser-cooling molecules. *Eur. Phys. J. D*, 31(2):395–402, 2004. URL <https://doi.org/10.1140/epjd/e2004-00167-2>.
- M. J. Dick. *Spectroscopy of selected calcium and strontium containing polyatomic molecules*. PhD thesis, University of Waterloo, 2007. URL <https://uwspace.uwaterloo.ca/bitstream/handle/10012/3010/MikeDickThesis.pdf>.
- C. E. Dickerson, H. Guo, A. J. Shin, B. L. Augenbraun, J. R. Caram, W. C. Campbell, and A. N. Alexandrova. Franck-Condon Tuning of Optical Cycling Centers by Organic Functionalization. *Phys. Rev. Lett.*, 126(12), 2021a. URL <https://doi.org/10.1103/physrevlett.126.123002>.
- C. E. Dickerson, H. Guo, G.-Z. Zhu, E. R. Hudson, J. R. Caram, W. C. Campbell, and A. N. Alexandrova. Optical cycling functionalization of arenes. *J. Phys. Chem. Lett.*, 12(16):3989–3995, 2021b. URL <https://doi.org/10.1021/acs.jpcllett.1c00733>.
- C. E. Dickerson, C. Chang, H. Guo, and A. N. Alexandrova. Fully saturated hydrocarbons as hosts of optical cycling centers. *arXiv:2209.09935*, 2022.
- S. Ding, Y. Wu, I. A. Finneran, J. J. Burau, and J. Ye. Sub-Doppler Cooling and Compressed Trapping of YO Molecules at μK Temperatures. *Phys. Rev. X*, 10:021049, Jun 2020. URL <https://link.aps.org/doi/10.1103/PhysRevX.10.021049>.
- S. C. Doret, C. B. Connolly, W. Ketterle, and J. M. Doyle. Buffer-Gas Cooled Bose-Einstein Condensate. *Phys. Rev. Lett.*, 103:103005, Sep 2009. URL <https://link.aps.org/doi/10.1103/PhysRevLett.103.103005>.

- J. M. Doyle, B. Friedrich, J. Kim, and D. Patterson. Buffer-gas loading of atoms and molecules into a magnetic trap. *Phys. Rev. A*, 52:R2515–R2518, Oct 1995. URL <https://link.aps.org/doi/10.1103/PhysRevA.52.R2515>.
- S. Eibenberger, J. Doyle, and D. Patterson. Enantiomer-specific state transfer of chiral molecules. *Phys. Rev. Lett.*, 118(12):123002, 2017. doi: 10.1103/PhysRevLett.118.123002.
- A. M. Ellis. Main group metal-ligand interactions in small molecules: New insights from laser spectroscopy. *Int. Rev. Phys. Chem.*, 20(4):551–590, 2001. URL <https://doi.org/10.1080/01442350110062542>.
- M. Endres, H. Bernien, A. Keesling, H. Levine, E. R. Anschuetz, A. Krajenbrink, C. Senko, V. Vuletic, M. Greiner, and M. D. Lukin. Atom-by-atom assembly of defect-free one-dimensional cold atom arrays. *Science*, 354(6315):1024–1027, 2016. URL <https://doi.org/10.1126/science.aah3752>.
- W. Ertmer, R. Blatt, J. L. Hall, and M. Zhu. Laser manipulation of atomic beam velocities: Demonstration of stopped atoms and velocity reversal. *Phys. Rev. Lett.*, 54:996–999, Mar 1985. doi: 10.1103/PhysRevLett.54.996. URL <https://link.aps.org/doi/10.1103/PhysRevLett.54.996>.
- N. Fitch and M. Tarbutt. *Laser-cooled molecules*, volume 70 of *Advances In Atomic, Molecular, and Optical Physics*. Academic Press, 2021. URL <https://www.sciencedirect.com/science/article/pii/S1049250X21000033>.
- N. J. Fitch and M. R. Tarbutt. Principles and Design of a Zeeman-Sisyphus Decelerator for Molecular Beams. *ChemPhysChem*, 17(22):3609–3623, 2016. URL <https://doi.org/10.1002/cphc.201600656>.
- K. Gaul, M. G. Kozlov, T. A. Isaev, and R. Berger. Chiral Molecules as Sensitive Probes for Direct Detection of P-Odd Cosmic Fields. *Phys. Rev. Lett.*, 125(12):123004, 2020. URL <https://doi.org/10.1103/physrevlett.125.123004>.
- O. Grasdijk, O. Timgren, J. Kastelic, T. Wright, S. Lamoreaux, D. Demille, K. Wenz, M. Aitken, T. Zelevinsky, T. Winick, and D. Kawall.

- CeNTREX: a new search for time-reversal symmetry violation in the ^{205}Tl nucleus. *Quantum Science and Technology*, 6:044007, 9 2021. ISSN 2058-9565. doi: 10.1088/2058-9565/ABDCA3. URL <https://iopscience.iop.org/article/10.1088/2058-9565/abdca3><https://iopscience.iop.org/article/10.1088/2058-9565/abdca3/meta>.
- P. D. Gregory, J. A. Blackmore, F. M. D, L. M. Fernley, S. L. Bromley, J. M. Hutson, and S. L. Cornish. Molecule–molecule and atom–molecule collisions with ultracold RbCs molecules. *New Journal of Physics*, 23(12):125004, Dec. 2021. doi: 10.1088/1367-2630/ac3c63. URL <https://doi.org/10.1088/1367-2630/ac3c63>.
- A. T. Grier, I. Ferrier-Barbut, B. S. Rem, M. Delehaye, L. Khaykovich, F. Chevy, and C. Salomon. Λ -enhanced sub-Doppler cooling of lithium atoms in D_1 gray molasses. *Phys. Rev. A*, 87:063411, Jun 2013. doi: 10.1103/PhysRevA.87.063411. URL <https://link.aps.org/doi/10.1103/PhysRevA.87.063411>.
- M. Guo, B. Zhu, B. Lu, X. Ye, F. Wang, R. Vexiau, N. Bouloufa-Maafa, G. Quéméner, O. Dulieu, and D. Wang. Creation of an ultracold gas of ground-state dipolar $^{23}\text{Na}^{87}\text{Rb}$ molecules. *Phys. Rev. Lett.*, 116(20):205303, 2016. URL <https://doi.org/10.1103/PhysRevLett.116.205303>.
- P. Haarhoff. The density of vibrational energy levels of polyatomic molecules. *Molecular Physics*, 7(2):101–117, Jan. 1964. doi: 10.1080/00268976300100871. URL <https://doi.org/10.1080/00268976300100871>.
- C. Hallas, N. B. Vilas, L. Anderegg, P. Robichaud, A. Winnicki, C. Zhang, L. Cheng, and J. M. Doyle. Optical trapping of a polyatomic molecule in an ℓ -type parity doublet state. *arXiv:2208.13762*, 2022.
- S. Haroche. Nobel lecture: Controlling photons in a box and exploring the quantum to classical boundary. *Rev. Mod. Phys.*, 85(3):1083, 2013.
- B. R. Heazlewood and T. P. Softley. Towards chemistry at absolute zero. *Nature Reviews Chemistry*, 5(2):125–140, Jan. 2021. doi: 10.1038/s41570-020-00239-0. URL <https://doi.org/10.1038/s41570-020-00239-0>.

- B. Hemmerling, E. Chae, A. Ravi, L. Anderegg, G. K. Drayna, N. R. Hutzler, A. L. Collopy, J. Ye, W. Ketterle, and J. M. Doyle. Laser slowing of CaF molecules to near the capture velocity of a molecular MOT. *J. Phys. B*, 49 (17):174001, 2016. URL <https://doi.org/10.1088/0953-4075/49/17/174001>.
- R. J. Hendricks, D. A. Holland, S. Truppe, B. E. Sauer, and M. R. Tarbutt. Vibrational branching ratios and hyperfine structure of ^{11}BH and its suitability for laser cooling. *Front. Phys.*, 2:51, 2014. URL <https://doi.org/10.3389/fphy.2014.00051>.
- E. Herbst and E. F. van Dishoeck. Complex organic interstellar molecules. *Annual Review of Astronomy and Astrophysics*, 47:427–480, 2009.
- D. Herschbach. Molecular collisions, from warm to ultracold. *Faraday Discussions*, 142:9–23, 2009. ISSN 13596640. doi: 10.1039/b910118g.
- G. Herzberg. *Molecular Spectra and Molecular Structure: Electronic Spectra and Electronic Structure of Polyatomic Molecules*, volume 3. Van Nostrand, 1966.
- E. Hirota. *High-Resolution Spectroscopy of Transient Molecules*. Springer Berlin Heidelberg, 1985.
- S. Hofsass, M. Doppelbauer, S. C. Wright, S. Kray, B. G. Sartakov, J. Pérez-Ríos, G. Meijer, and S. Truppe. Optical cycling of AlF molecules. *New Journal of Physics*, 23:075001, 6 2021. ISSN 1367-2630. doi: 10.1088/1367-2630/AC06E5. URL <https://iopscience.iop.org/article/10.1088/1367-2630/ac06e5><https://iopscience.iop.org/article/10.1088/1367-2630/ac06e5/meta>.
- C. M. Holland, Y. Lu, and L. W. Cheuk. On-demand entanglement of molecules in a reconfigurable optical tweezer array. *arXiv:2210.06309*, 2022.
- J. T. Hougen. Fermi resonance in linear triatomic molecules in Π electronic states. *The Journal of Chemical Physics*, 37(2):403–408, July 1962. doi: 10.1063/1.1701334. URL <https://doi.org/10.1063/1.1701334>.
- J. T. Hougen. Double group considerations, jahn-teller induced rovibronic effects, and the nuclear spin-electron spin hyperfine hamiltonian for a

- molecule of symmetry C_{3v} in an electronic 2E state. *Journal of Molecular Spectroscopy*, 81:73–92, 5 1980. ISSN 0022-2852. doi: 10.1016/0022-2852(80)90330-6.
- M.-G. Hu, Y. Liu, M. A. Nichols, L. Zhu, G. Quéméner, O. Dulieu, and K.-K. Ni. Nuclear spin conservation enables state-to-state control of ultracold molecular reactions. *Nature Chemistry*, 13(5):435–440, 2021.
- M. T. Hummon, T. V. T. an J. Klos, H.-I. Lu, E. Tsikata, W. C. Campbell, A. Dalgarno, and J. M. Doyle. Cold N-NH collisions in a magnetic trap. *Phys. Rev. Lett.*, 106:053201, 2011. URL <https://doi.org/10.1103/PhysRevLett.106.053201>.
- M. T. Hummon, M. Yeo, B. K. Stuhl, A. L. Collopy, Y. Xia, and J. Ye. 2D magneto-optical trapping of diatomic molecules. *Phys. Rev. Lett.*, 110(14):143001, 2013. URL <https://doi.org/10.1103/PhysRevLett.110.143001>.
- N. R. Hutzler. Polyatomic molecules as quantum sensors for fundamental physics. *Quantum Sci. Technol.*, 5(4):044011, 2020. URL <https://doi.org/10.1088/2058-9565/abb9c5>.
- N. R. Hutzler, H.-I. Lu, and J. M. Doyle. The buffer gas beam: An intense, cold, and slow source for atoms and molecules. *Chem. Rev.*, 112(9):4803–4827, 2012. URL <https://doi.org/10.1021/cr200362u>.
- T. A. Isaev and R. Berger. Polyatomic candidates for cooling of molecules with lasers from simple theoretical concepts. *Phys. Rev. Lett.*, 116(6):063006, 2016. URL <https://doi.org/10.1103/PhysRevLett.116.063006>.
- T. A. Isaev, A. V. Zaitsevskii, and E. Eliav. Laser-coolable polyatomic molecules with heavy nuclei. *J. Phys. B*, 50(22):225101, 2017. URL <https://doi.org/10.1088/1361-6455/aa8f34>.
- M. V. Ivanov, F. H. Bangerter, and A. I. Krylov. Towards a rational design of laser-coolable molecules: insights from equation-of-motion coupled-cluster calculations. *Phys. Chem. Chem. Phys.*, 21(35):19447–19457, 2019. URL <https://doi.org/10.1039/C9CP03914G>.

- M. V. Ivanov, F. H. Bangerter, P. Wójcik, and A. I. Krylov. Toward ultracold organic chemistry: Prospects of laser cooling large organic molecules. *J. Phys. Chem. Lett.*, 11(16):6670–6676, 2020a. URL <https://doi.org/10.1021/acs.jpcllett.0c01960>.
- M. V. Ivanov, S. Gulania, and A. I. Krylov. Two cycling centers in one molecule: Communication by through-bond interactions and entanglement of the unpaired electrons. *Journal of Physical Chemistry Letters*, 11:1297–1304, 2020b. ISSN 19487185. doi: 10.1021/acs.jpcllett.0c00021.
- P. Jansen, H. L. Bethlem, and W. Ubachs. Tipping the scales: Search for drifting constants from molecular spectra. *J. Chem. Phys.*, 140(1):010901, 2014. URL <https://doi.org/10.1063/1.4853735>.
- K. N. Jarvis, J. A. Devlin, T. E. Wall, B. E. Sauer, and M. R. Tarbutt. Blue-detuned magneto-optical trap. *Phys. Rev. Lett.*, 120:083201, Feb 2018. doi: 10.1103/PhysRevLett.120.083201. URL <https://link.aps.org/doi/10.1103/PhysRevLett.120.083201>.
- S. Kinsey-Nielsen, C. R. Brazier, and P. F. Bernath. Rotational analysis of the $\tilde{B}^2\Sigma^+ - \tilde{X}^2\Sigma^+$ transition of BaOH and BaOD. *J. Chem. Phys.*, 84(2): 698–708, 1986. doi: 10.1063/1.450566.
- W. Klemperer, K. K. Lehmann, J. K. G. Watson, and S. C. Wofsy. Can molecules have permanent electric dipole moments? *J. Phys. Chem.*, 97(10):2413–2416, 1993. URL <https://doi.org/10.1021/j100112a049>.
- J. Kobayashi, A. Ogino, and S. Inouye. Measurement of the variation of electron-to-proton mass ratio using ultracold molecules produced from laser-cooled atoms. *Nature Communications*, 10:1–5, 2019. ISSN 20411723. doi: 10.1038/s41467-019-11761-1. URL <http://dx.doi.org/10.1038/s41467-019-11761-1>.
- M. Koller, F. Jung, J. Phrompao, M. Zeppenfeld, I. M. Rabey, and G. Rempe. Electric-Field-Controlled Cold Dipolar Collisions between Trapped CH₃F Molecules. *Phys. Rev. Lett.*, 128:203401, May 2022. doi: 10.1103/PhysRevLett.128.203401. URL <https://link.aps.org/doi/10.1103/PhysRevLett.128.203401>.
- I. Kozyryev and N. R. Hutzler. Precision measurement of time-reversal symmetry violation with laser-cooled polyatomic molecules. *Phys. Rev. Lett.*,

- 119:133002, 2017. URL <https://doi.org/10.1103/PhysRevLett.119.133002>.
- I. Kozyryev, L. Baum, K. Matsuda, P. Olson, B. Hemmerling, and J. M. Doyle. Collisional relaxation of vibrational states of SrOH with He at 2 K. *New J. Phys.*, 17(4):045003, 2015. doi: 10.1088/1367-2630/17/4/045003.
- I. Kozyryev, L. Baum, K. Matsuda, and J. M. Doyle. Proposal for laser cooling of complex polyatomic molecules. *ChemPhysChem*, 17:3641, 2016a. doi: 10.1002/cphc.201601051.
- I. Kozyryev, L. Baum, K. Matsuda, B. Hemmerling, and J. M. Doyle. Radiation pressure force from optical cycling on a polyatomic molecule. *J. Phys. B*, 49(13):134002, 2016b. URL <https://doi.org/10.1088/0953-4075/49/13/134002>.
- I. Kozyryev, L. Baum, K. Matsuda, B. L. Augenbraun, L. Anderegg, A. P. Sedlack, and J. M. Doyle. Sisyphus laser cooling of a polyatomic molecule. *Phys. Rev. Lett.*, 118:173201, 2017. URL <https://doi.org/10.1103/PhysRevLett.118.173201>.
- I. Kozyryev, L. Baum, L. Aldridge, P. Yu, E. E. Eyler, and J. M. Doyle. Coherent bichromatic force deflection of molecules. *Phys. Rev. Lett.*, 120(6):063205, 2018. URL <https://doi.org/10.1103/PhysRevLett.120.063205>.
- I. Kozyryev, Z. Lasner, and J. M. Doyle. Enhanced sensitivity to ultralight bosonic dark matter in the spectra of the linear radical SrOH. *Phys. Rev. A*, 103:043313, Apr 2021. URL <https://link.aps.org/doi/10.1103/PhysRevA.103.043313>.
- R. V. Krems. Cold controlled chemistry. *Phys. Chem. Chem. Phys.*, 10(28):4079–4092, 2008. URL <https://doi.org/10.1039/B802322K>.
- T. Lahaye, C. Menotti, L. Santos, M. Lewenstein, and T. Pfau. The physics of dipolar bosonic quantum gases. *Rep. Prog. Phys.*, 72:126401, 2009.
- T. K. Langin and D. DeMille. Towards improved loading, cooling, and trapping of molecules in magneto-optical traps. *arXiv:2210.14223*, 2022.

- T. K. Langin, V. Jorapur, Y. Zhu, Q. Wang, and D. DeMille. Polarization enhanced deep optical dipole trapping of Λ -cooled polar molecules. *Phys. Rev. Lett.*, 127:163201, Oct 2021. doi: 10.1103/PhysRevLett.127.163201. URL <https://link.aps.org/doi/10.1103/PhysRevLett.127.163201>.
- G. Lao, G.-Z. Zhu, C. E. Dickerson, B. L. Augenbraun, A. N. Alexandrova, J. R. Caram, E. R. Hudson, and W. C. Campbell. Laser spectroscopy of aromatic molecules with optical cycling centers: Strontium(I) phenoxides. *The Journal of Physical Chemistry Letters*, 13(47):11029–11035, Nov. 2022. doi: 10.1021/acs.jpcllett.2c03040. URL <https://doi.org/10.1021/acs.jpcllett.2c03040>.
- Z. Lasner, A. Lunstad, C. Zhang, L. Cheng, and J. M. Doyle. Vibronic branching ratios for nearly closed rapid photon cycling of SrOH. *Phys. Rev. A*, 106:L020801, Aug 2022. doi: 10.1103/PhysRevA.106.L020801. URL <https://link.aps.org/doi/10.1103/PhysRevA.106.L020801>.
- J.-R. Li, W. G. Tobias, K. Matsuda, C. Miller, G. Valtolina, L. D. Marco, R. R. W. Wang, L. Lassabliere, G. Quemener, J. L. Bohn, and J. Ye. Tuning of dipolar interactions and evaporative cooling in a three-dimensional molecular quantum gas. *Nature Physics*, 17(10):1144–1148, Sept. 2021. doi: 10.1038/s41567-021-01329-6. URL <https://doi.org/10.1038/s41567-021-01329-6>.
- M. Li and J. A. Coxon. High-resolution analysis of the fundamental bending vibrations in the $\tilde{A}^2\Pi$ and $\tilde{X}^2\Sigma^+$ states of CaOH and CaOD: Deperturbation of Renner-Teller, spin-orbit and K-type resonance interactions. *J. Chem. Phys.*, 102(7):2663–2674, 1995. doi: 10.1063/1.468643. URL <https://doi.org/10.1063/1.468643>.
- J. Lim, J. R. Almond, M. A. Trigatzis, J. A. Devlin, N. J. Fitch, B. E. Sauer, M. R. Tarbutt, and E. A. Hinds. Laser cooled YbF molecules for measuring the electron’s electric dipole moment. *Phys. Rev. Lett.*, 120(12):123201, 2018. URL <https://doi.org/10.1103/PhysRevLett.120.123201>.
- H.-I. Lu. *Magnetic trapping of molecules via optical loading and magnetic slowing*. PhD thesis, Harvard University, Cambridge, MA, 2014. URL http://www.doylegroup.harvard.edu/files/bufferpubs/theses/hil_thesis.pdf.

- Y. Lu, C. M. Holland, and L. W. Cheuk. Molecular laser cooling in a dynamically tunable repulsive optical trap. *Phys. Rev. Lett.*, 128: 213201, May 2022. doi: 10.1103/PhysRevLett.128.213201. URL <https://link.aps.org/doi/10.1103/PhysRevLett.128.213201>.
- D. E. Maison, L. V. Skripnikov, and V. V. Flambaum. Theoretical study of $^{173}\text{YbOH}$ to search for the nuclear magnetic quadrupole moment. *Phys. Rev. A*, 100(3):032514, 2019. URL <https://doi.org/10.1103/physreva.100.032514>.
- K. Matsuda, L. D. Marco, J.-R. Li, W. G. Tobias, G. Valtolina, G. Quéméner, and J. Ye. Resonant collisional shielding of reactive molecules using electric fields. *Science*, 370(6522):1324–1327, Dec. 2020. doi: 10.1126/science.abe7370. URL <https://doi.org/10.1126/science.abe7370>.
- S. E. Maxwell, N. Brahms, R. Decarvalho, D. R. Glenn, J. S. Helton, S. V. Nguyen, D. Patterson, J. Petricka, D. Demille, and J. M. Doyle. High-flux beam source for cold, slow atoms or molecules. *Physical Review Letters*, 95:1–4, 2005a. ISSN 00319007. doi: 10.1103/PhysRevLett.95.173201. Ref. 5 in Nick’s beam paper.
- S. E. Maxwell, N. Brahms, R. deCarvalho, D. R. Glenn, J. S. Helton, S. V. Nguyen, D. Patterson, J. Petricka, D. DeMille, and J. M. Doyle. High-flux beam source for cold, slow atoms or molecules. *Phys. Rev. Lett.*, 95:173201, Oct 2005b. URL <https://link.aps.org/doi/10.1103/PhysRevLett.95.173201>.
- D. McCarron. Laser cooling and trapping molecules. *J. Phys. B*, 51(21): 212001, 2018. doi: 10.1088/1361-6455/aadfba. URL <https://doi.org/10.1088/1361-6455/aadfba>.
- D. J. McCarron, E. B. Norrgard, M. H. Steinecker, and D. DeMille. Improved magneto-optical trapping of a diatomic molecule. *New J. Phys.*, 17(3):035014, 2015. URL <https://doi.org/10.1088/1367-2630/17/3/035014>.
- D. J. McCarron, M. H. Steinecker, Y. Zhu, and D. DeMille. Magnetic trapping of an ultracold gas of polar molecules. *Phys. Rev. Lett.*, 121:013202, 2018. doi: 10.1103/PhysRevLett.121.013202. URL <https://link.aps.org/doi/10.1103/PhysRevLett.121.013202>.

- M. Mengel and F. C. De Lucia. Helium and hydrogen induced rotational relaxation of H₂CO observed at temperatures of the interstellar medium. *The Astrophysical Journal*, 543(1):271, 2000. URL <https://doi.org/10.1086/317108>.
- J. K. Messer and F. C. De Lucia. Measurement of Pressure-Broadening Parameters for the CO-He System at 4 K. *Phys. Rev. Lett.*, 53:2555–2558, Dec 1984. URL <https://link.aps.org/doi/10.1103/PhysRevLett.53.2555>.
- A. Micheli, G. K. Brennen, and P. Zoller. A toolbox for lattice-spin models with polar molecules. *Nat. Phys.*, 2(5):341–347, 2006. doi: 10.1038/nphys287.
- D. Mitra, N. B. Vilas, C. Hallas, L. Anderegg, B. L. Augenbraun, L. Baum, C. Miller, S. Raval, and J. M. Doyle. Direct laser cooling of a symmetric top molecule. *Science*, 369(6509):1366–1369, 2020.
- D. Mitra, Z. D. Lasner, G. Z. Zhu, C. E. Dickerson, B. L. Augenbraun, A. D. Bailey, A. N. Alexandrova, W. C. Campbell, J. R. Caram, E. R. Hudson, and J. M. Doyle. Pathway toward optical cycling and laser cooling of functionalized arenes. *Journal of Physical Chemistry Letters*, 13:7029–7035, 8 2022. ISSN 19487185. doi: 10.1021/ACS.JPCLETT.2C01430/SUPPL_FILE/JZ2C01430_SI_001.PDF. URL <https://pubs.acs.org/doi/abs/10.1021/acs.jpcllett.2c01430>.
- P. K. Molony, P. D. Gregory, Z. Ji, B. Lu, M. P. Köppinger, C. R. Le Sueur, C. L. Blackley, J. M. Hutson, and S. L. Cornish. Creation of ultracold ⁸⁷Rb¹³³Cs molecules in the rovibrational ground state. *Phys. Rev. Lett.*, 113(25):255301, 2014. URL <https://doi.org/10.1103/PhysRevLett.113.255301>.
- M. G. Moore and A. Vardi. Bose-enhanced chemistry: Amplification of selectivity in the dissociation of molecular bose-einstein condensates. *Physical Review Letters*, 88(16), Apr. 2002. doi: 10.1103/physrevlett.88.160402. URL <https://doi.org/10.1103/physrevlett.88.160402>.
- D. J. Nesbitt and R. W. Field. Vibrational energy flow in highly excited molecules: role of intramolecular vibrational redistribution. *The Journal*

- of Physical Chemistry*, 100(31):12735–12756, Jan. 1996. doi: 10.1021/jp960698w. URL <https://doi.org/10.1021/jp960698w>.
- K.-K. Ni, S. Ospelkaus, M. H. G. de Miranda, A. Pe'er, B. Neyenhuis, J. J. Zirbel, S. Kotochigova, P. S. Julienne, D. S. Jin, and J. Ye. A high phase-space-density gas of polar molecules. *Science*, 322(5899):231–235, 2008. URL <https://doi.org/10.1126/science.1163861>.
- K.-K. Ni, S. Ospelkaus, D. Wang, G. Quéméner, B. Neyenhuis, M. H. G. de Miranda, J. Bohn, J. Ye, and D. Jin. Dipolar collisions of polar molecules in the quantum regime. *Nature*, 464(7293):1324–1328, 2010. URL <https://doi.org/10.1038/nature08953>.
- K.-K. Ni, T. Rosenband, and D. D. Grimes. Dipolar exchange quantum logic gate with polar molecules. *Chem. Sci.*, 9(33):6830–6838, 2018. doi: 10.1039/c8sc02355g.
- M. A. Nichols, Y.-X. Liu, L. Zhu, M.-G. Hu, Y. Liu, and K.-K. Ni. Detection of long-lived complexes in ultracold atom-molecule collisions. *Phys. Rev. X*, 12:011049, Mar 2022. doi: 10.1103/PhysRevX.12.011049. URL <https://link.aps.org/doi/10.1103/PhysRevX.12.011049>.
- E. B. Norrgard, D. J. McCarron, M. H. Steinecker, M. R. Tarbutt, and D. DeMille. Submillikelvin dipolar molecules in a radio-frequency magneto-optical trap. *Phys. Rev. Lett.*, 116(6):063004, 2016. URL <https://doi.org/10.1103/PhysRevLett.116.063004>.
- E. B. Norrgard, D. S. Barker, S. Eckel, J. A. Fedchak, N. N. Klimov, and J. Scherschligt. Nuclear-spin dependent parity violation in optically trapped polyatomic molecules. *Communications Physics*, 2(1), 2019a. URL <https://www.nature.com/articles/s42005-019-0181-1>.
- E. B. Norrgard, D. S. Barker, S. Eckel, J. A. Fedchak, N. N. Klimov, and J. Scherschligt. Nuclear-spin dependent parity violation in optically trapped polyatomic molecules. *Communications Physics*, 2:1–6, 2019b. ISSN 23993650. doi: 10.1038/s42005-019-0181-1. URL <http://dx.doi.org/10.1038/s42005-019-0181-1>.
- A. V. Oleynichenko, L. V. Skripnikov, A. V. Zaitsevskii, and V. V. Flambaum. Laser-coolable AcOH⁺ ion for CP-violation searches. *Physical Review A*, 105:022825, 2 2022. ISSN 24699934. doi: 10.1103/PHYSREVA.

- 105.022825/FIGURES/3/MEDIUM. URL <https://journals.aps.org/prabstract/10.1103/PhysRevA.105.022825>.
- M. J. O'Rourke and N. R. Hutzler. Hypermetallic polar molecules for precision measurements. *Phys. Rev. A*, 100(022502):022502, 2019. URL <https://doi.org/10.1103/PhysRevA.100.022502>.
- S. Ospelkaus, K.-K. Ni, D. Wang, M. H. G. de Miranda, B. Neyenhuis, G. Quémener, P. Julienne, J. Bohn, D. Jin, and J. Ye. Quantum-state controlled chemical reactions of ultracold potassium-rubidium molecules. *Science*, 327(5967):853–857, 2010. URL <https://doi.org/10.1126/science.1184121>.
- J. W. Park, S. A. Will, and M. W. Zwierlein. Ultracold dipolar gas of fermionic $^{23}\text{Na}^{40}\text{K}$ molecules in their absolute ground state. *Phys. Rev. Lett.*, 114(20):205302, 2015. URL <https://doi.org/10.1103/PhysRevLett.114.205302>.
- D. Patterson and J. M. Doyle. Bright, guided molecular beam with hydrodynamic enhancement. *J. Chem. Phys.*, 126(15):154307, 2007. URL <https://doi.org/10.1063/1.2717178>.
- D. Patterson and J. M. Doyle. Sensitive chiral analysis via microwave three-wave mixing. *Phys. Rev. Lett.*, 111(2):023008, 2013.
- A. C. Paul, K. Sharma, M. A. Reza, H. Telfah, T. A. Miller, and J. Liu. Laser-induced fluorescence and dispersed-fluorescence spectroscopy of the $\tilde{A}^2E - \tilde{X}^2A_1$ transition of jet-cooled calcium methoxide (CaOCH_3) radicals. *J. Chem. Phys.*, 151(13):134303, 2019. doi: 10.1063/1.5104278.
- C. Pethick and H. Smith. *Bose-Einstein condensation in dilute gases*. Cambridge University Press, 2002.
- M. Petzold, P. Kaebert, P. Gersema, T. Poll, N. Reinhardt, M. Siercke, and S. Ospelkaus. Type-II Zeeman slowing: Characterization and comparison to conventional radiative beam-slowing schemes. *Phys. Rev. A*, 98(6):063408, 2018a. URL <https://doi.org/10.1103/physreva.98.063408>.
- M. Petzold, P. Kaebert, P. Gersema, M. Siercke, and S. Ospelkaus. A Zeeman slower for diatomic molecules. *New J. Phys.*, 20(4):042001, 2018b. URL <https://doi.org/10.1088/1367-2630/aab9f5>.

- W. D. Phillips. Nobel Lecture: Laser cooling and trapping of neutral atoms. *Rev. Mod. Phys.*, 70(3):721, 1998. URL <https://doi.org/10.1103/RevModPhys.70.721>.
- W. D. Phillips and H. Metcalf. Laser deceleration of an atomic beam. *Phys. Rev. Lett.*, 48:596–599, Mar 1982. doi: 10.1103/PhysRevLett.48.596. URL <https://link.aps.org/doi/10.1103/PhysRevLett.48.596>.
- N. H. Pilgram. Production and characterization of ytterbium monohydroxide (YbOH) for next-generation parity and time-reversal violating physics searches, 2023.
- N. H. Pilgram, A. Jadbabaie, Y. Zeng, N. R. Hutzler, and T. C. Steimle. Fine and hyperfine interactions in $^{171}\text{YbOH}$ and $^{173}\text{YbOH}$. *J. Chem. Phys.*, 154(24):244309, 2021. URL <https://doi.org/10.1063/5.0055293>.
- J. Piskorski. *Cooling, Collisions and nonSticking of Polyatomic Molecules in a Cryogenic Buffer Gas Cell*. PhD thesis, Harvard University, Cambridge, MA, 2014.
- J. Piskorski, D. Patterson, S. Eibenberger, and J. M. Doyle. Cooling, spectroscopy and non-sticking of trans-Stilbene and Nile Red. *ChemPhysChem*, 15(17):3800–3804, 2014.
- V. Plomp, Z. Gao, T. Cremers, M. Besemer, and S. Y. T. van de Meerakker. High-resolution imaging of molecular collisions using a zeeman decelerator. *The Journal of Chemical Physics*, 152(9):091103, Mar. 2020. doi: 10.1063/1.5142817. URL <https://doi.org/10.1063/1.5142817>.
- A. Prehn, M. Ibrügger, R. Glöckner, G. Rempe, and M. Zeppenfeld. Optoelectrical cooling of polar molecules to submillikelvin temperatures. *Phys. Rev. Lett.*, 116(6):063005, 2016. URL <https://doi.org/10.1103/PhysRevLett.116.063005>.
- M. Quack. On the measurement of the parity violating energy difference between enantiomers. *Chemical Physics Letters*, 132:147–153, 12 1986. ISSN 00092614. doi: 10.1016/0009-2614(86)80098-7.
- M. Quack, J. Stohner, and M. Willeke. High-resolution spectroscopic studies and theory of parity violation in chiral molecules. *Annual Review of Physical Chemistry*, 59:741–769, 2008. ISSN 0066426X. doi: 10.1146/annurev.physchem.58.032806.104511.

- M. Quack, G. Seyfang, and G. Wichmann. Perspectives on parity violation in chiral molecules: theory, spectroscopic experiment and biomolecular homochirality. *Chemical Science*, 13:10598–10643, 9 2022. ISSN 20416539. doi: 10.1039/D2SC01323A. URL <https://pubs.rsc.org/en/content/articlehtml/2022/sc/d2sc01323a>
<https://pubs.rsc.org/en/content/articlelanding/2022/sc/d2sc01323a>.
- S. F. Rice, H. Martin, and R. W. Field. The electronic structure of the calcium monohalides. a ligand field approach. *J. Chem. Phys.*, 82(11): 5023–5034, 1985. URL <https://doi.org/10.1063/1.448676>.
- F. Richter, D. Becker, C. Bény, T. A. Schulze, S. Ospelkaus, and T. J. Osborne. Ultracold chemistry and its reaction kinetics. *New J. Phys.*, 17(5):055005, 2015. URL <https://doi.org/10.1088/1367-2630/17/5/055005>.
- T. M. Rvachov, H. Son, A. T. Sommer, S. Ebadi, J. J. Park, M. W. Zwierlein, W. Ketterle, and A. O. Jamison. Long-lived ultracold molecules with electric and magnetic dipole moments. *Phys. Rev. Lett.*, 119:143001, Oct 2017. URL <https://link.aps.org/doi/10.1103/PhysRevLett.119.143001>.
- L. Satterthwaite, C. Pérez, A. L. Steber, D. Finestone, R. L. Broadrup, and D. Patterson. Enantiomeric analysis of chiral isotopomers via microwave three-wave mixing. *Journal of Physical Chemistry A*, 123:3194–3198, 2019. ISSN 15205215. doi: 10.1021/acs.jpca.9b02115.
- R. Sawant, J. A. Blackmore, P. D. Gregory, J. Mur-Petit, D. Jaksch, J. Aldegunde, J. M. Hutson, M. R. Tarbutt, and S. L. Cornish. Ultracold polar molecules as qudits. *New J. Phys.*, 22:013027, 2019. URL <https://doi.org/10.1088/1367-2630/ab60f4>.
- H. Sawaoka, A. Frenett, A. Nasir, T. Ono, B. L. Augenbraun, T. C. Steimle, and J. M. Doyle. Zeeman-sisyphus deceleration for heavy molecules with perturbed excited-state structure, 2022.
- B. C. Sawyer, B. K. Stuhl, M. Yeo, T. V. Tscherbul, M. T. Hummon, Y. Xia, J. Klos, D. Patterson, J. M. Doyle, and J. Ye. Cold heteromolecular dipolar collisions. *Physical Chemistry Chemical Physics*, 13:19059–19066, 2011. ISSN 14639076. doi: 10.1039/c1cp21203f. Ref. 101 in Nick’s beam paper.

- A. Schindewolf, R. Bause, X.-Y. Chen, M. Duda, T. Karman, I. Bloch, and X.-Y. Luo. Evaporation of microwave-shielded polar molecules to quantum degeneracy. *Nature*, 607(7920):677–681, July 2022. doi: 10.1038/s41586-022-04900-0. URL <https://doi.org/10.1038/s41586-022-04900-0>.
- J. C. Schnaubelt, J. C. Shaw, and D. J. McCarron. Cold ch radicals for laser cooling and trapping. 9 2021. doi: 10.48550/arxiv.2109.03953. URL <https://arxiv.org/abs/2109.03953v1>.
- E. S. Shuman, J. F. Barry, D. R. Glenn, and D. DeMille. Radiative force from optical cycling on a diatomic molecule. *Phys. Rev. Lett.*, 103(22):223001, 2009. URL <https://doi.org/10.1103/PhysRevLett.103.223001>.
- E. S. Shuman, J. F. Barry, and D. DeMille. Laser cooling of a diatomic molecule. *Nature*, 467(7317):820–823, 2010. URL <https://doi.org/10.1038/nature09443>.
- B. Spaun, P. B. Changala, D. Patterson, B. J. Bjork, O. H. Heckl, J. M. Doyle, and J. Ye. Continuous probing of cold complex molecules with infrared frequency comb spectroscopy. *Nature*, 533:517–520, 2016. ISSN 14764687. doi: 10.1038/nature17440.
- M. H. Steinecker, D. J. McCarron, Y. Zhu, and D. DeMille. Improved radio-frequency magneto-optical trap of SrF molecules. *ChemPhysChem*, 17(22):3664–3669, 2016. URL <https://doi.org/10.1002/cphc.201600967>.
- B. K. Stuhl, B. C. Sawyer, D. Wang, and J. Ye. Magneto-optical trap for polar molecules. *Phys. Rev. Lett.*, 101(24):243002, 2008. URL <https://doi.org/10.1103/PhysRevLett.101.243002>.
- M. R. Tarbutt. Magneto-optical trapping forces for atoms and molecules with complex level structures. *New J. Phys.*, 17(1):015007, 2015. doi: 10.1088/1367-2630/17/1/015007. URL <https://doi.org/10.1088/1367-2630/17/1/015007>.
- M. R. Tarbutt. Laser cooling of molecules. *Contemp. Phys.*, 59(4):356–376, 2018. URL <https://doi.org/10.1080/00107514.2018.1576338>.

- M. R. Tarbutt and T. C. Steimle. Modeling magneto-optical trapping of CaF molecules. *Phys. Rev. A*, 92(5):053401, 2015. URL <https://doi.org/10.1103/physreva.92.053401>.
- C. M. Tesch and R. de Vivie-Riedle. Quantum computation with vibrationally excited molecules. *Phys. Rev. Lett.*, 89:157901, Sep 2002. doi: 10.1103/PhysRevLett.89.157901. URL <https://link.aps.org/doi/10.1103/PhysRevLett.89.157901>.
- J. Toscano, H. J. Lewandowski, and B. R. Heazlewood. Cold and controlled chemical reaction dynamics. *Physical Chemistry Chemical Physics*, 22(17): 9180–9194, 2020. doi: 10.1039/d0cp00931h. URL <https://doi.org/10.1039/d0cp00931h>.
- S. Truppe, H. J. Williams, N. J. Fitch, M. Hambach, T. E. Wall, E. A. Hinds, B. E. Sauer, and M. R. Tarbutt. An intense, cold, velocity-controlled molecular beam by frequency-chirped laser slowing. *New J. Phys.*, 19(2): 022001, 2017a. URL <https://doi.org/10.1088/1367-2630/aa5ca2>.
- S. Truppe, H. J. Williams, M. Hambach, L. Caldwell, N. J. Fitch, E. A. Hinds, B. E. Sauer, and M. R. Tarbutt. Molecules cooled below the doppler limit. *Nature Physics*, 13:1173–1176, 8 2017b. ISSN 1745-2473. doi: 10.1038/nphys4241. URL <http://www.doi.org/10.1038/nphys4241>. First CaF MOT (Imperial). Cooled below the Doppler limit.
- S. Truppe, H. J. Williams, M. Hambach, L. Caldwell, N. J. Fitch, E. A. Hinds, B. E. Sauer, and M. R. Tarbutt. Molecules cooled below the Doppler limit. *Nat. Phys.*, 2017c. URL <https://doi.org/10.1038/nphys4241>.
- T. Tscherbul and R. Krems. Controlling electronic spin relaxation of cold molecules with electric fields. *Phys. Rev. Lett.*, 97(8):083201, 2006. URL <https://doi.org/10.1103/PhysRevLett.97.083201>.
- T. Tscherbul, Y. V. Suleimanov, V. Aquilanti, and R. Krems. Magnetic field modification of ultracold molecule-molecule collisions. *New J. Phys.*, 11(5):055021, 2009. URL <https://doi.org/10.1088/1367-2630/11/5/055021>.
- T. V. Tscherbul and R. V. Krems. Tuning bimolecular chemical reactions by electric fields. *Phys. Rev. Lett.*, 115(2):023201, 2015.

- T. Uzer and W. Miller. Theories of intramolecular vibrational energy transfer. *Physics Reports*, 199(2):73–146, Jan. 1991. doi: 10.1016/0370-1573(91)90140-h. URL [https://doi.org/10.1016/0370-1573\(91\)90140-h](https://doi.org/10.1016/0370-1573(91)90140-h).
- G. Valtolina, K. Matsuda, W. G. Tobias, J.-R. Li, L. D. Marco, and J. Ye. Dipolar evaporation of reactive molecules to below the fermi temperature. *Nature*, 588(7837):239–243, Dec. 2020. doi: 10.1038/s41586-020-2980-7. URL <https://doi.org/10.1038/s41586-020-2980-7>.
- S. Y. T. van de Meerakker and G. Meijer. Collision experiments with stark-decelerated beams. *Faraday Discussions*, 142:113, 2009. doi: 10.1039/b819721k. URL <https://doi.org/10.1039/b819721k>.
- N. B. Vilas, C. Hallas, L. Anderegg, P. Robichaud, A. Winnicki, D. Mitra, and J. M. Doyle. Magneto-optical trapping and sub-Doppler cooling of a polyatomic molecule. *Nature*, 606(7912):70–74, Jun 2022. doi: 10.1038/s41586-022-04620-5.
- M. Wall, K. Hazzard, and A. M. Rey. Quantum magnetism with ultracold molecules. In *From Atomic To Mesoscale: The Role of Quantum Coherence in Systems of Various Complexities*, pages 3–37. World Scientific, 2015a.
- M. L. Wall, K. Maeda, and L. D. Carr. Simulating quantum magnets with symmetric top molecules. *Ann. Phys. (Berl.)*, 525(10-11):845–865, 2013. URL <https://doi.org/10.1002/andp.201300105>.
- M. L. Wall, K. Maeda, and L. D. Carr. Realizing unconventional quantum magnetism with symmetric top molecules. *New J. Phys.*, 17(2):025001, 2015b. URL <https://doi.org/10.1088/1367-2630/17/2/025001>.
- Q. Wei, S. Kais, B. Friedrich, and D. Herschbach. Entanglement of polar symmetric top molecules as candidate qubits. *J. Chem. Phys.*, 135(15):154102, 2011. URL <https://doi.org/10.1063/1.3649949>.
- J. D. Weinstein, R. deCarvalho, T. Guillet, B. Friedrich, and J. M. Doyle. Magnetic trapping of calcium monohydride molecules at millikelvin temperatures. *Nature*, 395(6698):148–150, 1998. URL <https://doi.org/10.1038/25949>.

- K. Wenz, I. Kozyryev, R. L. McNally, L. Aldridge, and T. Zelevinsky. Large molasses-like cooling forces for molecules using polychromatic optical fields: A theoretical description. *Physical Review Research*, 2: 043377, 12 2020. ISSN 26431564. doi: 10.1103/PHYSREVRESEARCH.2.043377/FIGURES/23/MEDIUM. URL <https://journals.aps.org/prresearch/abstract/10.1103/PhysRevResearch.2.043377>.
- D. R. Willey, R. L. Crownover, D. N. Bittner, and F. C. De Lucia. Very low temperature spectroscopy: The pressure broadening coefficients for CH₃F between 4.2 and 1.9 K. *J. Chem. Phys.*, 89(10):6147–6149, 1988. doi: 10.1063/1.455430. URL <https://doi.org/10.1063/1.455430>.
- H. J. Williams, S. Truppe, M. Hambach, L. Caldwell, N. J. Fitch, E. A. Hinds, B. E. Sauer, and M. R. Tarbutt. Characteristics of a magneto-optical trap of molecules. *New J. Phys.*, 19(11):113035, 2017. URL <https://doi.org/10.1088/1367-2630/aa8e52>.
- H. J. Williams, L. Caldwell, N. J. Fitch, S. Truppe, J. Rodewald, E. A. Hinds, B. E. Sauer, and M. R. Tarbutt. Magnetic trapping and coherent control of laser-cooled molecules. *Phys. Rev. Lett.*, 120:163201, 2018. doi: 10.1103/PhysRevLett.120.163201. URL <https://link.aps.org/doi/10.1103/PhysRevLett.120.163201>.
- D. J. Wineland. Nobel lecture: Superposition, entanglement, and raising schrodinger’s cat. *Rev. Mod. Phys.*, 85(3):1103, 2013.
- P. Wójcik, T. Korona, and M. Tomza. Interactions of benzene, naphthalene, and azulene with alkali-metal and alkaline-earth-metal atoms for ultracold studies. *The Journal of Chemical Physics*, 150(23):234106, 2019. URL <https://doi.org/10.1063/1.5094907>.
- X. Wu, T. Gantner, M. Koller, M. Zeppenfeld, S. Chervenkov, and G. Rempe. A cryofuge for cold-collision experiments with slow polar molecules. *Science*, 358(6363):645–648, 2017. URL <https://doi.org/10.1126/science.aan3029>.
- Y. Wu, J. J. Bureau, K. Mehling, J. Ye, and S. Ding. High phase-space density of laser-cooled molecules in an optical lattice. *Physical Review Letters*, 127(26):263201, dec 2021. doi: 10.1103/physrevlett.127.263201.

- B. Yan, S. A. Moses, B. Gadway, J. P. Covey, K. R. A. Hazzard, A. M. Rey, D. S. Jin, and J. Ye. Observation of dipolar spin-exchange interactions with lattice-confined polar molecules. *Nature*, 501(7468):521–525, Sept. 2013. doi: 10.1038/nature12483. URL <https://doi.org/10.1038/nature12483>.
- H. Yang, J. Cao, Z. Su, J. Rui, B. Zhao, and J.-W. Pan. Creation of an ultracold gas of triatomic molecules from an atom–diatomic molecule mixture. *Science*, 378(6623):1009–1013, Dec. 2022. doi: 10.1126/science.ade6307. URL <https://doi.org/10.1126/science.ade6307>.
- X. Ye, M. Guo, M. L. González-Martínez, G. Quéméner, and D. Wang. Collisions of ultracold $^{23}\text{Na}^{87}\text{Rb}$ molecules with controlled chemical reactivities. *Science Advances*, 4(1), Jan. 2018. doi: 10.1126/sciadv.aaq0083. URL <https://doi.org/10.1126/sciadv.aaq0083>.
- S. F. Yelin, K. Kirby, and R. Côté. Schemes for robust quantum computation with polar molecules. *Phys. Rev. A*, 74(5):050301(R), 2006. URL <https://doi.org/10.1103/PhysRevA.74.050301>.
- M. Yeo, M. T. Hummon, A. L. Collopy, B. Yan, B. Hemmerling, E. Chae, J. M. Doyle, and J. Ye. Rotational state microwave mixing for laser cooling of complex diatomic molecules. *Phys. Rev. Lett.*, 114(22):223003, 2015. doi: 10.1103/physrevlett.114.223003. URL <https://doi.org/10.1103/physrevlett.114.223003>.
- P. Yu and N. R. Hutzler. Probing fundamental symmetries of deformed nuclei in symmetric top molecules. *Physical Review Letters*, 126:023003, 1 2021. ISSN 10797114. doi: 10.1103/PHYSREVLETT.126.023003/FIGURES/3/MEDIUM. URL <https://journals.aps.org/prl/abstract/10.1103/PhysRevLett.126.023003>.
- P. Yu, L. W. Cheuk, I. Kozyryev, and J. M. Doyle. A scalable quantum computing platform using symmetric-top molecules. *New J. Phys.*, 21:093049, 2019. URL <https://doi.org/10.1088/1367-2630/ab428d>.
- P. Yu, A. Lopez, W. A. Goddard, and N. R. Hutzler. Multivalent optical cycling centers: towards control of polyatomics with multi-electron degrees of freedom. *Physical Chemistry Chemical Physics*, 25(1):154–170, 2023. doi: 10.1039/d2cp03545f. URL <https://doi.org/10.1039/d2cp03545f>.

- A. Zakharova and A. Petrov. P, T-odd effects for the RaOH molecule in the excited vibrational state. *Physical Review A*, 103:032819, 3 2021. ISSN 24699934. doi: 10.1103/PHYSREVA.103.032819/FIGURES/6/MEDIUM. URL <https://journals.aps.org/pr/abstract/10.1103/PhysRevA.103.032819>.
- T. Zelevinsky, S. Kotochigova, and J. Ye. Precision test of mass-ratio variations with lattice-confined ultracold molecules. *Physical Review Letters*, 100, 1 2008. ISSN 00319007. doi: 10.1103/PHYSREVLETT.100.043201.
- M. Zeppenfeld, B. G. U. Englert, R. Glöckner, A. Prehn, M. Mielenz, C. Sommer, L. D. van Buuren, M. Motsch, and G. Rempe. Sisyphus cooling of electrically trapped polyatomic molecules. *Nature*, 491(7425):570–573, Nov. 2012. URL <https://doi.org/10.1038/nature11595>.
- C. Zhang, B. L. Augenbraun, Z. D. Lasner, N. B. Vilas, J. M. Doyle, and L. Cheng. Accurate prediction and measurement of vibronic branching ratios for laser cooling linear polyatomic molecules. *J. Chem. Phys.*, 155 (9):091101, 2021. URL <https://doi.org/10.1063/5.0063611>.
- Z.-Y. Zhang and J.-M. Liu. Quantum correlations and coherence of polar symmetric top molecules in pendular states. *Scientific Reports*, 7(1), Dec. 2017. doi: 10.1038/s41598-017-18148-6. URL <https://doi.org/10.1038/s41598-017-18148-6>.
- V. Zhelyazkova, A. Cournol, T. E. Wall, A. Matsushima, J. J. Hudson, E. A. Hinds, M. R. Tarbutt, and B. E. Sauer. Laser cooling and slowing of CaF molecules. *Physical Review A*, 89(5):053416, may 2014. doi: 10.1103/physreva.89.053416.
- G.-Z. Zhu, D. Mitra, B. L. Augenbraun, C. E. Dickerson, M. J. Frim, G. Lao, Z. D. Lasner, A. N. Alexandrova, W. C. Campbell, J. R. Caram, J. M. Doyle, and E. R. Hudson. Functionalizing aromatic compounds with optical cycling centers. *Nat. Chem.*, 14:995, 2022. URL <https://www.nature.com/articles/s41557-022-00998-x>.
- M. Zhu, C. W. Oates, and J. L. Hall. Continuous high-flux monovelocit atomic beam based on a broadband laser-cooling technique. *Phys. Rev. Lett.*, 67:46–49, Jul 1991. doi: 10.1103/PhysRevLett.67.46. URL <https://link.aps.org/doi/10.1103/PhysRevLett.67.46>.